SRF 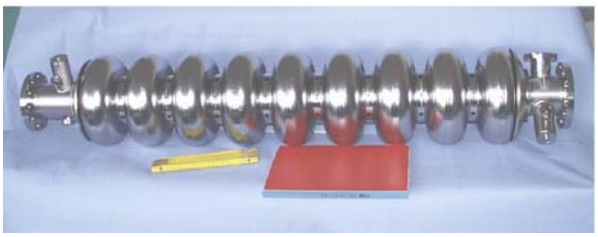

CARE/JRA1 Quarter report 1/2006

Research and Development on Superconducting Radio-Frequency Technology for Accelerator Application

Acronym: SRF

Co-Coordinators: D. Proch, DESY, T.Garvey, CNRS-Orsay

Participating Laboratories and Institutes:

Institute (Participating number)	Acronym	Country	Coordinator	SRF Scientific Contact	Associated to
DESY (6)	DESY	D	D. Proch	D. Proch	
CEA/DSM/DAPNIA (1)	CEA	F	R. Aleksan	O. Napoly	
CNRS-IN2P3-Orsay (3)	CNRS-Orsay	F	T. Garvey	T. Garvey	CNRS
INFN Legnaro (10)	INFN-LNL	I	S. Guiducci	E. Palmieri	INFN
INFN Milano (10)	INFN-Mi	I	S. Guiducci	P. Michelato	INFN
INFN Roma2 (10)	INFN-Ro2	I	S. Guiducci	S. Tazzari	INFN
INFN Frascati (10)	INFN-LNF	I	S. Guiducci	M. Castellano	INFN
Paul Scherrer Institute (19)	PSI	CH	V. Schlott	V. Schlott	
Technical University of Lodz (12)	TUL	PL	A. Napieralski	M. Grecki	
Warsaw University of Technology (14)	WUT-ISE	PL	R. Romaniuk	R. Romaniuk	
IPJ Swierk (13)	IPJ	PL	M. Sadowski	M. Sadowski	

Industrial Involvement:

Company Name	Country	Contact Person
ACCEL Instruments GmbH	D	M. Peiniger
WSK Mess- und Datentechnik GmbH	D	F. Schölz
E. ZANON SPA	I	G. Corniani
Henkel Lohnpoliertechnik GmbH	D	B. Henkel

Work supported by the European Community-Research Infrastructure Activity under the FP6 “Structuring the European Research Area” programme (CARE, contract number RII3-CT-2003-506395).

CARE/JRA1 Quarter report 1/2006

Research and Development on Superconducting Radio-Frequency Technology for Accelerator Application

Acronym: SRF

Co-Coordinators: D. Proch, DESY, T.Garvey, CNRS-Orsay

Participating Laboratories and Institutes:

Institute (Participating number)	Acronym	Country	Coordinator	SRF Scientific Contact	Associated to
DESY (6)	DESY	D	D. Proch	D. Proch	
CEA/DSM/DAPNIA (1)	CEA	F	R. Aleksan	O. Napoly	
CNRS-IN2P3-Orsay (3)	CNRS-Orsay	F	T.Garvey	T.Garvey	CNRS
INFN Legnaro (10)	INFN-LNL	I	S. Guiducci	E. Palmieri	INFN
INFN Milano (10)	INFN-Mi	I	S. Guiducci	P. Michelato	INFN
INFN Roma2 (10)	INFN-Ro2	I	S. Guiducci	S. Tazzari	INFN
INFN Frascati (10)	INFN-LNF	I	S. Guiducci	M. Castellano	INFN
Paul Scherrer Institute (19)	PSI	CH	V. Schlott	V. Schlott	
Technical University of Lodz (12)	TUL	PL	A.Napieralski	M. Grecki	
Warsaw University of Technology (14)	WUT-ISE	PL	R.Romaniuk	R. Romaniuk	
IPJ Swierk (13)	IPJ	PL	M. Sadowski	M. Sadowski	

Industrial Involvement:

Company Name	Country	Contact Person
ACCEL Instruments GmbH	D	M. Peiniger
WSK Mess- und Datentechnik GmbH	D	F. Schölz
E. ZANON SPA	I	G. Corniani
Henkel Lohnpoliertechnik GmbH	D	B. Henkel

1.) Milestones and Deliverables of the reporting period

3rd 18 months and 1st Quarterly report 2006

	Task	Milestones and Deliverables		planned end	expected end	Reference	task leader	contractor
1	**11.1.10**	**BPM Prototype(D)**	**New BPM ready for Installation**	**01.01.06**			M.Castellano	INFN-Lnl
2	**5.1.1.4**	**Final Report (D)**	**Best EP parameters**	**15.01.06**	**15.01.06**	**CARE-Report-06-010-SRF**	C.Antoine	CEA
3	5.2.2.4	Equipment ready	Roughness measurement finished	20.01.06			A.Matheisen	DESY
4	8.2.6	Status report	Report on magneto-strictive Tuner	31.01.06			Grecki	TUL
5	5.2.1.1.3	Status Report	Proof-of-Principle experiment hot wate	31.01.06	01.06.06		A.Matheisen	DESY
6	5.1.3.4	Commissioning	First operation of EP set-up	01.02.06			C.Antoine	CEA
7	**5.3.3.5**	**Final Report (D)**	**Automated EP is defined**	13.02.06			E.Palmieri	INFN-Lnl
8	5.4.1.5	Commissioning	Installation finished	28.02.06			D.Reschke	DESY
9	**9.3.3.8**	**Final Report (D)**	**Report on new LLRF hardware com**	**01.03.06**			R.Romaniuk	WUT-ISE
10	5.4.3.5	Commissioning	VT Cleaning Installation finished	07.03.06			D.Reschke	DESY
11	2.2.1.14	Report	Final Report for new components	17.03.06	01.03.06	CARE-Note-2006-002-SRF	P.Michelato	INFN-Mi
12	5.2.1.2.3	Design report	Electrode design fixed	31.03.06			A.Matheisen	DESY
13	**5.2.1.3.5**	**Final Report (D)**	**Process parameters fixed**	**31.03.06**	1.5.06		A.Matheisen	DESY
14	**3.1.3.5**	**Final Report (D)**	**Spinning parameters defined**	**18.05.06**			E.Palmieri	INFN-Lnl

2.) Publications

CARE-publication	Title	Authors	Journal/Conf.
	Magnetic Filters in UHV Arc-Discharges: Constructions, Field Modelling and Tests of Efficiency	P. Strzyżewski, J. Langner, R. Mirowski, M.J. Sadowski, S. Tazzari and J. Witkowski	Physica Scripta T123 (2006) 135-139
	Behaviour Of Gas Conditions During Vacuum Arc Discharges Used For Deposition Of Thin Films	P. Strzyzewski, L. Catani, A. Cianchi, J. Langner, J. Lorkiewicz, R. Mirowski, R. Russo, M. Sadowski, S. Tazzari and J. Witkowski	AIP CP 812 (2006) 485-488
	RRR of copper coating and low temperature electrical resistivity of materials for TTF couplers	M. Fouaidy, N. Hammoudi, IPNOrsay, France	PHYSICA C

CARE-Conf			
	Smart materials based system operated at 2K used at superconducting cavity tuner for VUV-FEL purpose	P. Sekalski, A. Napieralski, S. Simrock, C. Albrecht, L. Lilje, P. Bosland, M. Fouaidy, N. Hammoudi, A. Bosotti, R. Paparella	ACTUATORS 2006
	Low temperature properties of piezoelectric actuators used in SRF cavities cold tuning systems	G. Martinet, M. Fouaidy, N. Hammoudi, A. Olivier, F. Chatelet, S. Blivet, H. Saugnac IPNOrsay, France	EPAC 2006
	Electromechanical characterization of piezoelectric actuators subjected to a variable preloading force at cryogenic temperature	M. Fouaidy, M. Saki, N. Hammoudi, L. Simonet, IPN Orsay, France	EPAC2006
	Low temperature electromechanical and dynamic properties of piezostacks for superconducting RF cavities fast tuners	Fouaidy M., Martinet G., Hammoudi N., IPNOrsay, France	CRYOPRAGUE 2006
	Electromechanical System for Lorentz Force Compensation	P. Sekalski, A.Napieralski, S. Simrock	NSTI Nanotech 2006 (paper submitted)
	Automatic, resonant excitation based, system for Lorentz Force compensation for VUV-FEL	P. Sekalski, A.Napieralski, S. Simrock	EPAC 2006 (abstract submitted)

CARE-Note			
	Reports about new design for components: Cold Flanges	P. Michelato, L. Monaco, N. Panzeri	CARE-Note-2006-002-SRF
	Integration of piezoelectric actuators in the piezotuner developed at Saclay	M. Fouaidy, N. Hammoudi, G. Martinet, IPNOrsay, France, G. Devanz, P. Bosland, E. Jacques, Sylvie Regnaud, CEA Saclay, France	
	Electromechanical characterization of piezoelectric actuators subjected to a variable preloading force at cryogenic temperature	M. Fouaidy, M. Saki, N. Hammoudi, L. Simonet.	CARE-Note-2006-006-SRF

3.) List of talks

Subject	Speaker/Lab	Event	Date	Web site
Development of adaptive feed forward algorithm for Lorentz force compensation for VUV-FEL ACC1 cav5 purpose	P. Sekalski, DMCS-TUL	IEEE-SPIE Symposium	20. Jan 06	
Low temperature electromechanical and dynamic properties of piezostacks for superconducting RF cavities fast tuners	M. Fouaidy, IPN Orsay	CRYOPRAGUE 2006	17-21 July, 2006	

4.) Meetings / Workshops

Date	Title/Subject	Location	Number of attendees	Web-site address
20-21 Jan 2006	IEEE-SPIE ELHEP-ISE XVII SYMPOSIUM 2006	Warsaw, Poland	40	http://wilga.ise.pw.edu.pl/20061/downloads/program/program.htm
March 28-31, 2006	CARE-JRA1-WP4 (Thin film production) Collaboration Meeting	INFN, Tor Vergata University, Rome	8	None
May 11, 2006	Parameters of electropolishing / coordination of work task 5.1/5.2	DESY	4	None
June	EPAC	Edinburgh		http://epac06.org/
August	LINAC	Knoxville		http://www.sns.gov/linac06/

5.) Status of activities

Workpackage 2: Improved standard cavity fabrication

• Task 2.1 Reliability Analysis

The activity relative to the reliability analysis will be summarized in a dedicated paper and poster presentation at the 2006 EPAC. The abstract is entitled: "Performance Limitations of TTF Cavities in Accelerator Operation and their Relation to the Assembly Process".

N°	Task Name	Anfang	Ende	2006												2007							
				01	02	03	04	05	06	07	08	09	10	11	12	01	02	03	04	05	06	07	08
2.1	**Reliability Analysis**	**Do 01.01.04**	**Sa 31.12.05**																				
2.1.1	Review of data bank: cavity fabrication	Do 01.01.04	Fr 13.02.04																				
2.1.2	Review of data bank :cavity treatment	Mo 16.02.04	Di 30.03.04																				
2.1.3	Review of data bank: cavity VT performance	Mi 31.03.04	Do 13.05.04																				
2.1.4	Review of data bank: string assembly	Fr 14.05.04	Do 05.08.04																				
2.1.5	Review of data bank: string performance	Fr 06.08.04	Do 28.10.04																				
2.1.6	Establish correlations	Fr 29.10.04	Do 10.02.05																				
2.1.7	**Final report on reliability issue**	Sa 31.12.05	Sa 31.12.05	**31.12.**																			

• Task 2.2 Improved Component Design

During this period, the activity has been focalized on three different items:

- cold flanges experimental tests and analysis
- stiffening studies (end dish shape, etc.)
- e-beam welding.

Cold flanges experimental tests and analysis

The activity on cold flanges has continued both realizing new experimental measurements and FEM analysis.

As discussed in the "*Report about new design for components: Cold Flanges*" (CARE-Note-2006-002-SRF), our activity related to the analysis of cavity ancillary components has been mainly focused on the study of the cold connection flanges.

The new activity has been dedicated to an in-deep study of the seal mechanism, measuring the flattening of several gaskets due to the applied load. With these new data, we have obtained the information relative to the pressure needed to obtain the seal tightening for both gasket families we have studied (Al5754 and Al6060 alloys).

Furthermore, experimental tests on the beam line flange connection are in progress to evaluate its behavior when subjected to several thermal cycles, from room temperature to LN2 and back, in order to evaluate long term and fatigue problems. The experimental set-up is ready and the measurement has been just started.

As presented in the CARE-Note-2006-002-SRF a FE model for the analysis of beam line connection flanges has been developed and its results were compared with the obtained experimental data. Due to the lack of material characteristics information the analysis were performed only for the Al5754 gaskets. In the meantime, we were able to obtain the mechanical

characteristic of the Al6060 material by means of experimental tensile tests, allowing us to complete our numerical analysis for both gasket families.

Stiffening studies (end dish shape, etc.)

The TESLA cavity is equipped with two end dishes having conical shape and a thickness of 5 mm. No stiffening webs are used, but the end dishes are connected to the cavity by means of two ad-hoc shaped rings. At the helium tank side, two different solutions have been adopted. In proximity of the Saclay tuner, the end dish is connected to the tank by means of a bellow: therefore, in this region the tuner itself assures the structural continuity between the cavity and the helium tank. At the other side, additional rings allow the length accommodation between the cavity and the helium tank during the assembly.
In order to accomplish with the cavity requirements for ILC, a coaxial tuner may be used allowing, furthermore, the shortening of cavity total length. In this case, the helium tank must be modified and a first solution has been proposed for the test of the piezo blade tuner (see fig.1). This configuration has been chosen because of the minor modifications that have to be made, with respect to the present tank design. The drawback of this choice is the compliance of both the end dishes and of the connecting rings that noticeably reduce the effectiveness of the tuner device.
In order to achieve better results a different geometry has to be adopted. The solutions that we are investigating are similar to the ones we have chosen for the 700 MHz proton cavities, (see fig. 2). This choice allows obtaining a higher stiffness saving at the same time the possibility to accommodate the helium tank length with the total length of the cavity during the final assembly.
Task 2.2.1.14 finishing has been delayed to the end of July 2006, due to the increased effort needed for the system stiffness optimisation and in the 2.2.1.11-14 tasks.

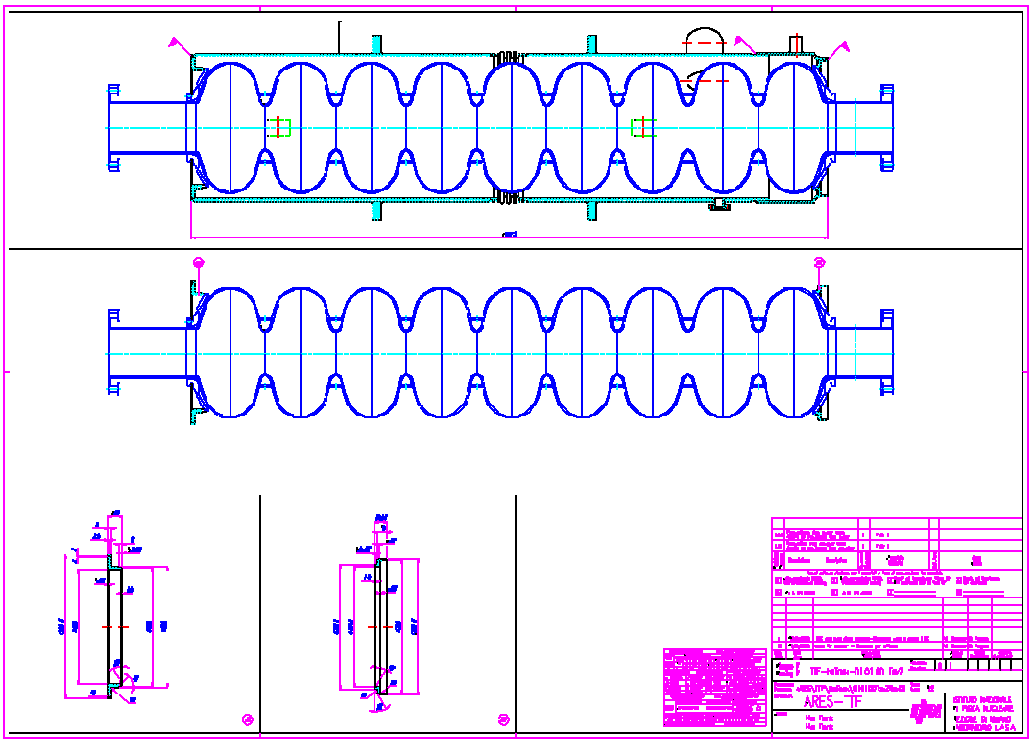

Fig. 1: Present configuration of helium tank and end dishes connections to be used for the piezo blade tuner test

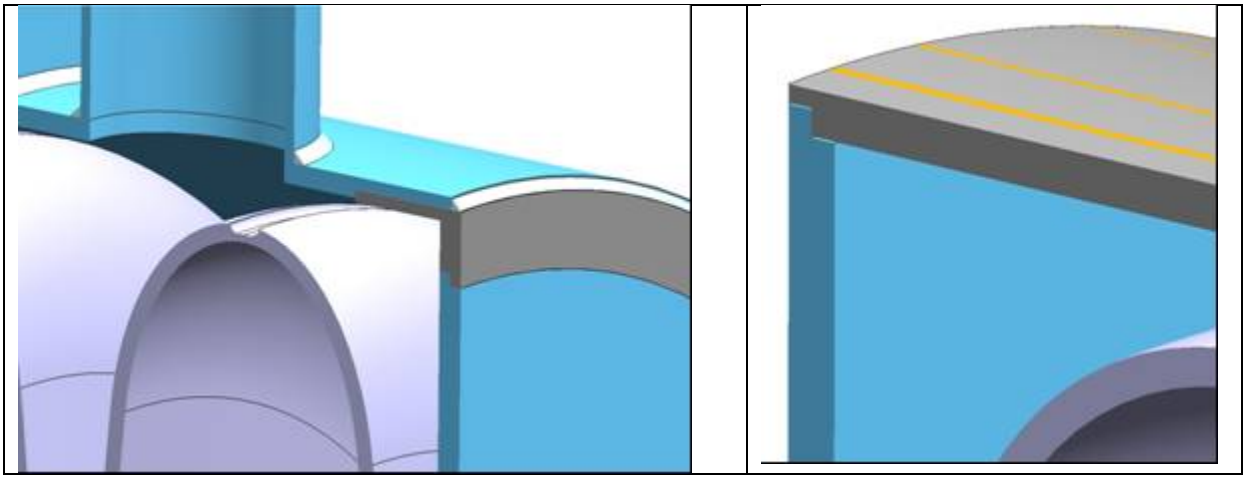

Fig. 2: Particular of proposed helium tank – end dish stiffer connections

Review of criticality in welding procedure

We have started this task, looking on the market of e-beam welding machine and we will soon start collecting information about their main parameters as electron energy, beam current, vacuum quality, pump down time, etc.

We are also critically analysing the possibility to e beam weld different materials (e.g. Nb to SS) using special metal interlayer

Update of MS-Project

N°	Task Name	Anfang	Ende
2.2	**Improved component design**	**Do 01.01.04**	**Do 11.09.08**
2.2.1	**Documentation retrieving**	**Do 01.01.04**	**Mo 31.07.06**
2.2.1.1	Start up meetings	Do 01.01.04	Mo 09.02.04
2.2.1.2	Access and study of Jlab, DESY, LLAN, KEK experience	Do 01.01.04	Mi 13.10.04
2.2.1.3	**Summary report on the status of the art on ancillaries**	Mi 13.10.04	Mi 13.10.04
2.2.1.4	Sealing material and shape design	Mi 13.10.04	Fr 29.07.05
2.2.1.5	Flange preliminary design	Mo 10.01.05	Fr 24.06.05
2.2.1.6	Material and geometric compatibility	Mo 27.06.05	Fr 02.09.05
2.2.1.7	Final assembly design	Do 14.10.04	Fr 09.09.05
2.2.1.8	End plate preliminary design	Do 14.10.04	Fr 09.09.05
2.2.1.9	**Report about new design for components**	Fr 16.09.05	Fr 16.09.05
2.2.1.10	Stiffness optimization	Do 14.10.04	Fr 10.02.06
2.2.1.11	Manufacturing procedure analysis	Mo 03.01.05	Fr 22.07.05
2.2.1.12	Final assembly design	Mo 05.09.05	Fr 17.02.06
2.2.1.13	Other ancillaries design	Do 14.10.04	Fr 24.02.06
2.2.1.14	**Final Report for new components**	Mo 31.07.06	Mo 31.07.06
2.2.2	**Review of criticality in welding procedures**	**Do 01.01.04**	**Fr 11.08.06**
2.2.2.1	Review of available parameters on vendor welding machine	Do 01.01.04	Fr 21.10.05
2.2.2.2	Definition of prototype requirements for tests	Mi 13.10.04	Mo 11.07.05
2.2.2.3	Welding test on specimens	Mo 24.10.05	Fr 24.02.06
2.2.2.4	Analysis of the results	Fr 29.07.05	Fr 11.08.06
2.2.2.5	**Report about welding parameters**	Fr 11.08.06	Fr 11.08.06
2.2.3	**Finalize new component design**	**Mo 14.08.06**	**Mo 30.07.07**
2.2.3.1	Do drawings	Mo 14.08.06	Mo 30.07.07
2.2.3.2	**New components design finished**	Mo 30.07.07	Mo 30.07.07
2.2.4	**Finalize new cavity design**	**Mo 14.08.06**	**Do 14.06.07**
2.2.4.1	Make drawings	Mo 14.08.06	Do 14.06.07
2.2.4.2	**New cavity design finished**	Do 14.06.07	Do 14.06.07
2.2.5	**Fabrication of new cavity**	**Mo 30.07.07**	**Do 11.09.08**
2.2.5.1	Fabrication	Mo 30.07.07	Do 11.09.08
2.2.5.2	New cavity finished	Do 11.09.08	Do 11.09.08

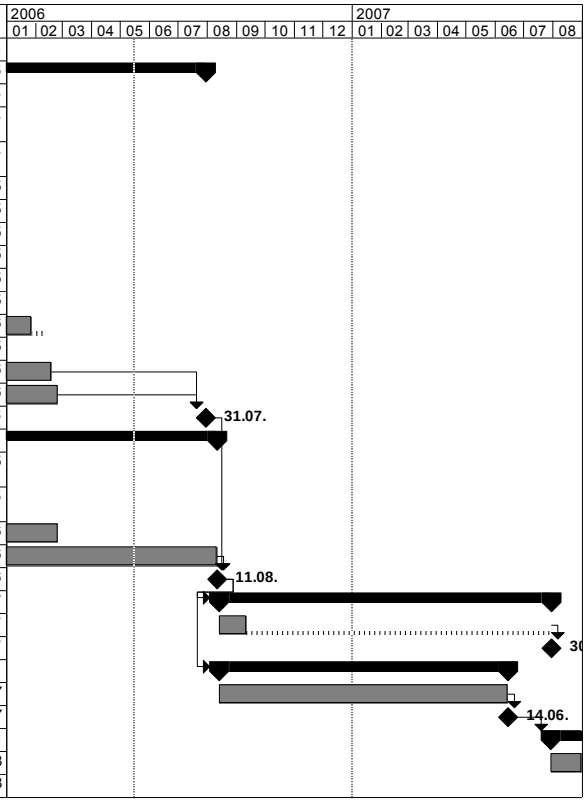

- **Task 2.3 EB welding**

In a three weeks shut down of the electro beam-welding machine, we demounted the old mechanical rotation drive and installed the new stage and box for the uhv-motor.

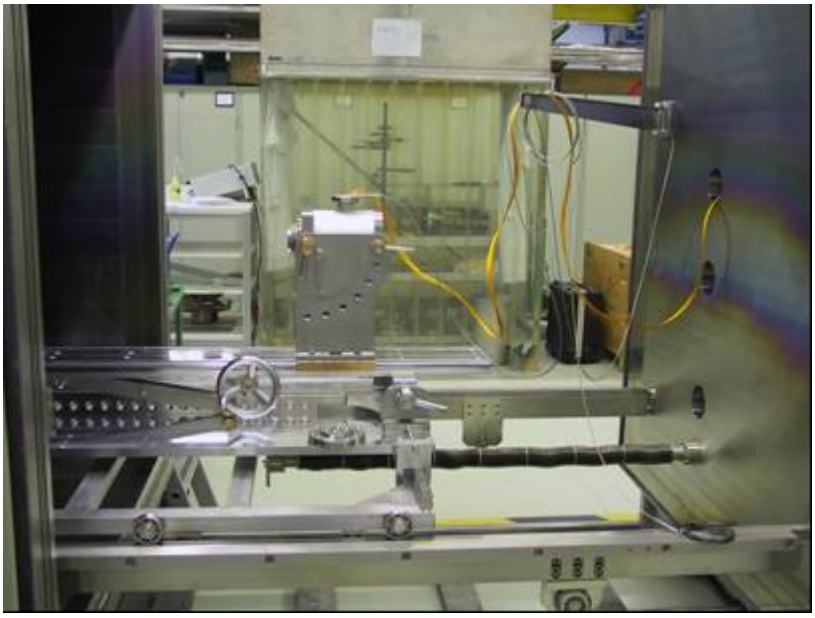

Figure 1: motor box and current supply with Kapton© isolation

With the new support and rotation drive changing the working angle of the motor or the stage is possible.

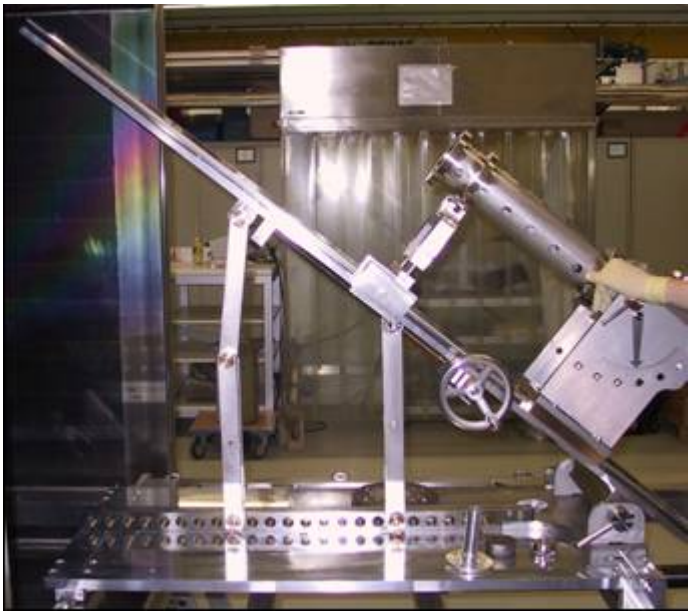

Figure 2: stage in a 38° angle

The installation of the motion-drive for the y-axis is prepared. The completion will take place next month.

Figure 3: full-enclosed y-drive with ball screw

Already the uhv-motor for the rotation drive is working successfully. Now we are welding for the single-cell-programme.

Update of MS-Project

N°	Task Name	Anfang	Ende
2.3	**EB welding**	**Do 01.01.04**	**Fr 04.01.08**
2.3.1	**Design tooling**	**Do 01.01.04**	**Mi 15.12.04**
2.3.1.1	Tools for flange welding	Do 01.01.04	Fr 20.02.04
2.3.1.2	Tools for pipe welding	Mo 23.02.04	Di 13.04.04
2.3.1.3	Tools for stiffening rings	Mi 14.04.04	Do 03.06.04
2.3.1.4	Tools for single cell welding	Fr 04.06.04	Mo 23.08.04
2.3.1.5	Tools for 9-cells	Di 24.08.04	Mi 15.12.04
2.3.1.6	**Tools design finished**	Mi 15.12.04	Mi 15.12.04
2.3.2	**Tools production**	**Mo 23.02.04**	**Fr 11.03.05**
2.3.2.1	Tools for flange welding	Mo 23.02.04	Di 30.03.04
2.3.2.2	Tools for pipe welding	Mi 14.04.04	Do 13.05.04
2.3.2.3	Tools for stiffening rings	Fr 04.06.04	Do 15.07.04
2.3.2.4	Tools for single cell welding	Di 24.08.04	Mi 27.10.04
2.3.2.5	Tools for 9-cells	Do 16.12.04	Fr 11.03.05
2.3.2.6	**Tools fabrication finished**	Fr 11.03.05	Fr 11.03.05
2.3.3	**Welding**	**Do 01.01.04**	**Fr 04.01.08**
2.3.3.1	Commissioning welding machine	Do 01.01.04	Fr 16.04.04
2.3.3.2	Test welding	Mo 19.04.04	Fr 03.09.04
2.3.3.3	**Start production welding of components**	Fr 11.03.05	Fr 11.03.05
2.3.3.4	Single cell welding	Mo 14.03.05	Fr 24.11.06
2.3.3.5	Multicell welding	Mo 19.12.05	Fr 04.01.08
2.3.3.6	**Welding of prototypes of components finish**	Fr 04.01.08	Fr 04.01.08

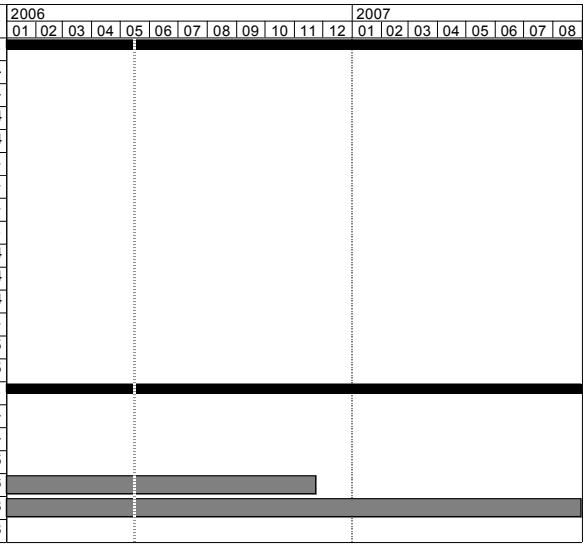

Work Package 3: Seamless Cavity Production

Task 3.1 Seamless cavity production by spinning

We have started to use the spinning machine. First test of the necking by the new machine have been proved to be satisfactory, nevertheless they need further investigation. The grat advantage of the new procedure is that now the necking step is automatically done during spinning. It must be kept into account indeed that before the cavity had to be disassembled from the lathe everytime we had to press the cavity in order to neck the material at the irises. In the present way fabrication times are then reduced even more. Some more investigation is needed for understanding how to find an uniform distribution of the thickness at the irises, and when fabricating last half-cell, the one close to the cut-off tubes. By means of the new machine, we have also tried the fabrication of a three cell 1,3 GHz resonator. The cavity has been then treated and also rf tested at low temperatures. The cavity has been spun from a seamless bulk Nb tube that was previously flowturned from a blank. Then the cavity was internally grinded, electropolished for 3 hours, HP-rinsed then cooled to 4,2 K. The resonator has been tried at 4,2 K, showing at that temperature a Q-factor of about 2e+08 and quenching around 2 MV/m, showing a high surface resistance, presumably due to the little grinding and little EP action. We will perform then more EP in order to improve performances.

In the meantime a new sealing configuration has been invented. Simply by spinning, the tube rim is plastically deformed in order to obtain a seamless flange (as in the attached figure). The cavity can be then easily sealed by indium wire. The great advantage is that it is an extremely low cost flange, making the EB weld unneeded. With high probability this kind of sealing would be not applicable for mass production of cavities, but it is certainly extremely useful for prototypes production.

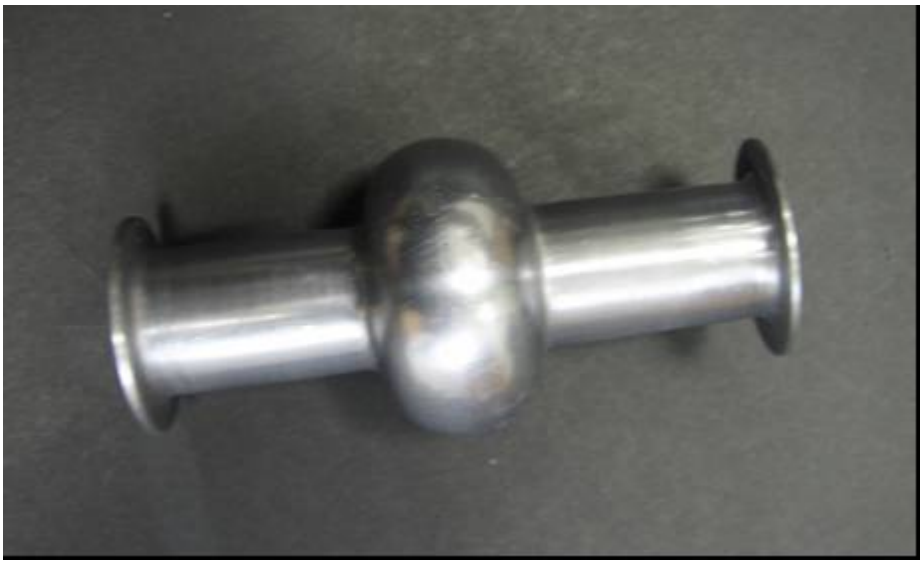

Update of MS-Project

N°	Task Name	Anfang	Ende
3.1	**Seamless by spinning**	**Do 01.01.04**	**Fr 04.01.08**
3.1.1	**Design spinning machine**	**Do 01.01.04**	**Fr 17.09.04**
3.1.1.1	Drawings of the matrices	Do 01.01.04	Fr 16.04.04
3.1.1.2	Drawings of the support system	Fr 16.04.04	Fr 17.09.04
3.1.1.3	**Drawings of spinning machine finished**	Fr 17.09.04	Fr 17.09.04
3.1.2	**Fabrication of spinning machine**	**Mo 20.09.04**	**Do 10.11.05**
3.1.2.1	Fabrication of machine parts	Mo 20.09.04	Fr 29.04.05
3.1.2.2	Software for the machine	Mo 20.09.04	Do 31.03.05
3.1.2.3	Assembly of machine	Fr 01.04.05	Fr 29.07.05
3.1.2.4	Commissioning of the machine	Mo 01.08.05	Do 10.11.05
3.1.2.5	**Spinning machine ready**	Do 10.11.05	Do 10.11.05
3.1.3	**Evaluation of spinning parameters**	**Mo 03.01.05**	**Do 18.05.06**
3.1.3.1	Drawings of the support system and turning mechanism	Mo 14.11.05	Do 26.01.06
3.1.3.2	Drawings of the necking mechanism	Mo 03.01.05	Fr 26.08.05
3.1.3.3	Fabrication of the tube necking machine	Fr 27.01.06	Do 23.03.06
3.1.3.4	Commissioning of the machine	Fr 24.03.06	Do 18.05.06
3.1.3.5	**Spinning parameters defined**	Do 18.05.06	Do 18.05.06
3.1.4	**Spinning of 1-celll cavities**	**Fr 19.05.06**	**Do 07.12.06**
3.1.4.1	Material and fabrication of bulk Nb test tubes	Fr 19.05.06	Do 07.09.06
3.1.4.2	Material and fabrication of bimetallic NbCu test tubes	Fr 08.09.06	Do 07.12.06
3.1.4.3	**1-cell spinning parameters defined**	Do 07.12.06	Do 07.12.06
3.1.5	**Extension of spinning apparatus to multicells**	**Fr 08.12.06**	**Do 11.01.07**
3.1.5.1	Computer simulation of the necking	Fr 08.12.06	Do 11.01.07
3.1.5.2	**Start of Multi-cell spinning**	Do 11.01.07	Do 11.01.07
3.1.6	**Spinning of multi-cell cavities cavities**	**Fr 12.01.07**	**Do 02.08.07**
3.1.6.1	Computer simulation of the spinning	Fr 12.01.07	Do 02.08.07
3.1.6.2	Spinning of bulk Nb 9-cell cavities	Fr 12.01.07	Do 12.07.07
3.1.6.3	**Parameters of multi-cell spinning defined**	Do 12.07.07	Do 12.07.07
3.1.7	**Series production of multi-cell cavities**	**Fr 13.07.07**	**Fr 04.01.08**
3.1.7.1	Spinning	Fr 13.07.07	Fr 04.01.08
3.1.7.2	**Multi-cell cavities finished**	Fr 04.01.08	Fr 04.01.08

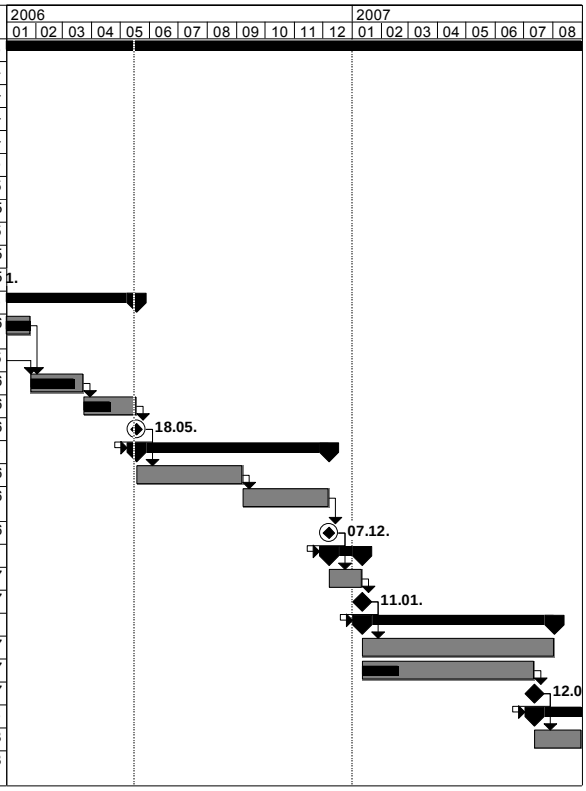

Task 3.2 Seamless by hydroforming

Numerical simulation of necking process

The numerical simulation was done in the finite element code ANSYS. The real geometry of the tubes after end reduction was taken into account.
Results of comparison of wall thickness after the first stage are shown in the Fig. 1. The comparison was made for Cu tubes with markers Rohr8 - Rohr13. For comparison the tube thicknesses were normalized to 4mm.

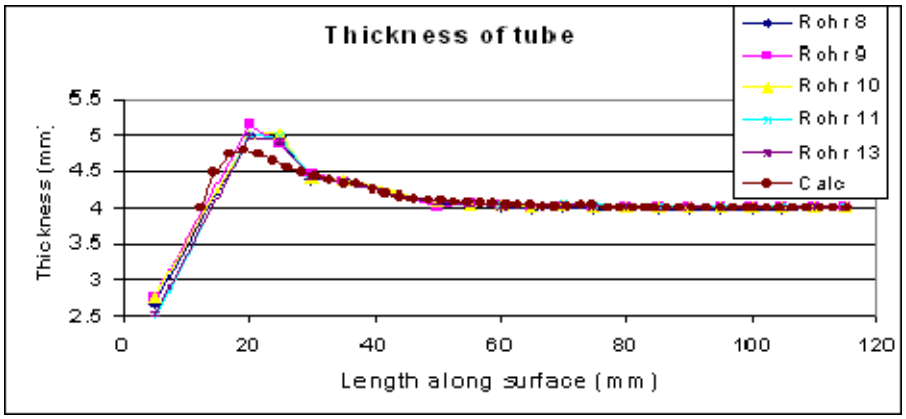

Fig. 1. Comparison of simulated and experimental wall thicknesses after necking.

The thickness of wall, obtained from simulation describes the experiment. The thickening of the tubes in the iris region is in accordance with dimension measurements of tubes with reduced ends.

Numerical simulation of hydroforming process

During the simulation of hydroforming process the tube form and stress distribution after necking was taken into account.
The applied loads (pressure and displacement) were used from real experiment on Rohr13. The results are compared in Fig. 2. The agreement with experimental data is acceptable.

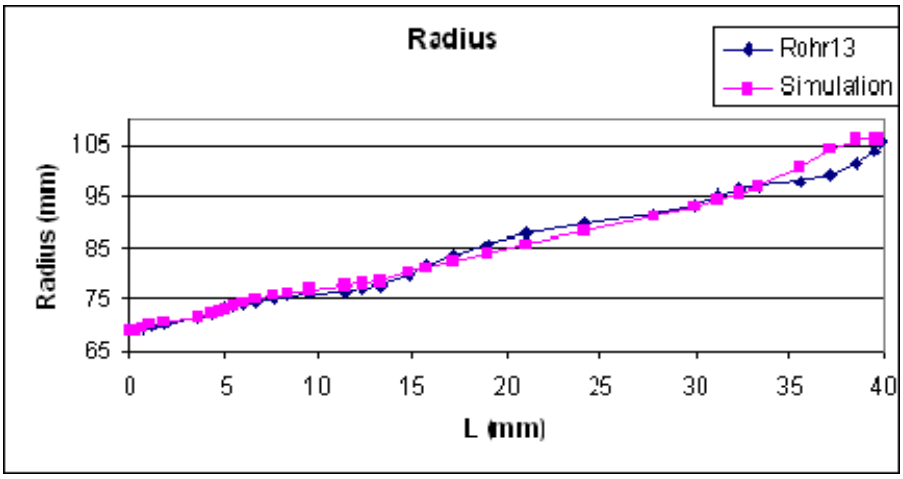

Fig. 2. Simulation of radius growth during hydroforming in comparison with experiment

Experiments on the tube necking at the iris

A lot of necking experiments was done on the copper tubes in order to optimize the necking parameters. Combination of radial and axial movements allows ensure a uniform circumferential wall thickness at the iris area without remarkable reduction of the wall thickness. The first necking of the niobium tube was successful both at tubes ends as well as in the tube irises. One example of the necking can be seen in Fig. 3

Fig. 3: Example of the Nb tube necking

Three 3-cell cell bulk Nb cavities have been fabricated without intermediate annealing from seamless tubes of dimensions: ID 150mm, wall thickness 3 mm. Intermediate constraint has the diameter of 182 mm (see Fig. 4).

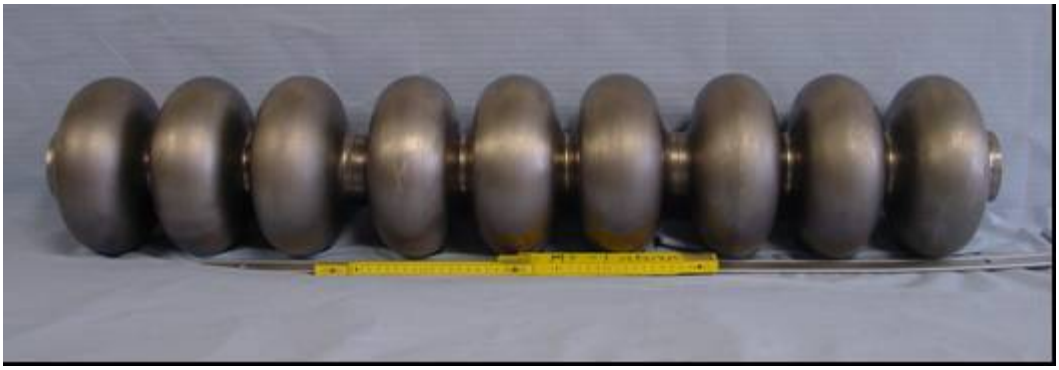

Fig. 4: Hydroformed three cells

Status of money spending

	Spent money	Value of new orders/ contracts	Expected spending of new orders/contracts until end 2006	Sum of column 2 & 4
Travel				
Consumables	*2500*	*2500*	*30000*	*32500*
Manpower	*9090*		*35000*	*44000*
Durable				
			Total sum	*76500*

Update of MS-Project

N°	Task Name	Anfang	Ende
3.2	**Seamless by hydroforming**	**Do 01.01.04**	**Fr 16.11.07**
3.2.1	**Design hydro forming machine**	**Do 01.01.04**	**Fr 17.09.04**
3.2.1.1	Drawings of the matrices	Do 01.01.04	Fr 17.09.04
3.2.1.2	Drawings of the support system	Do 01.01.04	Fr 17.09.04
3.2.1.3	**Drawings matrix & support finished**	Fr 17.09.04	Fr 17.09.04
3.2.2	**Construction of hydro forming machine**	**Do 01.01.04**	**Fr 01.07.05**
3.2.2.1	Hydraulic for machine	Do 01.01.04	Mi 14.07.04
3.2.2.2	Software for the machine	Mo 23.02.04	Fr 17.09.04
3.2.2.3	Machine fabrication	Mo 20.09.04	Mo 21.03.05
3.2.2.4	Commissioning of the machine	Di 22.03.05	Fr 01.07.05
3.2.2.5	**Hydro forming machine ready**	Fr 01.07.05	Fr 01.07.05
3.2.3	**Construction of tube necking machine**	**Do 01.01.04**	**Do 24.02.05**
3.2.3.1	Drawings of the support system and turning mechanism	Do 01.01.04	Fr 27.08.04
3.2.3.2	Drawings of the necking mechanism	Do 01.01.04	Fr 27.08.04
3.2.3.3	Fabrication of the tube necking machine	Do 23.09.04	Do 24.02.05
3.2.3.4	Software for the tube necking machine	Mo 03.05.04	Do 30.12.04
3.2.3.5	**Construction tube necking machine finishec**	Do 24.02.05	Do 24.02.05
3.2.4	**Development of seamless tubes for 9-cell cavitie**	**Do 01.01.04**	**Fr 01.07.05**
3.2.4.1	Material and fabrication of bulk Nb test tubes	Di 03.08.04	Fr 01.07.05
3.2.4.2	Material and fabrication of bimetallic NbCu test tubes	Do 01.01.04	Fr 01.07.05
3.2.4.3	**Seamless tubes ready**	Fr 01.07.05	Fr 01.07.05
3.2.5	**Development of tube necking**	**Mi 01.06.05**	**Fr 15.12.06**
3.2.5.1	Computer simulation of the necking	Mi 01.06.05	Fr 30.06.06
3.2.5.2	Experiments on tube necking at iris	Mo 02.01.06	Fr 15.12.06
3.2.5.3	**Tube necking machine operational**	Fr 15.12.06	Fr 15.12.06
3.2.6	**Hydro forming of seamless cavities**	**Mo 27.06.05**	**Fr 16.11.07**
3.2.6.1	Computer simulation of the hydro forming	Mo 27.06.05	Fr 24.11.06
3.2.6.2	Hydro forming of bulk Nb 9-cell cavities	Mo 18.12.06	Fr 16.11.07
3.2.6.3	**Hydro formed 9-cell cavities ready**	Fr 16.11.07	Fr 16.11.07

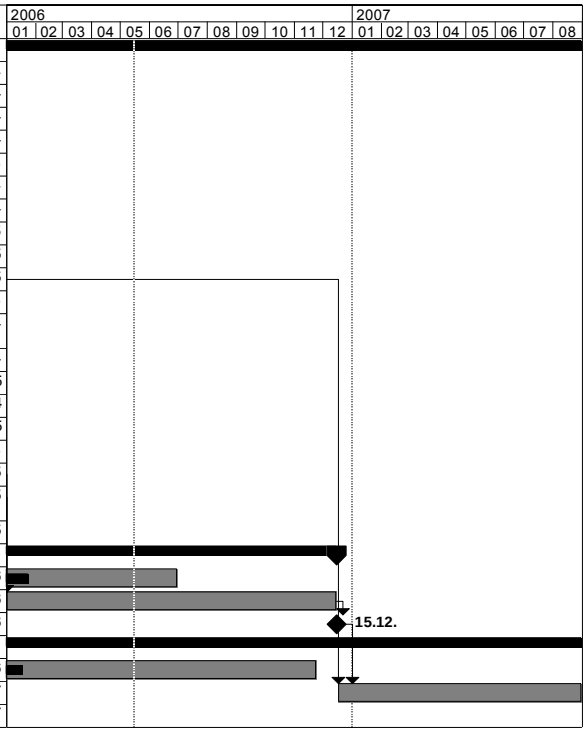

Work package 4: Thin film cavity production

4.1 Linear cathode coating

Design and construction of a micro-droplet filter

The first version of a magnetic filter was constructed in 2005 (see 2nd Quarter Report 2005). Unfortunately, its operational features determined during several experimental tests appeared to be not sufficient ones. Moreover, its geometrical dimensions were too large for the final application. Therefore, it was decided to design and manufacture two modified versions of the magnetic filter. The first version was based on the concept of the prototype filter, which used a concentric set of water-cooled Cu-tubes, but important modifications concerned smaller geometrical dimensions and better thermal stability. That version was given for the final manufacturing to an external company, which has just been postponed the delivery until June 30, 2006. The second version was in fact not a magnetic filter, but a Venetian-type blind system, which has been adapted to the cylindrical configuration. This version has just been manufactured, as shown in Fig. 1.

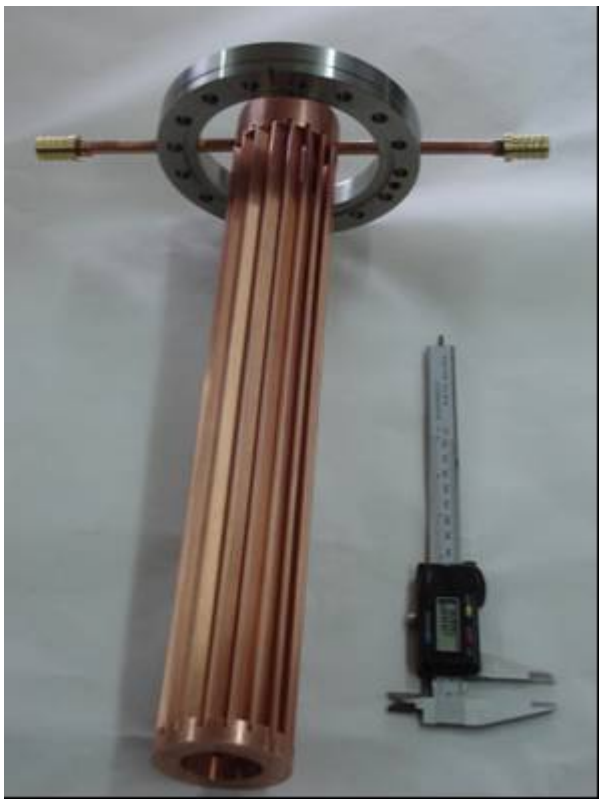

Fig. 1. General view of the cylindrical Venetian-type micro-droplet filter.

A new design of the cylindrical (linear) cathode

Experimental tests of the first prototype magnetic filter, which were performed within an auxiliary high-vacuum stand, showed that its design enables the arc discharge (between the cathode and magnetic filter walls) to be initiated. A relatively long and stable operation of the filter was possible due to the effective water-cooling system (see 2nd Quarter Report 2005). The first results of the micro-droplets filtering, as performed with the described prototype, were promising. Unfortunately, because of relatively large dimensions of the assembled prototype, it was impossible to install it within our main UHV-arc facility. The most important dimension was a smaller diameter of a TESLA-type cavity than that of the used vacuum chamber. Therefore, it appeared necessary to design new constructions of the magnetic filter as well as the cathode system.

The dimensions of the filter and cathode depend of course on the diameter of the cathode tube. The pure niobium tube, which was used for the cylindrical (linear) cathode manufacturing, had about 32 mm in diameter. Taking into account requirements connected with the micro-droplet filter, a 32-mm-dia. cathode cannot be applied within TESLA cavity for the final deposition processes. Therefore, it was decided to reduce the cathode diameter. Two new pure-niobium tubes were ordered at the Tokyodenkai Co. Their dimensions were chosen as follows: outer diameter equal to 24 mm, and wall of 3 mm in thickness. The first tube of about 50 cm in length will be used in the main UHV-arc facility for coating a single RF cavity, and the second tube of about 120 cm in length will be designed for future experiments with a triple-cavity structure. A scheme of the new cathode structure, showing the connections of the niobium tube with the other parts of the UHV facility, is presented in Fig.2.

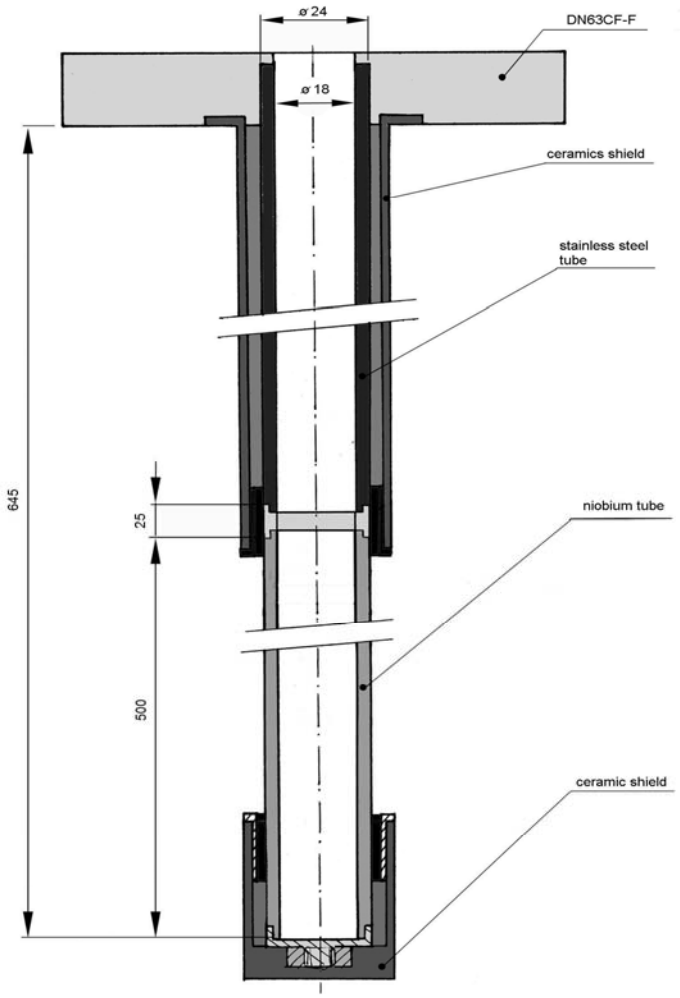

Fig. 2. Sketch of a new cathode design.

The new niobium cathode is currently being prepared for the final assembling together with the subsequent application of two different micro-droplet filters (1^0 - made of copper tubes with magnetic ion channels, and 2^0 - the so-called Venetian blind system) within the main UHV linear-arc facility.

Nb thin film characterization

In order to characterize the Nb films two subsequent deposition processes under the UHV conditions were performed. The basic pressure in both cases was below $5 \cdot 10^{-10}$ Torr. The described depositions were performed upon one side-polished sapphire substrates of surface dimensions equal to 10 mm x 10 mm. Differences relied only on the arc discharge currents, respectively 55A (sample 1) and 80A (sample 2). The samples were mounted to the inner surface of cavity-like vacuum chamber, at a distance of about 9 cm from the niobium cathode. Since the substrates were mounted upon the grounded anode, no additional bias was applied. The both depositions were performed under extremely clean conditions at very low pressure. Before the

deposition processes all the substrates were cleaned carefully within an ultrasonic bath. After their placement within the UHV-arc facility the residual gas composition was checked by means of a mass spectrometer (before, during and after each process).

The samples were characterized by means of the Time-of-Flight Secondary Ion Mass Spectrometry (TOF-SIMS), RRR measurements and micro-droplets distribution analyses. Another analyzes of the deposited layers, like the Atomic Force Microscope (AFM) and Glow Discharge – Optical Emission Spectroscopy (GD-OES) will also be performed in the near future.

ToF-SIMS measurements of deposited samples

Information about the surface chemical composition and depth profile were obtained by means of a time-of-flight (ToF)-SIMS mass spectrometer, delivered by the Ion-ToF GmbH, Muenster, Germany. The instrument was equipped with an O_2+ primary-ion gun and high mass resolution time-of-flight mass analyzer. During an analysis the sample surface was irradiated with pulses of 1 keV ions, and an average ion current amounted to 40 nA. Secondary ions emitted from the bombarded surface were mass-separated and counted with the ToF analyzer. Results of some measurements are presented in Figs 3a and 3b.

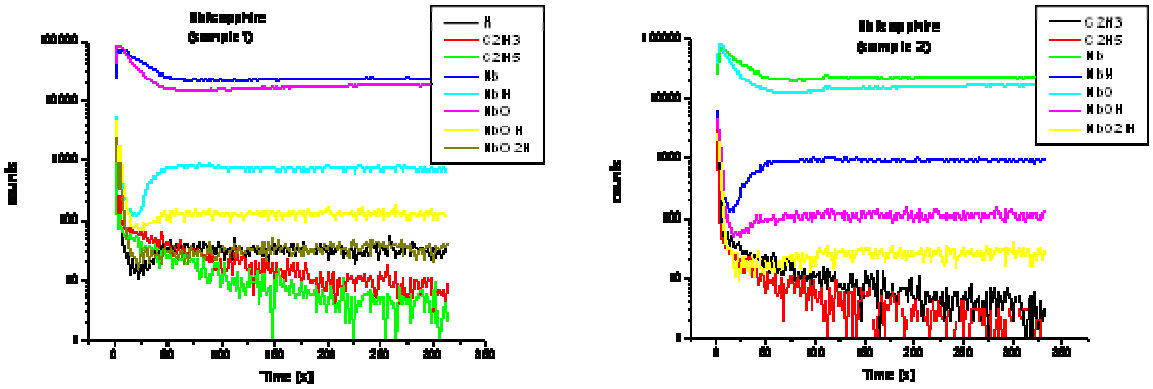

Fig. 3. Results of the SIMS measurements.

One can easily see that the deposited Nb-layers were clean enough. Chemical compositions of both samples appeared to be similar ones, and the deposited layers consisted mainly of Nb, NbO, NbH and NbOH species. The presence of some impurities (like Cs, Na and K) has also been confirmed, but their levels were very low (not shown here). Unfortunately, it was impossible to check the contamination by oxygen, due to the use of ions of this element for the surface bombardment, but in next step the SIMS measurements will be performed with the use of non-reactive gas ions (like Ar- or Kr-species).

RRR measurements of the samples

Residual Resistivity Ratio (RRR) parameters of the Nb-layers were measured at the Tor Vergata University, Rome. Unfortunately, in spite of very clean conditions during depositions, results of the RRR measurements appeared to be unsatisfactory (in range of 3-4). One of the

explanations is the deposition of many micro-droplets upon the investigated Nb- surfaces. They could increase the surface roughness. Moreover, SEM pictures (presented in the previous report) showed that many micro-droplets are surrounded by small gaps (in relation to the Nb layer). A large number of such gaps could cause higher surface resistance. Therefore, it was decided to repeat the RRR measurements at another laboratory in order to confirm the obtained results and to investigate an influence of the micro-droplets on the RRR value upon other samples.

Measurements of micro-droplets distributions

Surface distributions of micro-droplets (upon the samples prepared at IPJ Swierk) were measured by our colleagues at the Tor Vergata University, Rome. Some results are presented in Fig. 4.

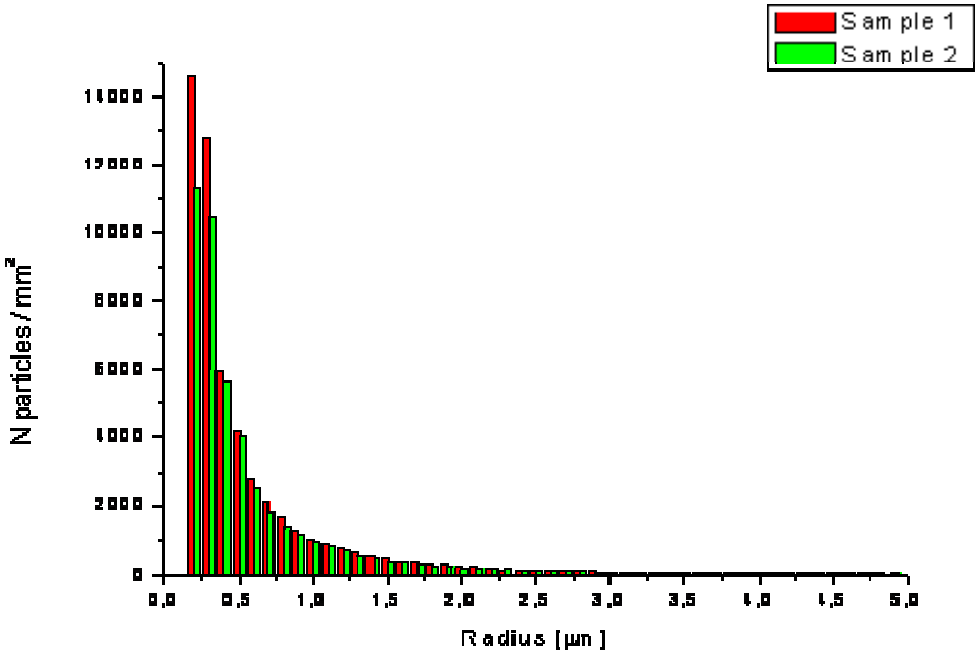

Fig. 4. Statistics of the micro-droplets deposited upon surfaces of two samples coated at IPJ in Swierk and analyzed at Tor Vergata University in Rome.

A new Keying Module for cavity biasing

During the previous year the both teams involved in the WP4 task, i.e. laboratories in Swierk and Rome, decided to switch from the DC operation and/or the sample bias to a pulsed bias of the kHz range. Such a solution should improve a quality of the coated layers and make possible to control a substrate temperature during the deposition process. In order to fulfil the above requirements, a new U.I.P. Keying Module was designed and constructed at IPJ, Swierk, as shown in Fig. 5. At the moment, this module is tested at the Tor Vergata laboratory in Rome.

The U.I.P. Keying Module was designed especially to power different vacuum chambers, which are used in laboratories and industry for PVD processes applied in surface treatment

technologies. The power electronics was based on the switched mode technology, which ensures the low audio-noise generation, high efficiency, low output current and small dimensions and weight.

The U.I.P. Keying Module can transform a DC input signal into the pulse output signal. Its frequency, shape and filling factor can be varied according to requirements of the keying signal needed for the coating facility.

Fig. 5. General view of the U.I.P Keying Module used for pulse biasing of RF cavities.

The main electrical and mechanical parameters of the U.I.P Keying Module were established as follows:

Mains voltage:	220 – 230 V
Mains frequency:	50 – 60 Hz
Output frequency:	0 – 100 kHz
Output voltage:	(-800) – 0 V
Output current:	0 – 5 A
Control modes:	external source of keying pulses, e.g a signal generator
Filling:	10 – 90 %
Fusing:	315 mA
Ambient operating temp.:	0 – 35^{o} C
Size (WxHxD):	135 x 220 x 300 mm
Weight:	3.5 kg
Storage temperature:	(-25) – 55 ^{o}C

The operational parameters of the U.I.P. Keying Module, e.g. the frequency, voltage and filling, are limited mainly by power transistors (Ultra Fast Speed IGBT – IRG4PH50U, made by International Rectifier). The device enables the fast switching of the output signal to be performed. The optimal operation frequency of the transistors is 40 kHz. Higher frequencies (up to 100 kHz) are achievable, but some signal degradation might be observed.

The U.I.P. Keying Module can be controlled by two independent pulse signals, formed by a signal generator or a computer (e.g. by LabView program). This module should be connected in series between the DC power supply unit and the RF cavity or substrate holder.

Updating of MS-Project

N°	Task Name	Anfang	Ende
4.1	**Linear-arc cathode coating**	**Do 01.01.04**	**Fr 26.10.07**
4.1.1	**Installation & commissioning of coating apparatu**	**Do 01.01.04**	**Di 12.12.06**
4.1.1.1	Modification of a prototype facility for single cells	Do 01.01.04	Di 14.09.04
4.1.1.2	Optimization of a triggering system	Mo 22.03.04	Mo 11.10.04
4.1.1.3	**Prototype facility ready**	Mo 11.10.04	Mo 11.10.04
4.1.1.4	Study of arc current reduction and stabilization	Mo 11.10.04	Mo 07.02.05
4.1.1.5	Optimization of pow ering system	Mo 07.02.05	Mo 14.03.05
4.1.1.6	**Coating apparatus operational**	Mo 14.03.05	Mo 14.03.05
4.1.1.7	**Coating single cells**	**Mo 14.03.05**	**Di 12.12.06**
4.1.1.7.1	Coating of single cells w ithout micro droplet filtering	Mo 14.03.05	Fr 30.06.06
4.1.1.7.2	Design and construction of a micro droplet filt	Mo 14.03.05	Fr 30.06.06
4.1.1.7.3	**Droplet filter ready**	Fr 30.06.06	Fr 30.06.06
4.1.1.7.4	Coating of single cell w ith micro droplet filterin	Mo 02.01.06	Di 12.12.06
4.1.2	**Coating multi-cell**	**Mo 03.07.06**	**Fr 26.10.07**
4.1.2.1	Design and commissioning	Mo 03.07.06	Mi 22.08.07
4.1.2.2	First multicell coating	Fr 26.10.07	Fr 26.10.07

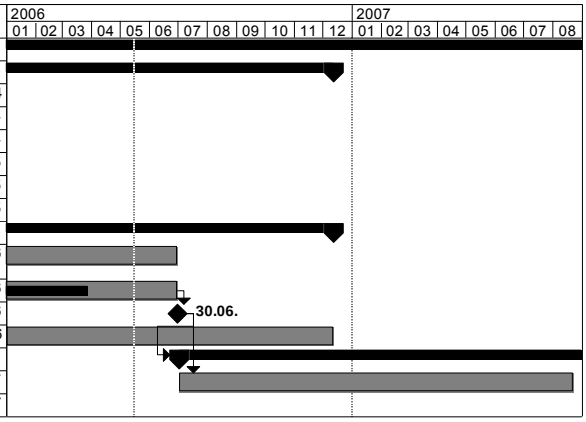

4.2 Planar-Arc Cathode Coating

Nb deposition activities on the planar arc stand

Measurements of Nb layer homogeneity have been performed in the planar arc stand at the Tor Vergata laboratory using a set of sapphire witness-samples. The deposition rate reached about 300 (+/- 20%) nm/min at a distance 35 mm off the system axis, and it proved to be reproducible one.

A series of niobium depositions has been also performed to test a dependence of super-conducting parameters and composition (of the reached surface layer) on the substrate bias and the coated surface orientation respectively the plasma propagation direction. Four sets of samples, consisting of 12 copper and 6 sapphire flat samples each, have been Nb-coated at an arc current of 110 A and the optimized magnetic field distribution, at the substrate bias values of -23 V (close to the floating potential) , -40 V (the minimum voltage to reach ion current saturation), - 60 V and –80 V. The samples have been mounted on three specially designed copper-holders, which allowed samples orientation at angles of 0^0, 30^0 , 45^0, 60^0 , 75^0 or 90^0, respectively, to the horizontal position (see Fig. 1), whereas the plasma beam in the system propagates vertically. Four of the copper samples coated at the horizontal position (0^0) at different bias are now being studied with SEM and they will undergo X-ray analysis. Four of the sapphire “horizontal” samples coated at different bias voltages are now tested for RRR and Tc.

The remaining four copper samples will undergo preparation for RRR measurements of an isolated Nb-layer after etching the copper substrate.

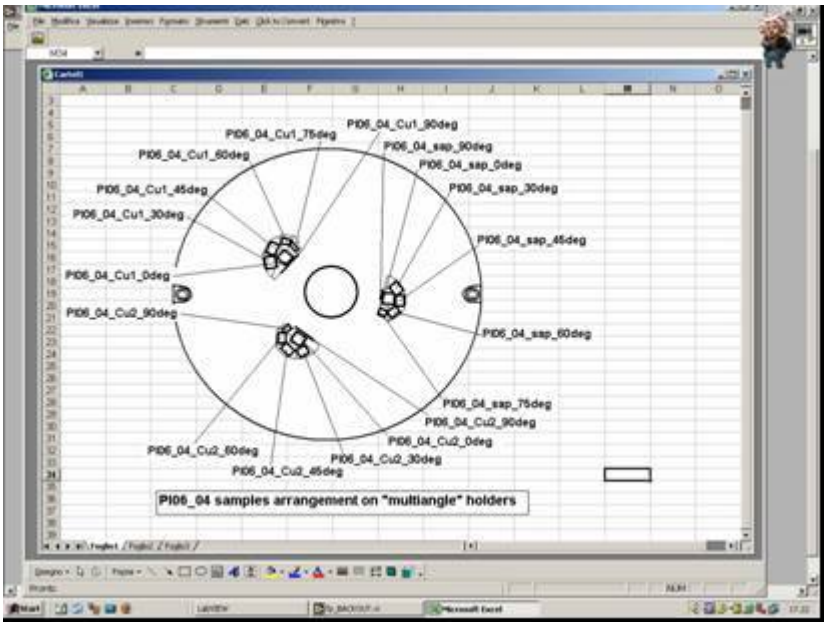

Fig. 1. Arrangement of copper- and sapphire-samples upon the "multi-angle" holders.

Nb deposition within the "old" 90^{o}-filter system

The old UHV planar arc stand, equipped with a 90^{o} magnetic filter, had been used to perform three coating procedures at the beginning of 2006.

a) The first procedure concerned coating of two modified circular copper-samples to be tested for Q-value and surface resistance dependence on magnetic RF field (courtesy of H. Padamsee). The shape of the samples has been modified, as compared with that of the samples coated in our laboratory and tested in Cornell in 2005 (see JRA1 Annual Report 2005). Surface curvature radii have significantly been increased to avoid insufficient film thickness at the corners. The estimated layer thickness, as reached on both samples, was ca. 2400 nm in the centre, and 1000 nm at a distance of 4.5 cm from the centre (at a rim of the sample). The coated samples have been sent away to the Cornell University for further tests.
b) The two subsequent procedures concerned the niobium coating of pure Nb-samples (in order to deposit Nb-layers up to 200 nm in thickness), which were prepared for measurements to be carried out at the Jefferson Laboratory (courtesy of Dr. Wu). This project is aimed at testing of the Nb-coatings as regards the field emission. Together with Nb substrates there were coated two sapphire witness samples for SEM and RRR tests.

Installation of a new T-type magnetic filter device

After the procedures described above the "old" magnetic filter was dismounted, and the magnetic structure of a new vacuum planar-arc device with a T-type magnetic filter has been assembled, as shown in Fig.2. (Fig.2).

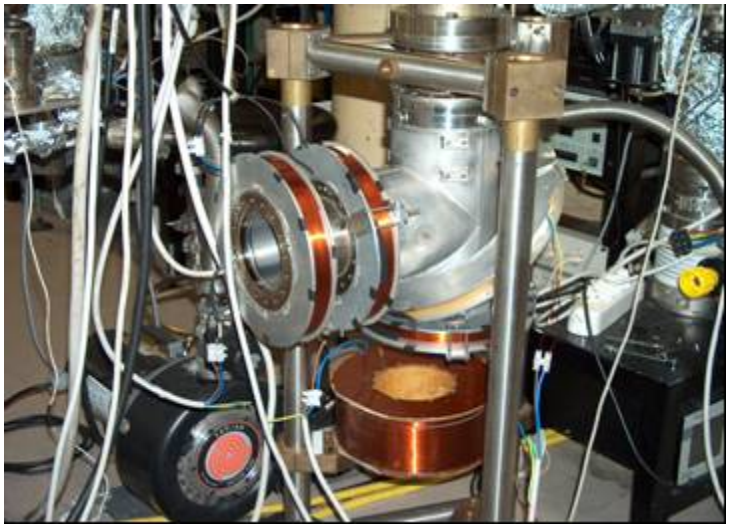

Fig. 2. The new T-filter device under assembly.

The magnetic field distribution inside the new filter was measured with appropriate probes. Simultaneously, some numerical simulations of the magnetic field distribution were performed at the A. Soltan Institute for Nuclear Studies (IPJ), as shown in Figs. 3a and 3b.

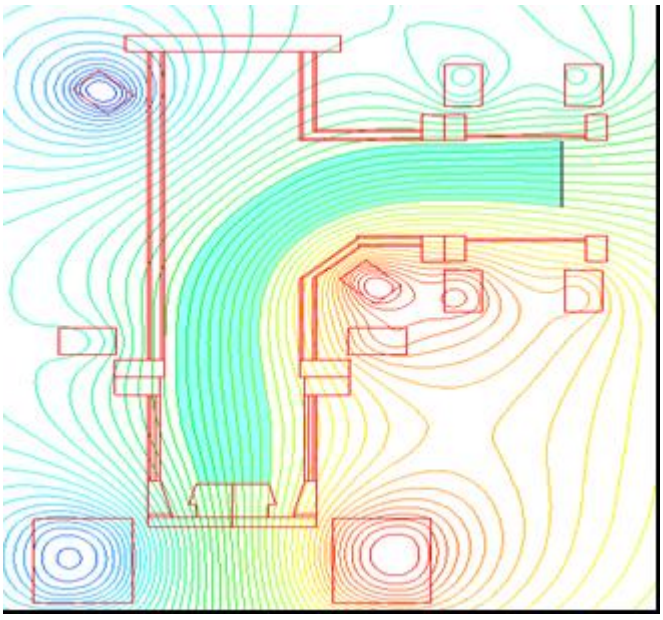

Fig.3a. Distribution of the magnetic field lines within a new T-type filter (courtesy of P. Strzyzewski, IPJ Swierk).

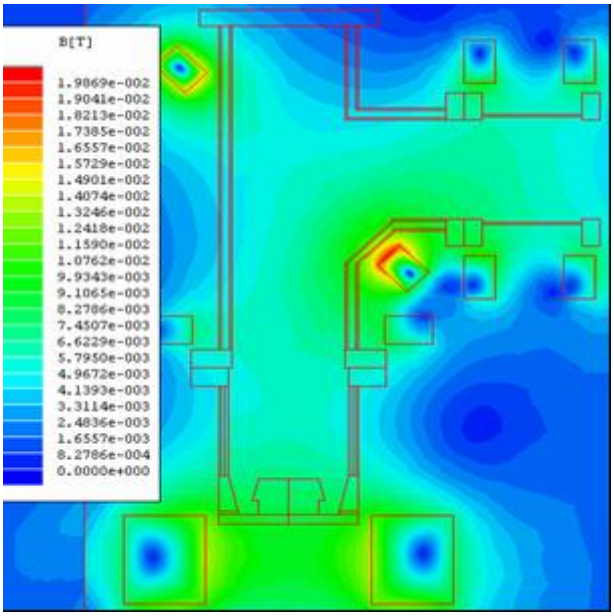

Fig.3. Values of the magnetic field within a new T-type filter (courtesy of P. Strzyzewski, IPJ Swierk).

The performed simulations showed that some additional correction coils are necessary in order to optimize the plasma transmission. They will be manufactured and used in future.

Cavity test stand

The test stand has been prepared to allow studying various film deposition parameters, using a single cell, cavity-like, insulated chamber, consisting of two halves and equipped with sensors and sample holders. This chamber was connected to a planar arc system and the device has been brought into full operation, as presented in Fig. 4.

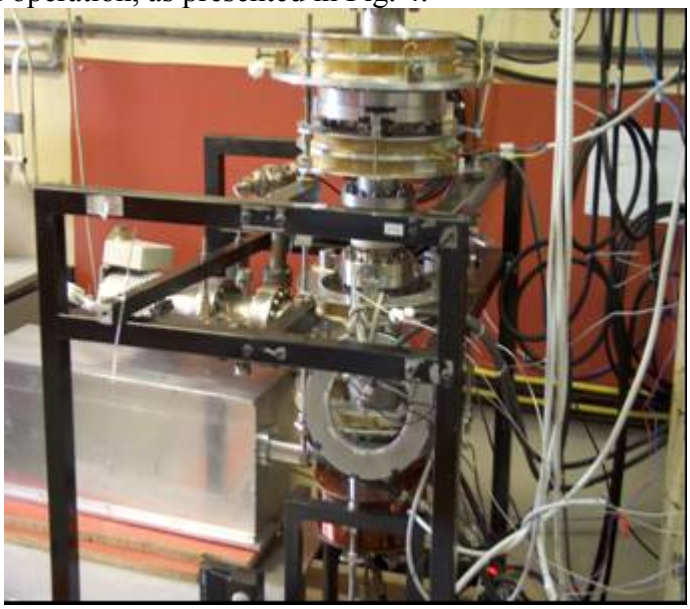

Fig.4. Present view of the cavity test stand with a new laser used as for arc triggering.

A new pulsed power supply unit, designed and manufactured at the IPJ-Swierk, has been used to apply a pulsed bias voltage to the cavity. A new set of isolated ion current collectors, which were installed inside the top half-cell, has been shown in Fig. 5.

Fig. 5. View of the ion current collectors installed inside the upper half-cell.

It was believed that the pulsing of the bias voltage is necessary to optimize the layer thickness distribution upon the inner cavity surface. Bias voltage pulse frequency and duty cycle have to be matched to plasma dynamics inside the cavity. An example of a time dependence of ion current, as collected by the cavity surface at a pulse frequency of 1 kHz and duty cycle of 50%, is shown in Fig. 6.

Fig.6. Time variations of the ion current, as collected by the "cavity" wall during the application of pulsed bias voltage. The upper trace shows the current readout, the second trace presents a

differential signal with the reduced noise, at the lowest trace shows changes of the bias voltage. The frequency was 1 kHz, duty factor 50%, and maximum bias voltage – 60 V.

The first tests, which were performed with the pulsed bias voltage, showed that the plasma transport system (determined by the magnetic field distribution) from the cathode to the cavity needs further optimization to be performed during next experiments.

Updating of MS-Project

N°	Task Name	Anfang	Ende
4.2	**Planar-arc cathode coating**	**Do 01.01.04**	**Sa 30.06.07**
4.2.1	**Modification of a planar-arc & trigger system**	**Do 01.01.04**	**Fr 27.05.05**
4.2.1.1	Modification	Do 01.01.04	Fr 16.04.04
4.2.1.2	Optimization of the laser triggering system	Mo 19.04.04	Fr 03.09.04
4.2.1.3	**Planar arc system fully tested**	Fr 03.09.04	Fr 27.05.05
4.2.2	**Routine Operation of planar arc system**	**Mo 06.09.04**	**Fr 30.06.06**
4.2.2.1	Characterization of samples coated at different conditions	Mo 06.09.04	Fr 30.06.06
4.2.2.2	Characterization of Nb-coated sapphire sam	Mo 06.12.04	Fr 30.06.06
4.2.2.3	Characterization of Nb-coated copper sampl	Mi 09.02.05	Fr 30.06.06
4.2.2.4	**Summary report on quality of planar arc coating**	Fr 27.05.05	Fr 27.05.05
4.2.3	**Studies of other HTC superconducting coating**	**Mo 30.05.05**	**Sa 30.06.07**
4.2.3.1	Study of superconducting properties	Mo 30.05.05	Sa 30.06.07
4.2.3.2	**Report on quality of superconducting properties**	Sa 30.06.07	Sa 30.06.07

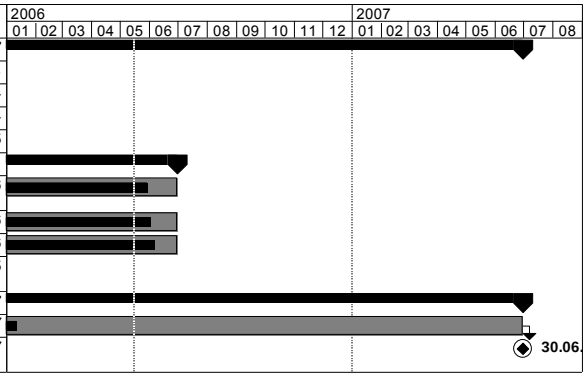

Work package 5: Surface preparation

Task 5.1 EP on single cells

5.1.1 EP on sample

Effect of water concentration in Electro polishing mixture has been put forward to explain the aging of the bath. Mixtures with lower H_2O concentration are investigated in terms of lifetime and surface state.
Tests with high fluorinated acid mixtures showed that the resulting removal speed depends a lot on anode cathode distance (tests with rotative anodes device).

5.1.2 Single Cell cavities

Tests with water and nitrogen flow showed leaks coming from the tank that should contain the acid mixture. This is a vital part of the set-up. As a result, a new tank has been ordered and should be delivered at the end of May. As a consequence, task 5.1.3.5 has been delayed. Once the tank is commissioned, final implantation will be finished and tests with the acid mixture will start (beginning of june 2006).

5.1.3.4 First operation of EP set-up

- Power supply, monitoring system and nitrogen flow security system have been checked during a cavity anodization with dilute H_2SO_4 mixture.

- The EP single cell set-up was tested with water. These tests showed that the acid tank had leaks. As a result, hydrogen and acid exhausts treatment are not efficient.
  A new tank has been ordered and tests with acid will start after commissioning.

- Security aspects:

Security committee allows to lead first tests with acids to control the set-up during an operation and check effectiveness of acid exhausts treatment system.
The risk analysis that has been submitted to the security committee involves explosion aspects. We are waiting the response concerning that precise point.
Continuous EP operation will result from acceptance of these aspects.

Status of money spending

	Spent money	Value of new orders/ contracts	Expected spending of new orders/contracts until end 2004	Sum of column 2 & 4
Travel				
Consumables		*4728 €*		
Manpower				
Durable				
			Total sum	

Updating of MS-Project

N°	Task Name	Anfang	Ende
5.1	**EP on single cells**	**Do 01.01.04**	**Fr 22.08.08**
5.1.1	**EP on samples**	**Do 01.01.04**	**Do 31.03.05**
5.1.1.1	Establishing method of surface characterization	Do 04.03.04	Fr 28.05.04
5.1.1.2	**Surface characterization fixed**	Fr 28.05.04	Fr 28.05.04
5.1.1.3	Series of EP with samples for surface investigations	Do 01.01.04	Do 31.03.05
5.1.1.4	**Best EP parameters**	Do 31.03.05	Do 31.03.05
5.1.2	**Single cell cavities**	**Do 01.01.04**	**Do 31.03.05**
5.1.2.1	Order Nb and fabricate 3 cavities	Do 01.01.04	Do 31.03.05
5.1.2.2	**3 cavities fabricated**	Do 31.03.05	Do 31.03.05
5.1.3	**Build EP chemistry for single cells**	**Do 01.01.04**	**Sa 31.12.05**
5.1.3.1	Design of EP set-up	Do 01.01.04	Fr 27.02.04
5.1.3.2	Fabrication of EP set-up	Do 01.04.04	Mo 28.02.05
5.1.3.3	Commissioning of EP set-up	Do 30.09.04	Sa 31.12.05
5.1.3.4	**First operation of EP set-up**	Sa 31.12.05	Sa 31.12.05
5.1.4	**Operation of single cell EP**	**Mo 02.01.06**	**Fr 02.06.06**
5.1.4.1	Continous single cell operation	Mo 02.01.06	Fr 02.06.06
5.1.4.2	**Define working parameters for single cells**	Fr 02.06.06	Fr 02.06.06
5.1.5	**Continuous operation, search for best paramete**	**Mo 05.06.06**	**Fr 22.08.08**
5.1.5.1	Parametrising EP procedure	Mo 05.06.06	Fr 22.08.08
5.1.5.2	**EP parameters fixed**	Fr 22.08.08	Fr 22.08.08

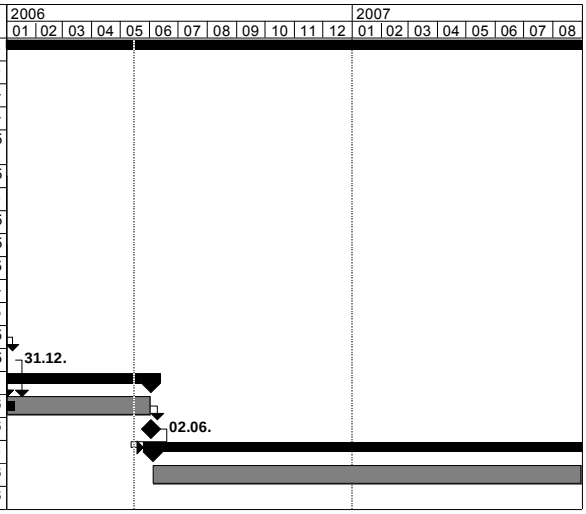

Task 5.2 Surface preparation

The Ep stet up is running continuously. Basing on the results of task 5.2.1.3.2 a U/I devise is installed in the Ep apparatus. This devise allows online measurements of the U/I curve of the acid in use. In comparison to the parameter results obtained in a.2.1.3.2 it allows to determine the aging of the acid bath online.

During the routinely done Ep processes all parameters are fixed now. This action was done to understand the wide spread of performance results. Actually it is not clear whether the cavity fabrication, the material or the EP process parameters are responsible for this spread. Several cavities reached 35 MV/m with the parameter in use. The assumption is made that this parameter set is close to optimum. Under that condition the parameters are fixed to get more statistical results that can be analysed in this respect.

Action Items

- Data recording of the parameters necessary to run the ELSYCA software

Discussion needed

- for industrialization of Ep and change goal of task 5.2.4
- Data recording at Saclay under Action Item 5.1 as input parameters for item 5.2.1.3.3 / Bath mixture
- Use of date of single cell program/ Use of single cells for to study Oxy polishing .

Status of money spending

	Spent money	**Value of new orders/ contracts**	**Expected spending of new orders/contracts until end 2006**	**Sum of column 2 & 4**
Travel	*WP 5.1 and WP 5.2 coordination 3 TEURO*		*7 TEURO*	*10 TEURO*
Consumables			*5 TEURO*	*5 TEURO*
Manpower		*0,5 man year 55 TEURO at DESY*		*27,5 TEURO*
Durable			*3 TEURO*	
			Total sum	*42,5 TEURO*

Update of MS-Project

5	WP5 SURFACE PREPARATION	01.01.04	02.07.08	22%
5.2	EP on multi-cells	01.01.04	19.09.08	35%
5.2.1	Transfer of parameters from 1 cell to multi cell equipment	01.01.04	01.12.05	66%
5.2.1.1	Finish EP setup nine-cells at DESY	01.01.04	01.11.05	100%
5.2.1.1.1	Improved gas cleaning system	01.01.04	05.05.04	100%
5.2.1.1.2	Design for hot water rinsing	06.05.04	15.07.05	**100%**
5.2.1.1.3	Proof-of-Principle experiment hot water rinsing	01.11.05	01.11.05	0%
5.2.1.2	Optimize electrode shape	10.09.04	01.12.05	**70%**
5.2.1.2.1	Develop computer model / Evaluate software	10.09.04	27.01.05	100%
5.2.1.2.2	Design improved electrode	01.02.05	18.06.06	0%

5.2.1.2.3	Electrode design fixed	01.12.05	01.08.06	0%
5.2.1.3	Fix process parameters/ Quality control	01.01.04	01.12.05	**80%**
5.2.1.3.1	Setup chemical lab	01.01.04	24.03.04	100%
5.2.1.3.2	Bath aging	25.03.04	16.06.04	**100%**
5.2.1.3.3	Bath mixture	25.03.04	08.09.06	**80%**
5.2.1.3.4	Alternative (salt) mixtures	04.01.05	05.05.05	100%
5.2.1.3.5	Process parameters fixed	01.12.05	01.12.05	**80%**
5.2.2	Laser roughness	04.01.05	20.01.06	6%
5.2.2.1	Evaluate existing systems	04.01.05	05.05.05	**100%**
5.2.2.2	Specify laser system	06.05.05	08.09.05	0%
5.2.2.3	Built laser system	09.09.05	20.01.06	0%
5.2.2.4	Roughness measurement finished	20.01.06	20.01.06	0%
5.2.3	Oxipolishing as final chemical cleaning	13.01.05	01.04.08	38%
5.2.3.1	Laboratory studies	13.01.05	22.04.05	30%
5.2.3.2	Design of OP system	24.02.05	18.05.05	70%
5.2.3.3	Setup one-cell system	19.05.05	31.01.07	77%
5.2.3.4	Proof-of-Principle experiment Oxipolishing	31.01.07	31.01.07	0%
5.2.3.5	Design OP for nine-cells	16.12.05	29.05.07	**80%**
5.2.3.6	Build OP for 9-cells	30.05.07	25.09.07	0%
5.2.3.7	OP for 9-cells ready	25.09.07	25.09.07	0%
5.2.3.8	Study op with 9-cell cavities	26.09.07	01.04.08	0%
5.2.3.9	Evaluate experiments	01.04.08	01.04.08	0%
5.2.4	Transfer Electropolishing technology to industry	06.05.05	19.09.08	**30%**
5.2.4.1	Qualify industry with one-cells	06.05.05	02.06.06	100%
5.2.4.2	Industrial design study on setup for multi-cells	29.11.05	26.12.06	10%
5.2.4.3	Report on industrial design	26.12.06	26.12.06	0%
5.2.4.4	Fabricate EP multi-cell industrial prototype	26.12.06	07.05.07	0%
5.2.4.5	Commission EP multi-cell industrial prototype	07.05.07	27.08.07	0%
5.2.4.6	EP multi-cell industrial prototype ready	27.08.07	27.08.07	0%
5.2.4.7	Operate EP multi-cell industrial prototype	27.08.07	19.09.08	0%
5.2.4.8	Final report on industrial EP	19.09.08	19.09.08	0%

Comments on Task

5.2.1.1.2

Activities on Hot water rinsing will be stopped. A report on the status is under preparation

5.2.1.2

The test apparatus to determine the acid parameters for the input to the computer program necessary to start the calculation of current distribution did not withstand the Ep mixture. The calculation of optimized parameters is delayed by the missing data. A new set up with inert electrodes was build and is send to ELSYCA in Brussels.

5.2.2.1

At the University of Wuppertal a surface analysis apparatus is set up. It allows determine the surface roughness of samples. Actually it is in use to set up a quality control system for cavity assembly and preparation. After this procedure is fixed a test run to qualify this set up

5.2.3.5

The design of a nine cell OP system is finished. The application on a nine cell cavity is stopped actually. These activities have to be delayed due to other activities with higher priority on the DESY 9 cell infrastructure.

5.2.4

The transfer is delayed and on hold now. It is under discussion to send out a contract to industry to electro polish about 30 new 9 cell cavities. It does not make sense to start up parallel activity under CARE with the same goal if industrialization.
It has to be discussed whether to use the money foreseen for task 5.2.4 for the contract of industrial electro polishing or to invest this money in a quality control procedure for acid mixtures. This action may stabilize the EP process and may be applied for the cavity fabrication as quality control step for the high gradient programme.

Task 5.3 Automated Electro-Polishing

The automated EP bench has been completed. The EP facility can serve both Cu and Nb cavities. The Automated program has been tested directly on a cavity for what concerns the EP of Copper, still on samples for what concerns Niobium. The reason for that is the presence of oscillations that could somehow false the presence of the minimum of the differential conduction. Indeed while due the Niobium peculiar oscillations are due to the forming and breaking of the oxide growing onto the Niobium surface meanwhile Electropolishing, the minimum in the first derivative of the I-V polarization curve corresponds to the minimum in the differential conductance, that in other words corresponds to the maximum resistance of the viscous layer grown during the Electropolishing. At the moment we are specifically testing on samples how to easy discriminate the mimnimum of the differential conductance from the wells of the oxide growth oscillations. However even if still subject of implementation, the software is ready for being moved to other laboratories of the collaboration, in order to be tested.

Updating of MS-Project

N°	Task Name	Anfang	Ende
5.3	**Automated EP (AEP)**	**Do 01.01.04**	**Do 03.01.08**
5.3.1	**Prototype EP installation**	**Do 01.01.04**	**Di 08.02.05**
5.3.1.1	Design installation	Do 01.01.04	Fr 05.03.04
5.3.1.2	Fabricate/ order components	Mo 08.03.04	Fr 02.07.04
5.3.1.3	Assemble EP installation	Mo 05.07.04	Di 08.02.05
5.3.1.4	**First operation of automated EP**	Di 08.02.05	Di 08.02.05
5.3.2	**EP computer control**	**Mo 08.03.04**	**Mo 21.02.05**
5.3.2.1	Design control architecture	Mo 08.03.04	Di 27.04.04
5.3.2.2	Developed softw are	Mi 28.04.04	Di 10.08.04
5.3.2.3	Test of softw are	Di 04.01.05	Mo 21.02.05
5.3.2.4	**Software ready**	Mo 21.02.05	Mo 21.02.05
5.3.3	**Operation of AEP prototype**	**Di 22.02.05**	**Mo 13.02.06**
5.3.3.1	Correlate surface finish/ conductance	Di 22.02.05	Mo 13.06.05
5.3.3.2	Determine optimum conductance	Di 14.06.05	Mi 14.09.05
5.3.3.3	Optimize automated operation	Do 15.09.05	Fr 02.12.05
5.3.3.4	Design report on AEP	Mo 05.12.05	Mo 13.02.06
5.3.3.5	**Automated EP is defined**	Mo 13.02.06	Mo 13.02.06
5.3.4	**Alternative electrolytes**	**Di 01.03.05**	**Mo 30.10.06**
5.3.4.1	Review of EP chemistry	Di 01.03.05	Di 24.05.05
5.3.4.2	**Proposal for alternative electrolytes**	Di 24.05.05	Di 24.05.05
5.3.4.3	Experiments w ith alternative electrolytes	Di 14.02.06	Mo 30.10.06
5.3.4.4	**Conclude experimental results**	Mo 30.10.06	Mo 30.10.06
5.3.5	**Define best AEP**	**Di 31.10.06**	**Do 03.01.08**
5.3.5.1	Compare standard/new electrolyte method	Di 31.10.06	Fr 05.01.07
5.3.5.2	Modify AEP installation for best electrolyte	Mo 08.01.07	Fr 06.04.07
5.3.5.3	Operate modified AEP	Mo 09.04.07	Do 25.10.07
5.3.5.4	Design report on best AEP	Fr 26.10.07	Do 03.01.08
5.3.5.5	**Conclude on best electrolyte**	Do 03.01.08	Do 03.01.08

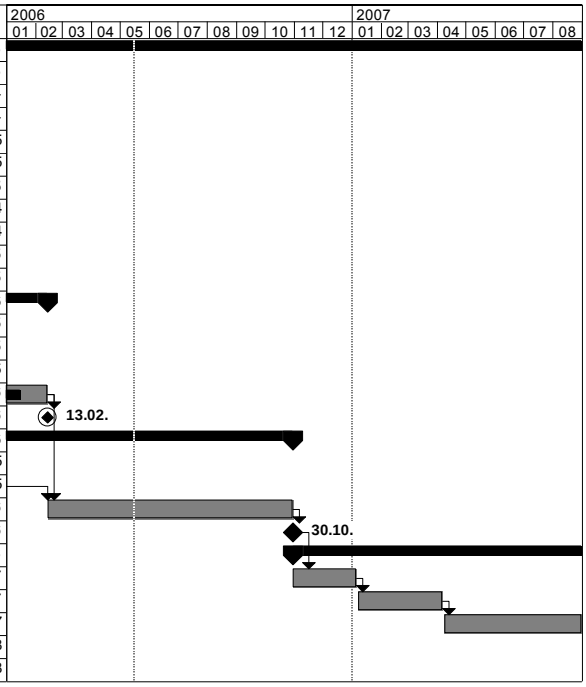

Task 5.4 Dry ice cleaning

During the first quarter of 2006 the commissioning of the dry-ice cleaning system continues successfully. Several cavities are cleaned both for system tests and for rf measurement of the cavity. Gradients up to 34 MV/m are achieved in single-cell cavities. Nevertheless several minor problems could be identified and solved.
To fulfil the requirements of personal safety for routine operation the installation of a gas alarm system started. It will be operational in May/June 06. Though the installation is not fully completed, the commissioning (see below) is ongoing.
During the first commissioning phase in 2005 the infra-red (IR) heater system was identified to be insufficient. A heater system is necessary to prevent a significant cooling and freezing of the cavity caused by the heat removal during operation of the dry-ice jet. A new dedicated design of an optimized, high power IR heater had to be developed, constructed and installed. This caused a delay during commissioning of app. six months. The new heater system fully meets its requirements and allows continuous dry-ice cleaning without freezing of the cavity.

Dry-ice cleaning system with the new IR heater

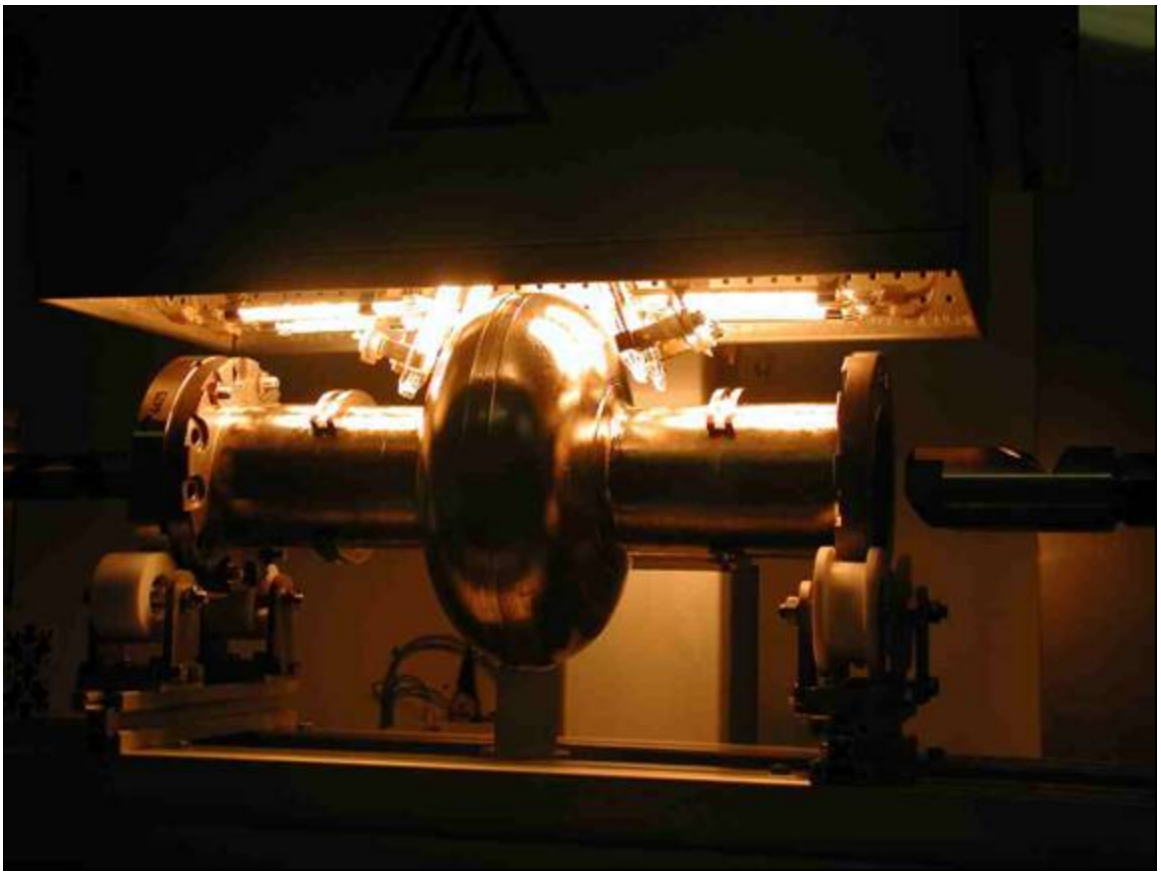

The new IR heater system in operation

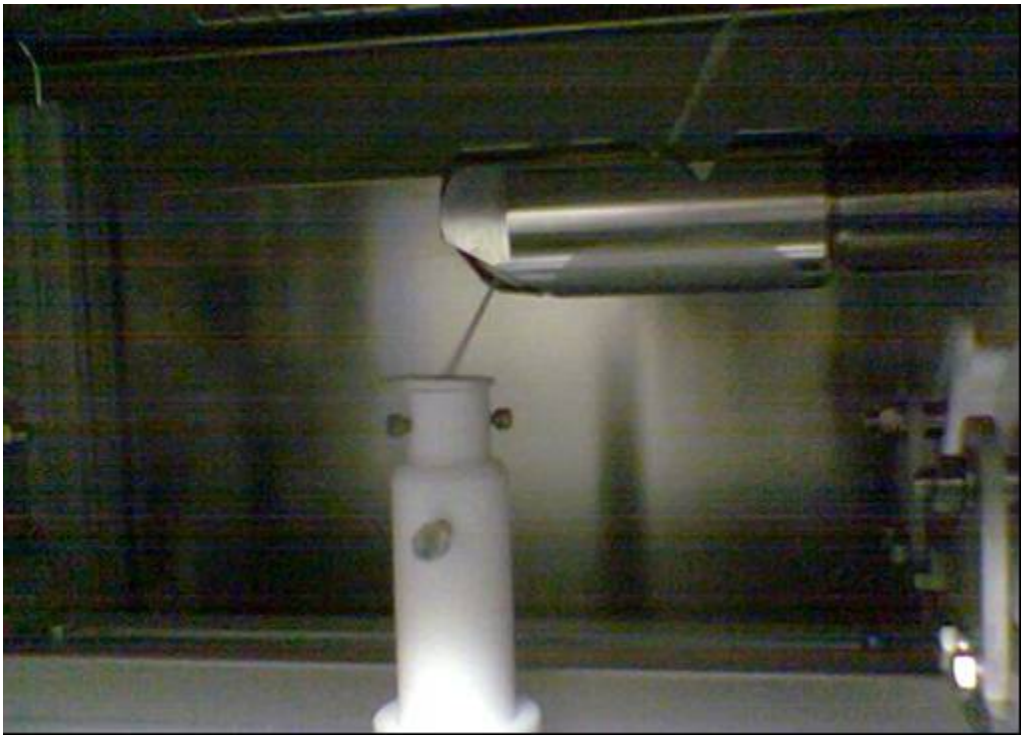

Cleaning of a niobium sample for field emission investigations (WP6.3)

Updating of MS-Project

N°	Task Name	Anfang	Ende
5.4	**Dry ice cleaning**	**Do 01.01.04**	**Mi 30.12.09**
5.4.1	**Installation of full system for 1-3 cell cavities**	**Do 01.01.04**	**Mo 11.04.05**
5.4.1.1	Installation of CO2 piping	Do 01.01.04	Mi 31.03.04
5.4.1.2	Installation of motion system	Do 01.04.04	Mi 30.06.04
5.4.1.3	Installation of control system	Do 01.07.04	Di 08.02.05
5.4.1.4	Commissioning	Mi 09.02.05	Mo 11.04.05
5.4.1.5	**Installation finished**	Mo 11.04.05	Mo 11.04.05
5.4.2	**Optimization of cleaning parameters**	**Di 12.04.05**	**Fr 14.07.06**
5.4.2.1	Sample cleaning	Di 12.04.05	Fr 09.09.05
5.4.2.2	1-cell cavity cleaning	Fr 09.09.05	Mi 08.02.06
5.4.2.3	Fix best cleaning parameters	Fr 10.02.06	Fr 14.07.06
5.4.2.4	**Cleaning parameters fixed**	Fr 14.07.06	Fr 14.07.06
5.4.3	**VT 9-cell cleaning apparatus**	**Mo 04.09.06**	**Fr 30.11.07**
5.4.3.1	Design 9-cell apparatus VT	Mo 04.09.06	Do 28.12.06
5.4.3.2	Fabricated 9-cell apparatus	Fr 29.12.06	Do 29.03.07
5.4.3.3	Installation of 9-cell apparatus	Fr 30.03.07	Fr 29.06.07
5.4.3.4	Commissioning of 9-cell apparatus	Sa 30.06.07	Fr 30.11.07
5.4.3.5	**VT Cleaning Installation finished**	Fr 30.11.07	Fr 30.11.07
5.4.4	**VT Cleaning of 9-cell cavities**	**Mo 03.12.07**	**Mi 30.12.09**
5.4.4.1	Continuous cleaning	Mo 03.12.07	Mi 30.12.09
5.4.4.2	**Evaluation of experimental results**	Mi 30.12.09	Mi 30.12.09
5.4.5	**Design & construction of H9-cell cleaning apparatus**	**Mo 03.12.07**	**Fr 03.04.09**
5.4.5.1	Design 9-cell apparatus VT	Mo 03.12.07	Mi 02.04.08
5.4.5.2	Fabricated 9-cell apparatus	Do 03.04.08	Mo 04.08.08
5.4.5.3	Installation of 9-cell apparatus	Di 05.08.08	Mo 03.11.08
5.4.5.4	Commissioning of 9-cell apparatus	Di 04.11.08	Fr 03.04.09
5.4.5.5	**Start H9-cell cleaning**	Fr 03.04.09	Fr 03.04.09
5.4.6	**Cleaning of horizontal nine-cell cavity**	**Mo 06.04.09**	**Mi 30.12.09**
5.4.6.1	Continuous cleaning	Mo 06.04.09	Mi 30.12.09
5.4.6.2	**Evaluation of experimental results**	Mi 30.12.09	Mi 30.12.09

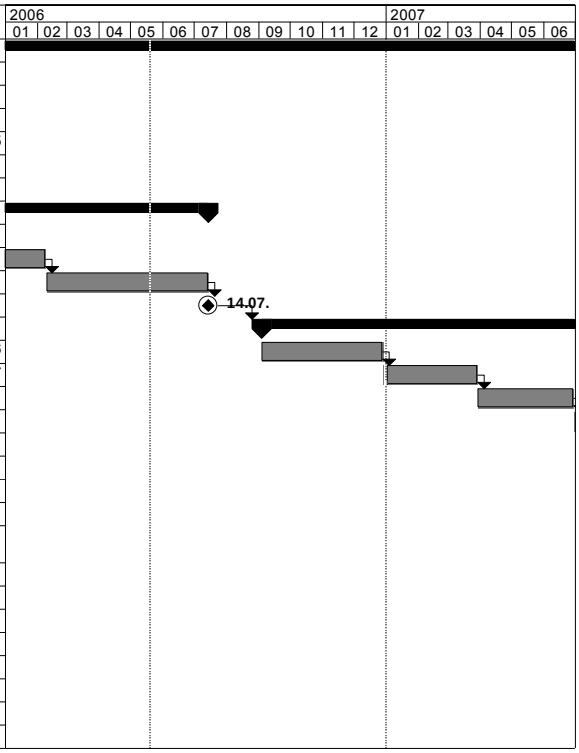

Work package 6: Material Analysis

Task 6.1 SQUID Scanner

Scanning of artificially produced defects

A niobium test sheet with artificially imbedded flaws (tantalum inclusions of size 0,1-0,05 mm close to surface) was produced (Fig. 1) and scanned with SQUID scanner. Holes of different diameter and depth were drilled and filled with tantalum. After that these location were heated by defocused electron beam up to melting. Finally the sheet surface was completely grinded, so that the defect positions were barely seen.

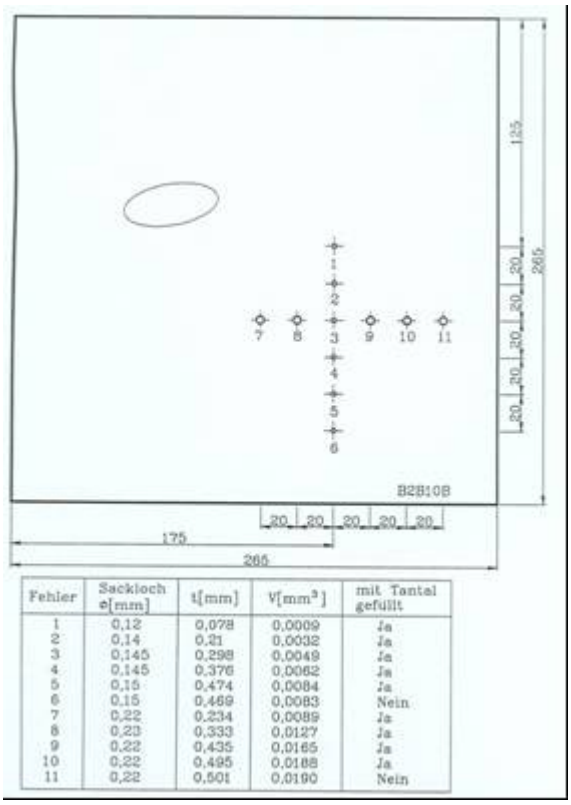

Fehler	Sackloch e[mm]	t[mm]	V[mm³]	mit Tantal gefüllt
1	0,12	0,078	0,0009	Ja
2	0,14	0,21	0,0032	Ja
3	0,145	0,298	0,0049	Ja
4	0,145	0,376	0,0062	Ja
5	0,15	0,474	0,0084	Ja
6	0,15	0,469	0,0083	Nein
7	0,22	0,234	0,0089	Ja
8	0,23	0,333	0,0127	Ja
9	0,22	0,435	0,0165	Ja
10	0,22	0,495	0,0188	Ja
11	0,22	0,501	0,0190	Nein

Fig. 1: Nb test sheet wit Ta inclusions

SQUID scanning was done with the excitation coil of 1 mm diameter and 40 windings. The scanning speed was ca. 10cm/sec. The exciting frequency was 6 KHz. Scanning results can be seen in Fig. 2. All artificially produced defects were identified.

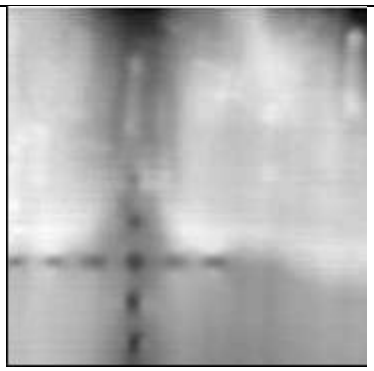

Fig. 2a: SQUID scanning results of Nb test sheets

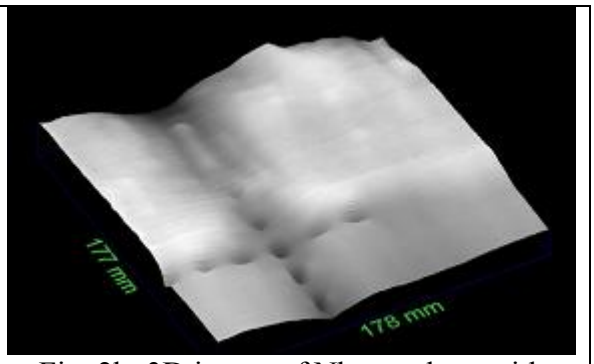

Fig. 2b: 3D image of Nb test sheet with artificial Ta defects by SQUID scanning

Fabrication of more systematic artificial defects is in work. Draft of the defect distribution can be seen in Fig.3. Following materials are foreseen to be imbedded; tantalum, cooper, iron, niobium, stainless steal.

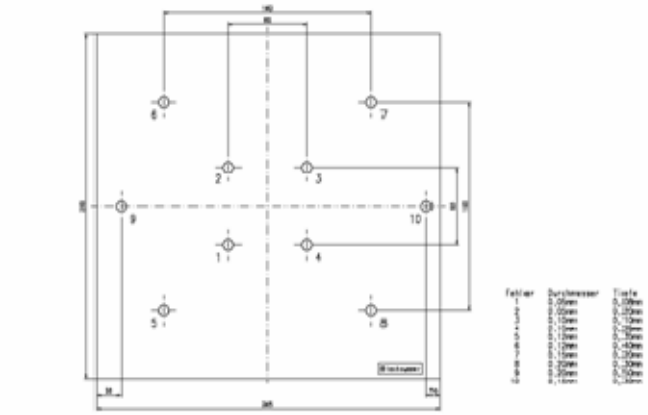

Fig. 3: Draft of niobium sheet with imbedded defects

Status of money spending

	Spent money	**Value of new orders/ contracts**	**Expected spending of new orders/contracts until end 2006**	**Sum of column 2 & 4**
Travel				
Consumables			*10000*	*10000*
Manpower	*4890*		*14670*	*19560*
			Total sum	***29560***

Updating of MS-Project

N°	Task Name	Anfang	Ende
6.1	**SQUID scanning**	**Do 01.01.04**	**Mo 31.12.07**
6.1.1	**Produce calibration defects**	**Do 01.01.04**	**Do 12.08.04**
6.1.1.1	Production of surface defects	Do 01.01.04	Fr 18.06.04
6.1.1.2	Production of bulk defects	Do 12.02.04	Do 12.08.04
6.1.1.3	**Calibration defects finished**	Do 12.08.04	Do 12.08.04
6.1.2	**Design components of Squid scanner**	**Do 01.01.04**	**Di 30.11.04**
6.1.2.1	Design of the scanning table and support	Do 01.01.04	Mi 30.06.04
6.1.2.2	Design of the SQUID cooling system	Mi 28.01.04	Di 30.11.04
6.1.2.3	**Design Scanner finished**	Di 30.11.04	Di 30.11.04
6.1.3	**Construction of scanning apparatus**	**Mi 01.12.04**	**Fr 16.12.05**
6.1.3.1	Fabrication of the SQUID	Mi 01.12.04	Mi 30.03.05
6.1.3.2	Fabrication and purchase of components for SQUID apparatus	Mi 01.12.04	Do 30.06.05
6.1.3.3	Softw are for the SQUID scanner	Mi 01.12.04	Do 30.06.05
6.1.3.4	Commissioning and calibration of scanning apparatus	Mo 04.07.05	Fr 16.12.05
6.1.3.5	**Scanning apparatus operational**	Fr 16.12.05	Fr 16.12.05
6.1.4	**Scanning of sheets with artificial defects**	**Fr 16.12.05**	**Do 08.02.07**
6.1.4.1	Scanning of sheets w ith artificial surface defects	Fr 16.12.05	Do 01.06.06
6.1.4.2	Scanning of sheets w ith artificial bulk defects	Fr 02.06.06	Do 16.11.06
6.1.4.3	Development of algorithm for material defects classification	Mo 20.11.06	Do 08.02.07
6.1.4.4	**Classification of defects finished**	Do 08.02.07	Do 08.02.07
6.1.5	**Scanning of production sheets**	**Mo 12.02.07**	**Mo 31.12.07**
6.1.5.1	Scanning of sheets of different producers	Mo 12.02.07	Do 20.09.07
6.1.5.2	Identification of defects by (EDX, SURFA etc.)	Mo 02.04.07	Fr 28.09.07
6.1.5.3	Conclusive comparison w ith eddy current data	Fr 21.09.07	Mo 31.12.07
6.1.5.4	**Final report on SQUID scanning**	Mo 31.12.07	Mo 31.12.07

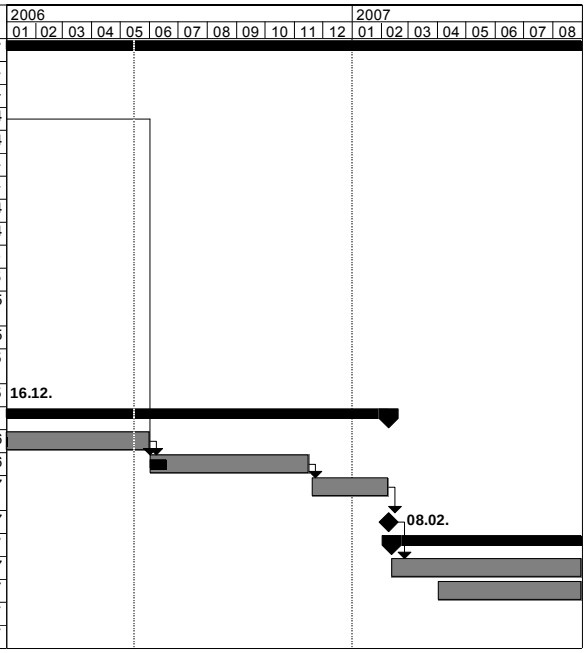

Task 6.2 Flux gate magnetometry

Referring to tomography of the electrolytic cells in order to configure the effect of cathode geometry on Electropolishing, we fabricated a few elementary rectangular cells for the procedure calibration and several shaped electrolytic cell having the possibility to test different cathode shapes.

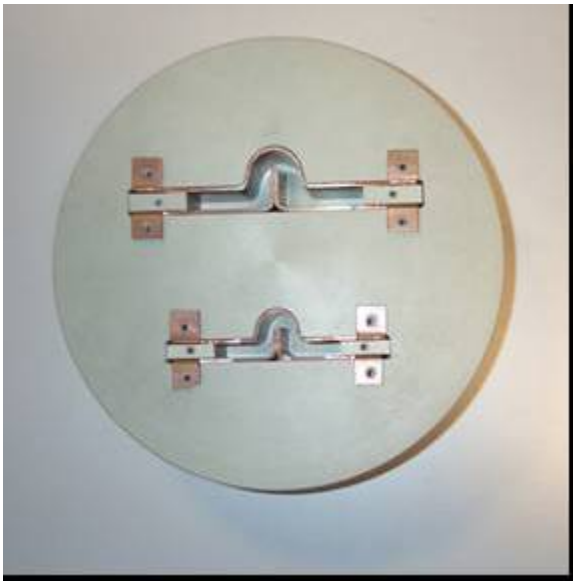

Fig. 1 The cavity shaped electrolytic cells with a cathode that totally enters into the cell.

The electrolytic solution was 55% Phosphoric acid and 45% n-buthanol, the electropolishing process was driving in voltage and the magnetic field sensors, in this case a Flux-Gate 1st order electronic gradiometer, was oriented to detect the in plane component of the magnetic field gradient, Gx, due the current distribution flowing between the electrodes.

Images of ongoing electropolishing process have been carried out moving the sensors back and forth over the whole cell length, with a speed of 3mm/s and a continuous acquisition mode with 6 data points/mm. To monitor the electropolishing process of copper surface Flux-Gate sensors have been applied because of their capability to detect the magnetic field produced in the electropolishing process. The Flux-Gate sensor is a solid state device based on the non linearity of the magnetic characteristic of its sensing ferromagnetic core. It can measure the d.c or the low frequency a.c. magnetic field component, with a field sensitivity ranging from 1e-11 to 1e-4 Tesla. A flux-Gate sensor is made of a high permeability cylindrical core around which there are two coaxial coils: bias coil and sensing coil. This sensor detect directly variation of the magnetic field generally using a Phase Sensitive Detection (PSD), in this way it can work in a bandwidth ranging from d.c. to 5 kHz.

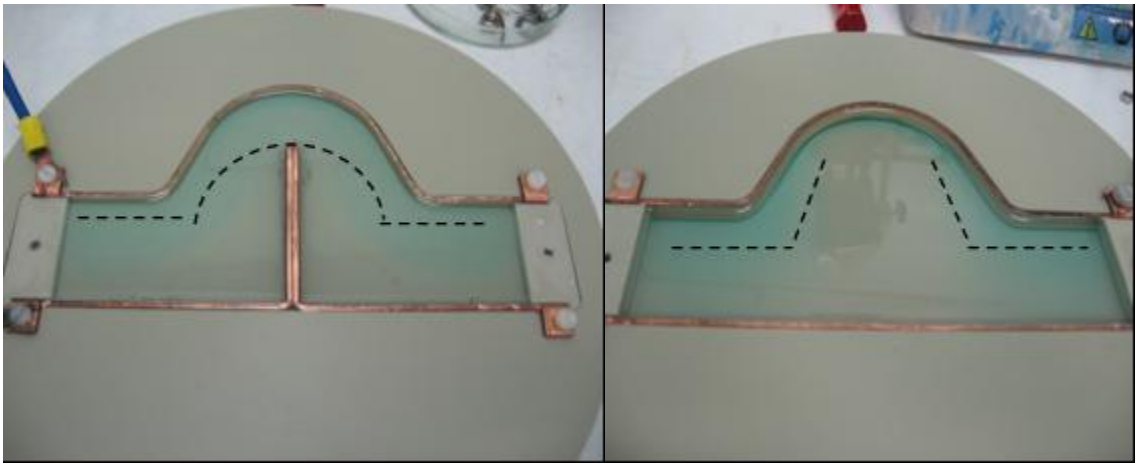

Figure 2 : The electrolytic cells analysed: a cavity like electrode with flat and shaped cathode, respectively. The dot lines follow the viscous layer due to uniform electropolishing process.

In next figure the imaging of the current distributions obtained applying the FFT technique to the corresponding magnetic field data detected by flux gates is reported. It could be noted that the current distribution is uniform along the total length of the cell, because the plateau of the polarization curve (at 4V) guarantees an uniform corrosion.

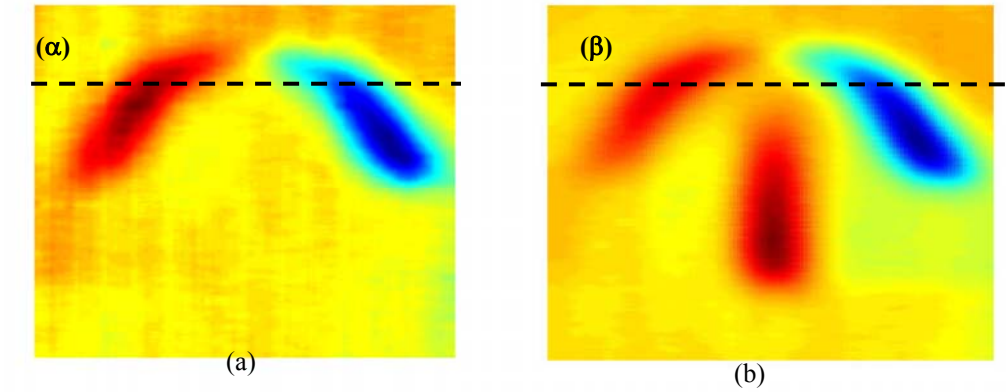

Figure 3: Magnetic field distribution for the cells with different cathode shapes: flat (a) and shaped (b)

The measurements show good agreement between the visual inspection of the viscous layer, and the magnetic tomography, implying that flux gate Magnetometry could be successfully applied in closed geometries.

Updating of MS-Project

N°	Task Name	Anfang	Ende
6.2	**Flux gate magnetometry**	**Do 01.01.04**	**Mi 11.06.08**
6.2.1	**Produce calibration defects**	**Do 01.01.04**	**Sa 01.01.05**
6.2.1.1	Production of surface defects	Do 01.01.04	Fr 07.05.04
6.2.1.2	Production of bulk defects	Do 01.01.04	Do 01.07.04
6.2.1.3	**Calibration defects finished**	Sa 01.01.05	Sa 01.01.05
6.2.2	**Design components of flux gate head**	**Do 01.01.04**	**Mo 20.12.04**
6.2.2.1	Design electronics	Do 01.01.04	Fr 16.04.04
6.2.2.2	Design of flux gate head	Mo 02.08.04	Fr 17.12.04
6.2.2.3	Design of operations softw are	Do 01.01.04	Fr 04.06.04
6.2.2.4	**Design flux gate head finished**	Mo 20.12.04	Mo 20.12.04
6.2.3	**Fabrication of flux gate detector**	**Mo 21.06.04**	**Mo 19.12.05**
6.2.3.1	Fabrication of flux gate head	Mo 03.01.05	Fr 29.04.05
6.2.3.2	Fabrication of mechanics	Mo 21.06.04	Di 12.07.05
6.2.3.3	Implementation of softw are	Di 12.07.05	Mo 19.09.05
6.2.3.4	Commissioning of flux gate detector	Mo 19.09.05	Mo 21.11.05
6.2.3.5	Calibration of flux gate detector	Mo 21.11.05	Mo 19.12.05
6.2.3.6	**Flux gate detector operational**	Mo 19.12.05	Mo 19.12.05
6.2.4	**Commissioning of flux gate detector**	**Mo 19.12.05**	**Do 04.01.07**
6.2.4.1	Operational tets tests	Mo 19.12.05	Fr 21.07.06
6.2.4.2	Evaluation of test results	Fr 21.07.06	Do 04.01.07
6.2.4.3	**Flux gate scanner commissioned**	Do 04.01.07	Do 04.01.07
6.2.5	**Operation of flux gate detector**	**Do 04.01.07**	**Mo 17.09.07**
6.2.5.1	Regular operation	Do 04.01.07	Mi 06.06.07
6.2.5.2	Report of operation	Mi 06.06.07	Mo 17.09.07
6.2.5.3	**Conclusion of flux gate scanning operation**	Mo 17.09.07	Mo 17.09.07
6.2.6	**Comparison with SQUID scanner**	**Mo 17.09.07**	**Mi 11.06.08**
6.2.6.1	Compare measurements	Mo 17.09.07	Mi 11.06.08
6.2.6.2	**Conclude SQUID scanner vs. flux gate detector**	Mi 11.06.08	Mi 11.06.08

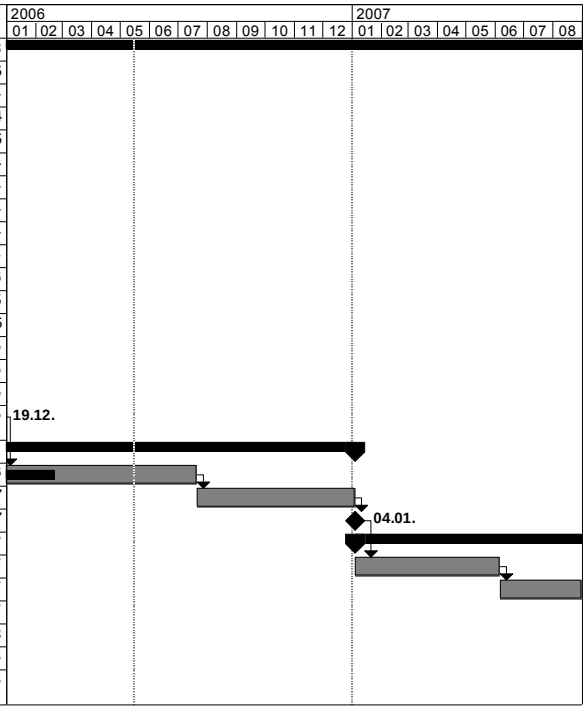

Task 6.3 DC field emission scanning

To study the improvement of surface quality by applying dry ice cleaning (DIC) as a final surface cleaning procedure, a series of systematic field emission scanning and local measurements of emitters were performed on two circular Nb samples (28 mm diameter) and four square shaped Cu samples (7mm×7mm). The samples' description, surface treatments and measurement details are given below:

<table>
<tr><th>Sample</th><th>Surface treatment/ Production method</th><th>Intermediate measurements</th><th>Final treatment</th><th>Measurement, Analysis</th></tr>
<tr><td>Nb (SEP1)</td><td>EP</td><td rowspan="2">FE measurement, SEM, EDX</td><td rowspan="5">Dry Ice Cleaning</td><td rowspan="2">FE measurement, SEM, EDX</td></tr>
<tr><td>Nb (SEP2)</td><td>EP+ HPR</td></tr>
<tr><td>Cu 1</td><td rowspan="2">Cut out of Diamond turned cavity cell</td><td>FE measurement</td><td rowspan="3">FE measurements</td></tr>
<tr><td>Cu 2</td><td>--</td></tr>
<tr><td>Cu 4</td><td rowspan="2">Cut out of Normal, high quality cavity cell</td><td>--</td></tr>
<tr><td>Cu 6</td><td>FE measurement</td></tr>
</table>

The main results of this work can be summarized as follows:

- Both Nb and Cu samples showed clearly the improved surfaces after DIC with:

  No field emission up to (60, 90) and (90, 120) MV/m;

  Emitter density N up to (2, 3) and (4, 12) /cm^2 at 120 MV/m
- The shift in onset field towards 90 MV/m for 1 Nb sample while 120 MV/m for all other samples has been observed. The emitter number density at 120 MV/m was reduced to less than one fourth of the emitters before DIC.
- Some strong emitters were localized by high resolution scans and showed nearly stable Fowler-Nordheim-like I-V curves with reduced local field enhancement factors between 17 to 84 for Nb and 20 to 48 for Cu samples, which are typical for particulates and surface irregularities.
- High resolution SEM on Nb samples revealed two types of emitters: remnants of a thin conductive object (shown in fig.1) and a scratch-like surface defect. No foreign element was detected by EDX.

SEM image of an emitter before and after DIC, showing destructive effect of DIC on the emitter:

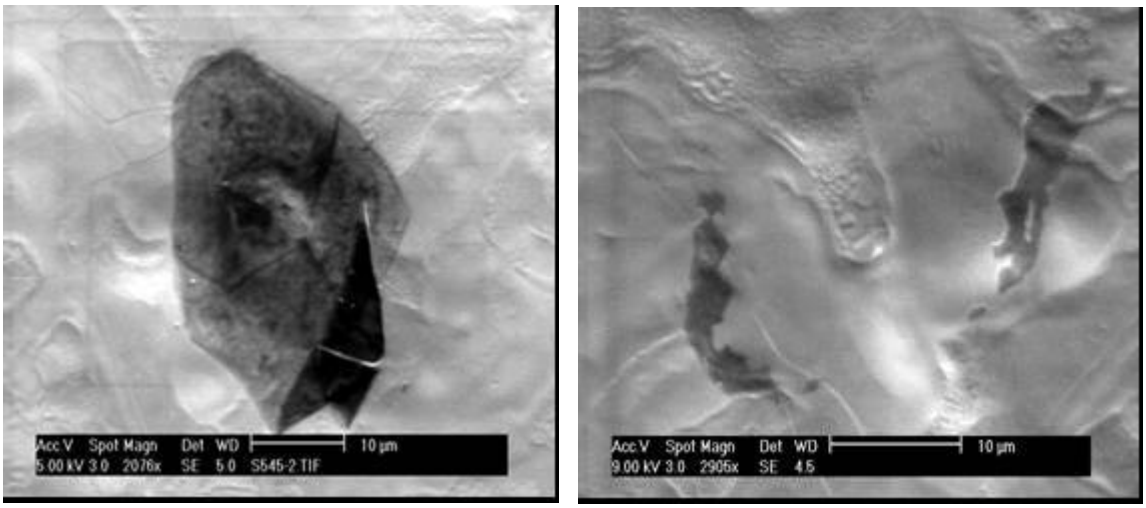

Fig1. SEM images of an emitter before and after dry ice cleaning. Most of the part of the emitting particle has been destroyed by DIC, but remnants still emitting with reduced strength.

The measurements for quality control analysis have also been started on the new series of samples prepared inside the cavity.

Updating of MS-Project

N°	Task Name	Anfang	Ende
6.3	**DC field emission studies of Nb samples**	**Do 01.01.04**	**Mi 26.12.07**
6.3.1	**Quality control scans**	**Do 01.01.04**	**Mi 26.12.07**
6.3.1.1	Modification of Scanning apparatus	Do 01.01.04	Fr 02.04.04
6.3.1.2	Calibration of Scanning apparatus	Mo 05.04.04	Fr 04.06.04
6.3.1.3	**Start scanning activity**	Fr 04.06.04	Fr 04.06.04
6.3.1.4	BCP and HPR samples	Mo 07.06.04	Do 26.05.05
6.3.1.5	EP and HPR samples	Fr 10.09.04	Mi 03.08.05
6.3.1.6	BCP/EP and DIC samples	Mi 05.01.05	Fr 10.06.05
6.3.1.7	**First report on BCP/EP and DIC surface**	Fr 10.06.05	Fr 10.06.05
6.3.1.8	Continue QA scanning	Mo 13.06.05	Mi 26.12.07
6.3.1.9	**Evaluation of scanning results**	Mi 26.12.07	Mi 26.12.07
6.3.2	**Detailed measurements on strong emitters**	**Mo 13.06.05**	**Mi 26.12.07**
6.3.2.1	Calibrate apparatus for high current	Mo 13.06.05	Mi 30.11.05
6.3.2.2	**Start strong emitter evaluation**	Mi 30.11.05	Mi 30.11.05
6.3.2.3	I/V curves and current limits	Do 01.12.05	Mi 26.12.07
6.3.2.4	SEM and AES	Do 01.12.05	Mi 26.12.07
6.3.2.5	Influence of heat treatment and ion impact	Do 01.12.05	Mi 26.12.07
6.3.2.6	**Evaluate strong emitter investigations**	Mi 26.12.07	Mi 26.12.07

Work package 7: Couplers.

Work-package 7 of JRA1 concerns the development of power couplers. This WP is broken down into three main tasks:
7.1 – New proto-type couplers.
7.2 – Fabrication of a titanium-nitride coating bench for the coupler ceramic windows.
7.3 – Conditioning studies of proto-type couplers.

For task 7.1 we have designed two new-proto-types named TTF-V and TW60 respectively.
Both types of couplers are now being produced in industry, and are expected in May (TTF5) and June (TW60). 4 couplers of each type are expected.
A test transition for this 8 couplers is also expected.

The status of the production of these couplers is the following:

- for TTF5 couplers: the ceramics are brazed, the TiN coating is expected soon, the copper coating process is validated, all parts are machined and most sub-assemblies are welded.
- for TW60 couplers: a first ceramic is brazed (for validation), all parts (including ceramics) are machined, welding and brazing will follow
- for test transition: the transition is finished (machining, welding, brazing), there is some leak problems due to rectangular dismountable flange with Helicoflex seals but we have some alternatives in mind (as brazed flanges for examples) so we are sure that this test transition will be delivered with the first couplers at the latest.

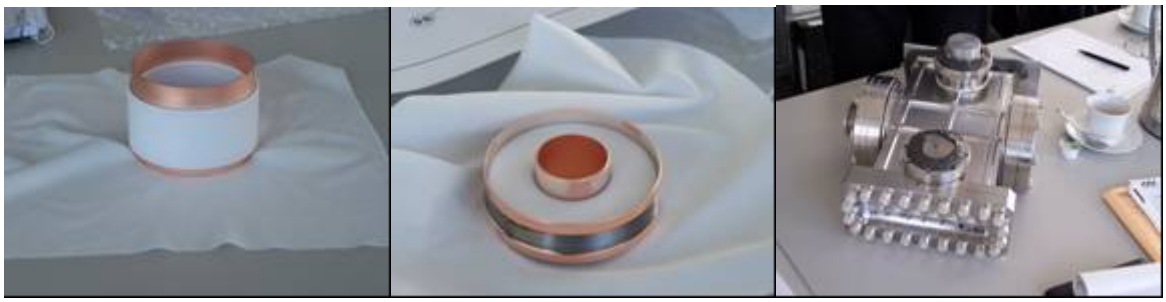

From left to right: TTF5 brazed production ceramic, TW60 validation ceramic, test transition

As far as the task 7.2 is concerned we have to admit a certain delay (4-5 months on the last milestone) on the time schedule due to the difficulty to find an industrial partner that can assure the construction of the prototype with the required performances in a reasonable time schedule and budget.
At the end we are defining collaboration with an Italian research consortium that is capable to fulfil our demand. This collaboration will imply also a better participation of the LAL personnel to the development and testing phases of the coating station. At the end the sputtering solution seems the preferred one. The technical drawings and the scheme of the machine are already in production. In the meanwhile we are defining the administrative details to assure the faster possible procedure.

Concerning the task 7.3 we are still waiting for the new prototypes. In the meanwhile a full work of preparation for the new tests has been performed. A lot of simulations have validated the

models as far as the thermal response, the multipacting activity and the Q ext parameter are concerned. Actually we are calculating the transverse kick effect of the coupling field of the prototypes couplers in the cavity on the beam.
Few technical modifications have also been implemented in the conditioning station to be able to receive the new prototypes.
A lot of experience is been acquired working on the conditioning of the TTFIII couplers. All the improvements on the conditioning procedure that have been studied in this activity will be applied to the new prototypes conditioning studies. Actually the TTFIII couplers are been tested in DESY on a SC cavity giving excellent results.

Status of money spending

	Spent money	**Value of new orders/ contracts**	**Expected spending of new orders/contracts until end 2004**	**Sum of column 2 & 4**
Travel	*17100*			
Consumables	*45100*			
Manpower	*56400*			
Durable	*313000*			
Overheads	*22600*			
			Total sum	

Updating of MS-Project

N°	Task Name	Anfang	Ende
7.1	**New Prototype Coupler**	**Do 01.01.04**	**Sa 15.07.06**
7.1.1	RF Simulations of Coupler	Do 01.01.04	Mi 30.06.04
7.1.2	Report on Simulation	Mi 30.06.04	Mi 30.06.04
7.1.3	Detailed Engineering Drawings	Do 01.07.04	Fr 31.12.04
7.1.4	Engineering complete	Fr 31.12.04	Fr 31.12.04
7.1.5	Call for tenders	Mo 03.01.05	Fr 01.04.05
7.1.6	Prototype Fabrication in Industry	Di 05.04.05	Mi 31.05.06
7.1.7	Low Power tests	Mi 31.05.06	Fr 30.06.06
7.1.8	**Ready for High Power Tests**	Sa 15.07.06	Sa 15.07.06
7.2	**Fabrication of TiN Coating System**	**Mo 03.01.05**	**Fr 01.12.06**
7.2.1	Mechanical design of vacuum chamber	Mo 03.01.05	Fr 29.04.05
7.2.2	Fabrication drawings	Mo 02.05.05	Di 30.08.05
7.2.3	Construction of vacuum chamber	Do 01.09.05	Fr 01.09.06
7.2.4	Define vacuum needs	Mo 03.04.06	Fr 30.06.06
7.2.5	Appropriation of vacuum equipment	Mo 03.07.06	Sa 30.09.06
7.2.6	Design of electronic circuitry	Do 01.09.05	Do 30.03.06
7.2.7	Fabrication of electronics in industry	Mo 03.04.06	Fr 29.09.06
7.2.8	Installation and Test at Orsay	Mo 02.10.06	Do 30.11.06
7.2.9	**First Window Coating**	Fr 01.12.06	Fr 01.12.06
7.3	**Conditioning Studies of Proto-type Couplers**	**Mo 02.01.06**	**Fr 30.11.07**
7.3.1	Conditioning of couplers	Mo 02.01.06	Fr 30.11.07
7.3.2	Evaluate conditioning results	Mi 04.01.06	Fr 30.11.07
7.3.3	**Final report on conditioning**	**Fr 30.11.07**	**Fr 30.11.07**

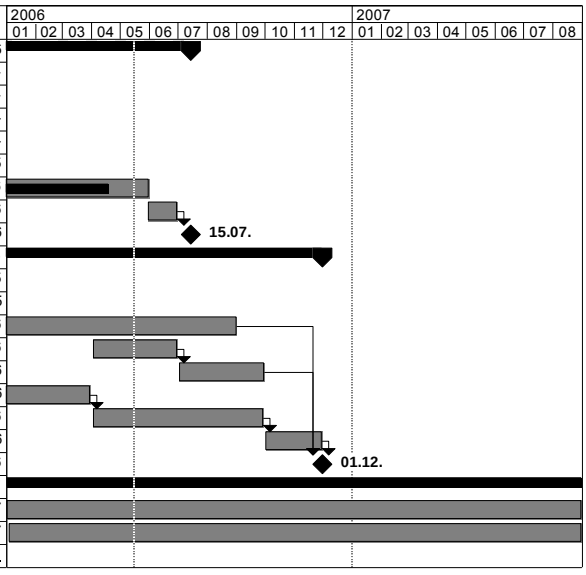

Work package 8: Tuners

Task 8.1 UMI Tuner

The new INFN coaxial blade tuner is an evolution of a coaxial tuner solution we originally developed for TTF superstructures and that performed as expected in terms of stiffness, frequency sensitivity and tuning capabilities both in CHECHIA and during TTF operations. Now, in order to compensate the Lorentz forces detuning foreseen at 35 MV/m, fast elements have been integrated in the tuning system. The tuner construction is finished, as well as the modified helium tank, which have been split in two halves joined by a bellow in order to allow the variation of the cavity length. All the parts have already been constructed by ZANON, and the assembling of two complete prototypes, has been done.
The two cavities helium tanks are shown in figure 1, where the welded titanium rings to support the coaxial tuners and the bellows to accomplish the tuning movements can be seen. Four stiffener bars are inserted. They can be used both for transportation and safety means in case of piezostack breakdown.

Figure 4: TTF cavities modified helium tanks

The ring-blade assembly that provides the slow tuning to the cavity is shown in figure 2. This is the main tuner mechanism and consists of a three-ring bending system. One of the external rings is rigidly connected to the helium tank, while the central one is divided in two halves. The rings are connected by welded thin titanium plates (blades) at an angle which transforms the azimuthally rotation (in opposite directions) of the two halves of the central ring into a variation of the distance between the end rings, producing elastic change of the cavity length.

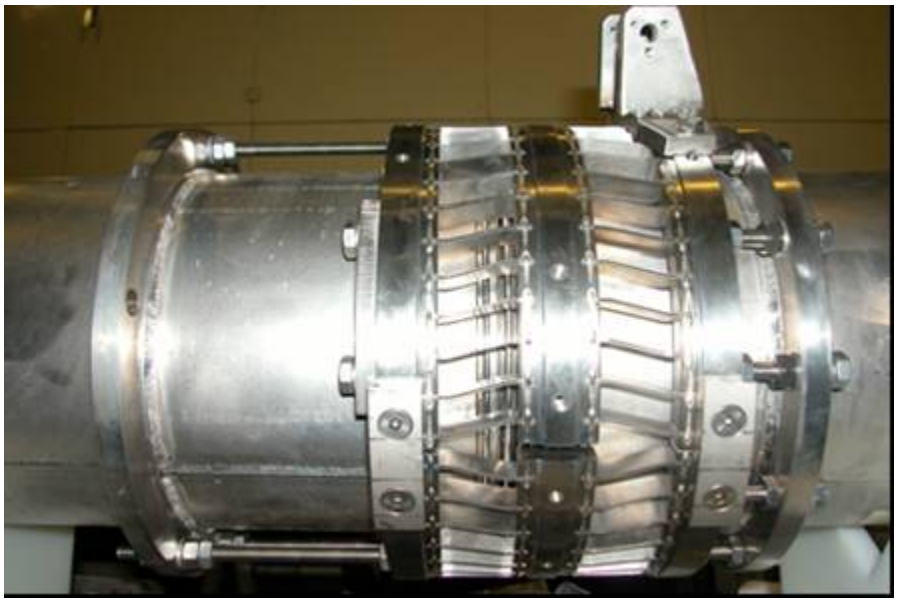

Figure 5: Ring blade assembly mounted on the helium tank.

Each tuner can accommodate up to four piezostack actuators. This part, during operation, can provide the fast tuning capabilities needed for Lorentz force detuning compensation and microphonics stabilization. A 40 mm length aluminum dummy piezostack mounted on its support, in order to verify the mechanical constraints, with-out risking damaging the real piezostack actuators (see figure 3). The cavity elasticity is used to provide the piezostack preload. During the first tests two Noliac 40 mm length and 10 mm^2 cross-section will be employed for each tuner, while longer piezostack actuators (70 mm) with 15 mm^2 cross-section, are already being acquired from Noliac for further testing.

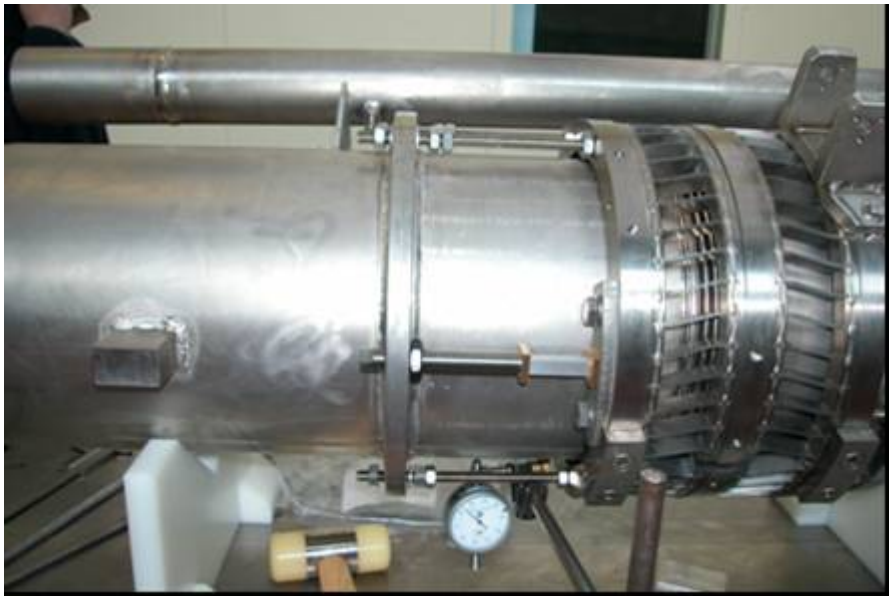

Figure 6: Dummy piezostack block inserted in the coaxial tuner

In figure 4 the leverage mechanism is shown. The azimuthally rotation of the central rings is provided by a leverage system connected to a stepping motor. The leverage system amplifies the

torque of the stepping motor, contemporarily increasing the tuning sensitivity. A movement test has been performed at the machine shop with the motor connected to its electric driver. The system performed satisfactory but only ±1.2 mm of axial displacement has been achieved, due to a non optimized provisional assembling. With the proper assembling the axial displacement foreseen for the blade tuner is w = ±1.5 mm.

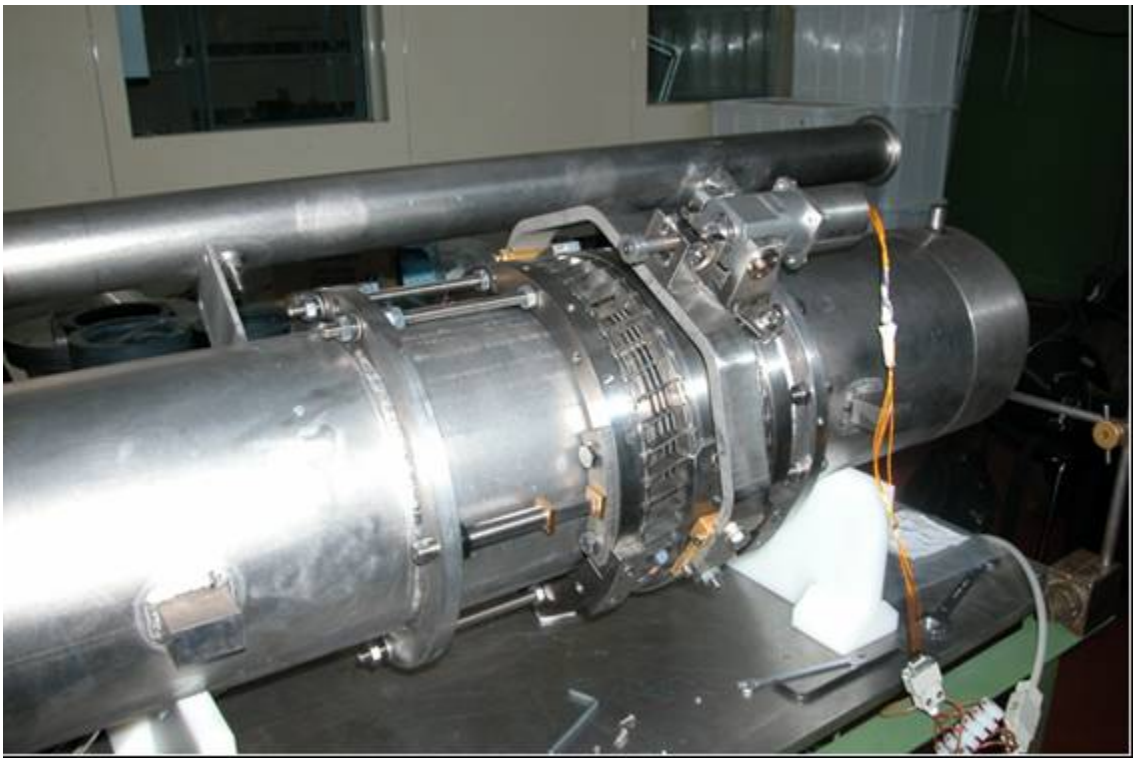

Figure 7: Complete assembly provided with leverage mechanism and stepping motor.

Now the tuning assemblies are at DESY waiting for the cavities to be welded to the helium tanks. After this operation, two cold tests will be performed at DESY and BESSY facilities.

Updating of MS Project

N°	Task Name	Anfang	Ende
8.1	**UMI TUNER**	**Do 01.01.04**	**Mo 31.12.07**
8.1.1	Control electronics	Do 01.01.04	Fr 02.07.04
8.1.2	Mechanical tuner design, leverage system/motor	Mo 03.01.05	Do 29.09.05
8.1.3	Integration piezo design	Mo 03.01.05	Mo 09.05.05
8.1.4	Choice of transducer/actuator	Mo 09.05.05	Mi 10.08.05
8.1.5	**Report UMI tuner**	Mi 10.08.05	Mi 10.08.05
8.1.6	Tuner fabrication	Mi 10.08.05	Di 07.02.06
8.1.7	Piezo fabrication and bench tests	Di 07.02.06	Di 06.02.07
8.1.8	Cavity-tuner-coupler integration	Mi 04.01.06	Sa 30.06.07
8.1.9	Pulsed RF tests	Mo 02.07.07	Mo 31.12.07
8.1.10	**Evaluation of tuner operation**	Mo 31.12.07	Mo 31.12.07

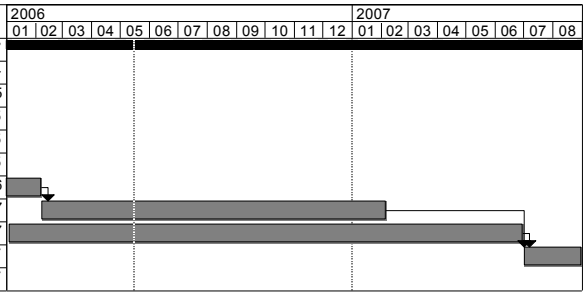

Task 8.2 Magnetostrictive tuner

The prototype of magnetostrictive tuner is ready for the test with the cavity. The control system as well as the driver is already prepared. Due to the movement of the CRYHOLAB stand test the proper experiment with magnetostrictive tuner is postponed. According to the recently updated schedule, the test will be performed before end of the 2006.
The control algorithm was developed for both piezostack and magnetostrictive operation. The test with piezostack mounted in VUV-FEL shows that the Lorentz force was compensated in at least 4 steps by 90% for gradient of 20MV/m.

Updating of MS-Project

N°	Task Name	Anfang	Ende
8.2	**Magneto-strictive Tuner**	**Do 01.01.04**	**Di 31.01.06**
8.2.1	Complete specification	Do 01.01.04	Fr 30.01.04
8.2.2	Conceptual design	Mo 02.02.04	Mi 31.03.04
8.2.3	Prototype and performance evaluation	Do 01.04.04	Fr 04.02.05
8.2.4	Finalize tuner and drive electronics design	Do 01.07.04	Do 14.04.05
8.2.5	Test of tuner	Do 14.04.05	Di 31.01.06
8.2.6	**Report on magneto-strictive Tuner**	Di 31.01.06	Di 31.01.06

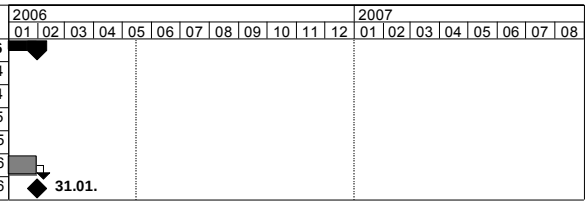

Task 8.3 CEA Tuner

The fabrication of the new CEA tuner is finished. The tuner was mounted in CRYHOLAB and then tested. The detailed report of the investigation is in charge of WP 10.

Updating of MS-Project

N°	Task Name	Anfang	Ende
8.3	**CEA Tuner**	**Mo 05.01.04**	**Mi 01.06.05**
8.3.1	Design Piezo + Tuning System	Mo 05.01.04	Fr 18.06.04
8.3.2	Fabrication	Mo 21.06.04	Do 31.03.05
8.3.3	Installation RF	Fr 01.04.05	Mi 01.06.05
8.3.4	**Start of Integrated Experitments**	Mi 01.06.05	Mi 01.06.05

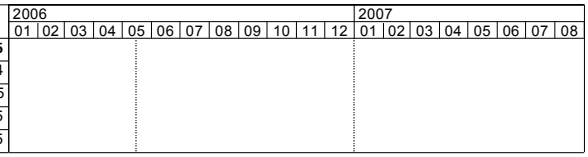

Task 8.4: IN2P3 activities

In the frame of CARE WP8, IPN Orsay had prepared two piezoelectric actuators PICMA#6 and PICMA#7 (Fig. 1) for their integration (item #8.4.5) in the new PiezoTuning System (PTS) developed at Saclay. As it is a critical part of the PTS, the fixture of the actuators was carefully designed in order to avoid shear forces and/or torsion forces to the actuator and fit very precisely (e.g. ~10 μm) into the PTS in order to avoid loss of mechanical contact during cool down to 2 K.

To fulfil these requirements, a cone on sphere system is used. In the actual PTS, the cavity acting as a spring is used for preloading the piezostacks.

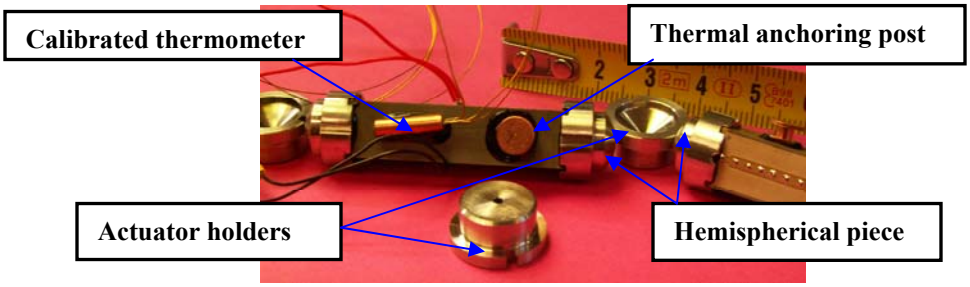

Fig. 1 : Piezoelectric actuators ready for integration into Saclay PTS

The critical dimensions were measured with a high precision in the industry (micrometer and 3D machine). In particular, the following overall lengths (Fig. 2) values (actuator and with their holders) were measured: L_6=51mm $_{-0}^{+5\mu m}$ and L_7=51mm $_{-0}^{+7\mu m}$ for the piezostacks PICMA#6 and PICMA#7 respectively.

Fig. 2: Definition of the overall length L

Moreover, each actuator is equipped with an Allen-Bradley thermometer which was calibrated (Fig.3) at IPN Orsay facility in the temperature range 1.56 K-71 K.

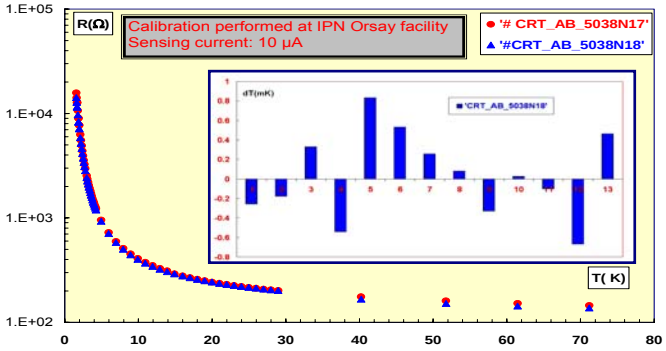

Fig. 3: Calibration curves and fit error histogram (insert) in superfluid helium region (1.56 K-2.1 K).

The actuators were integrated into the PTS then the assembly was mounted on the cavity C45 and installed in CRYHOLAB test facility (Fig. 4). The whole device is now ready for cryogenic tests which started on April 11, 2006.

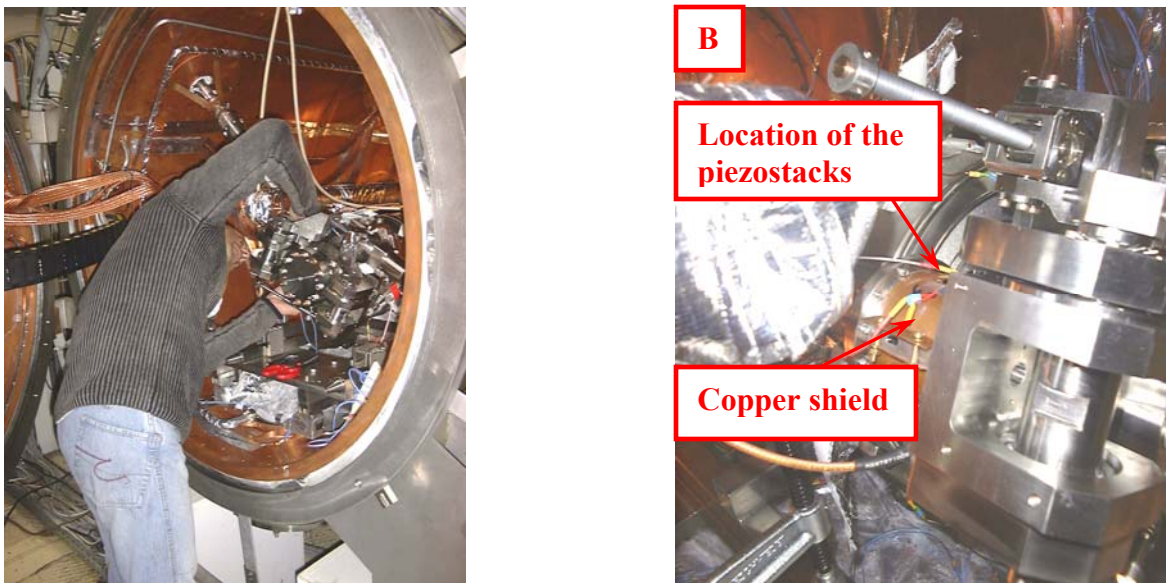

Fig. 4: A) Mounting the PTS in CRYHOLAB, B) close view to the fixture of actuators.

In order to investigate (subtasks #8.4.6 and #8.4.è) the electro-acoustic behaviour of the TESLA cavity #C45 and to measure the performance of the PTS developed at Saclay with PICMA actuators, the following tests in CRYHOLAB were performed during three weeks (10-27 April 2006):

1) Measurements of the transfer functions,
2) Study of the mechanical modes of the cavity including quality factors,
3) Measurements of the actuators response to the applied preloading force,
4) Study Lorentz detuning and detuning compensation with PTS (Pulsed RF tests).

The measurements (items#1-3) are finished and good results were obtained: the experimental data will be presented and discussed in a next report. The pulsed RF tests were started: the status of this activity is summarized in WP#10 quarter report (Cryostats integration tests).

Status of money spending

	Spent money	Value of new orders/ contracts	Expected spending of new orders/contracts until end 2006	Sum of column 2 & 4
Travel	*7.3*		*2.5*	*9.8*
Consumables	*28.7*		*10*	*38.7*
Manpower	*44.3*			*44.3*
Durable	*0*	*0*	*0*	*0*
			Total sum	*92.8*

Updating of MS-Project

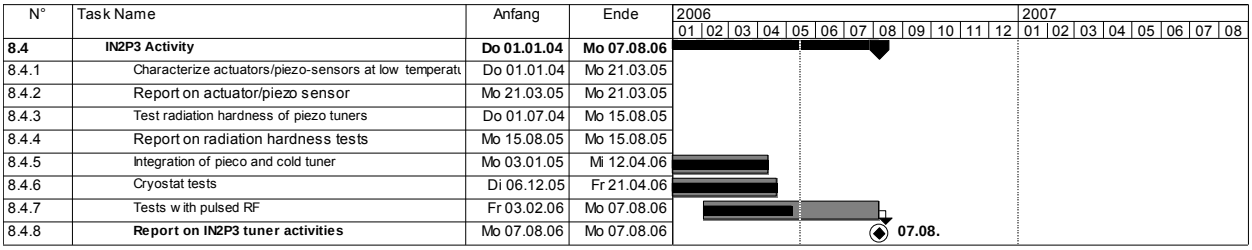

N°	Task Name	Anfang	Ende
8.4	**IN2P3 Activity**	**Do 01.01.04**	**Mo 07.08.06**
8.4.1	Characterize actuators/piezo-sensors at low temperatu	Do 01.01.04	Mo 21.03.05
8.4.2	Report on actuator/piezo sensor	Mo 21.03.05	Mo 21.03.05
8.4.3	Test radiation hardness of piezo tuners	Do 01.07.04	Mo 15.08.05
8.4.4	Report on radiation hardness tests	Mo 15.08.05	Mo 15.08.05
8.4.5	Integration of pieco and cold tuner	Mo 03.01.05	Mi 12.04.06
8.4.6	Cryostat tests	Di 06.12.05	Fr 21.04.06
8.4.7	Tests w ith pulsed RF	Fr 03.02.06	Mo 07.08.06
8.4.8	**Report on IN2P3 tuner activities**	Mo 07.08.06	Mo 07.08.06

Work package WP 9: LOW-LEVEL RF (LLRF)

9.1 Operability and technical performance

9.1.1 Transient detector

Progress: In line with schedule.

During the reporting period transient detection system was improved with fine-tuning circuitry for RF Notch filter adjustment. Two circuits based on different ideas were assembled and tested: fine-tuning with motorized attenuator and phase shifter and fine tuning with IQ modulator. The performed tests have proved the better efficacy of the second idea then the first one. With this new fine-tuning circuitry it is possible to keep the filter properly adjusted without temperature stabilization. IQ modulator can constantly adjust magnitude and phase with feedback to keep it correct with an accuracy of 1e-3 degree in phase and 1e-5 in magnitude (Figure 8, Figure 9). With this new concept transient detection system is able to run continuously without interruption.

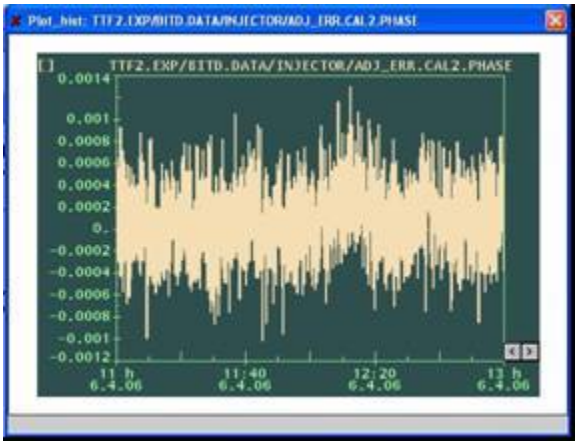

Figure 8 RF Notch filter phase adjustment error [deg]

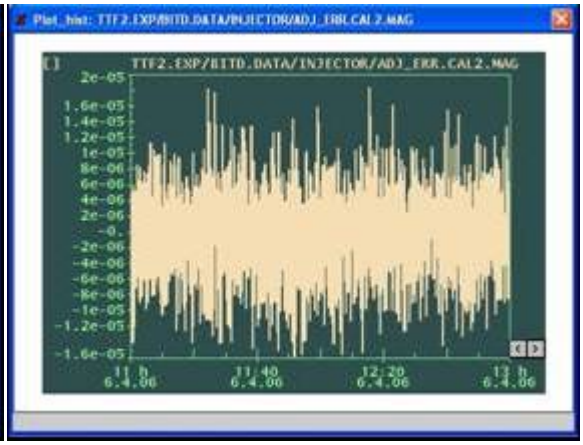

Figure 9 RF Notch filter magnitude adjustment error

Concepts for transient detection system cost reduction were proposed. One of these ideas is based on the use of fast integrators. With them it will be not necessary to use high-speed ADC boards. To test this idea algorithms used in this method were implemented in currently running system. These tests have finished successfully.
Measurement accuracy can be improved by reducing measurement noise. The idea with moving amplifier to the front of the filter was tested and tests showed that this way measurement noise could be reduced.
System for transient detection was tested during March accelerator studies period. These tests were successful and showed that the system is working correctly and in conformance with the theory. Measurement results are available in TTF logbook (http://ttfinfo.desy.de/TTFelog/):
/TTFelog/data/2006/12/25.03_n
/TTFelog/data/2006/12/25.03_n
/TTFelog/data/2006/11/19.03_M

Milestones and deliverables: None defined in contract for this period
Significant achievements and impact:
Filter for transient detection was improved with fine-tuning circuitry. This circuitry can continuously adjust filter to keep required filter attenuation.
Deviations from plan:
None

9.1.2 LLRF Automation
Progress: In line with schedule.

Automation:
During first three months of 2006 the following pieces of system have been improved and preliminarily put into practice.

Finite State Machine for RF-power station:
This part of the solution is implemented as regular Finite State Machine and its role is to facilitate the process of automation of the RF-power station. Automaton cares for proper hardware startup, shutdown, and attempts to guard preset high voltage level and quality. Due to the fact that FSM deals with very expensive and operation critical elements some aspects of safety had to be considered. Many of the machine/operation safety aspects are assured by design.

One of important features of FSM design was to make it easy to deploy among different power-stations so the FSM structure is abstracted to the level that it deals with only very general aspects of automation. Details concerning communication with the hardware are seamed in Matlab scripts, which compiled binary versions are invoked by the automaton.

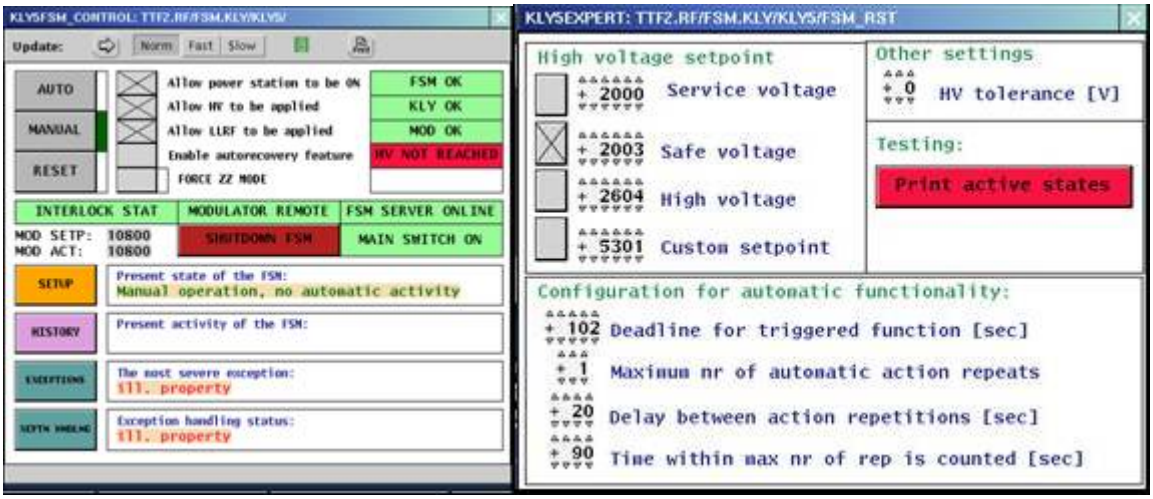

Figure 10 Main panel of the FSM explains what are the basic features of the solution.

Rule-based exception handler for RF-power station:
This part deals mainly with information coming from technical interlock system and its role is to facilitate exception handling, automatic recovery, and operator's decision support capabilities. Solution is based on rule-based knowledge base classifying the interlock signals and their compounds into four main categories:

Implementation of the exception handler has been performed in Prolog. Virtual machine of the

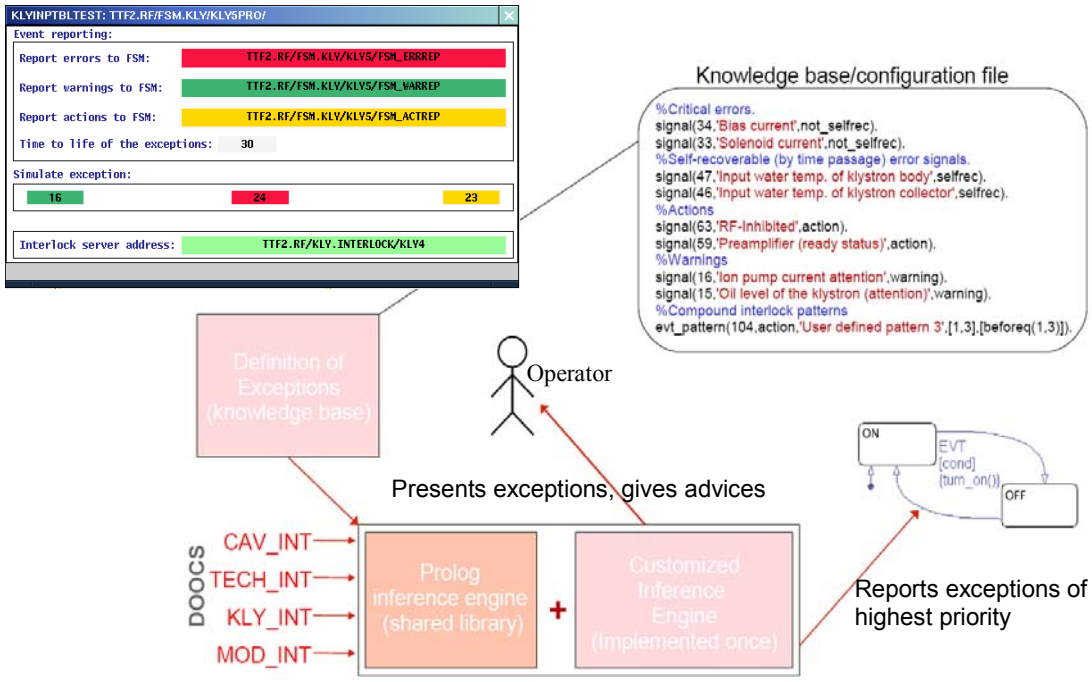

Figure 11 Conceptual view on exception handler

Pro log has been dynamically linked to the DOOCS server. Precompiled byte-code of both the knowledge base and set of rules is being automatically compiled along with DOOCS server sources and than merged to the image of the process.

During initialization virtual machine finds the base and rules. Then servers starts to listen to the interlock signals. Encountered patterns of interlock signals are matched and recognized, than decision mechanism implemented as a set of Prolog's rules attempts to guess most significant (probably causal) pattern. When “guilty” pattern is recognized, it is then passed to the state machine that if in automated mode allows the “remedy” procedure to be fired.

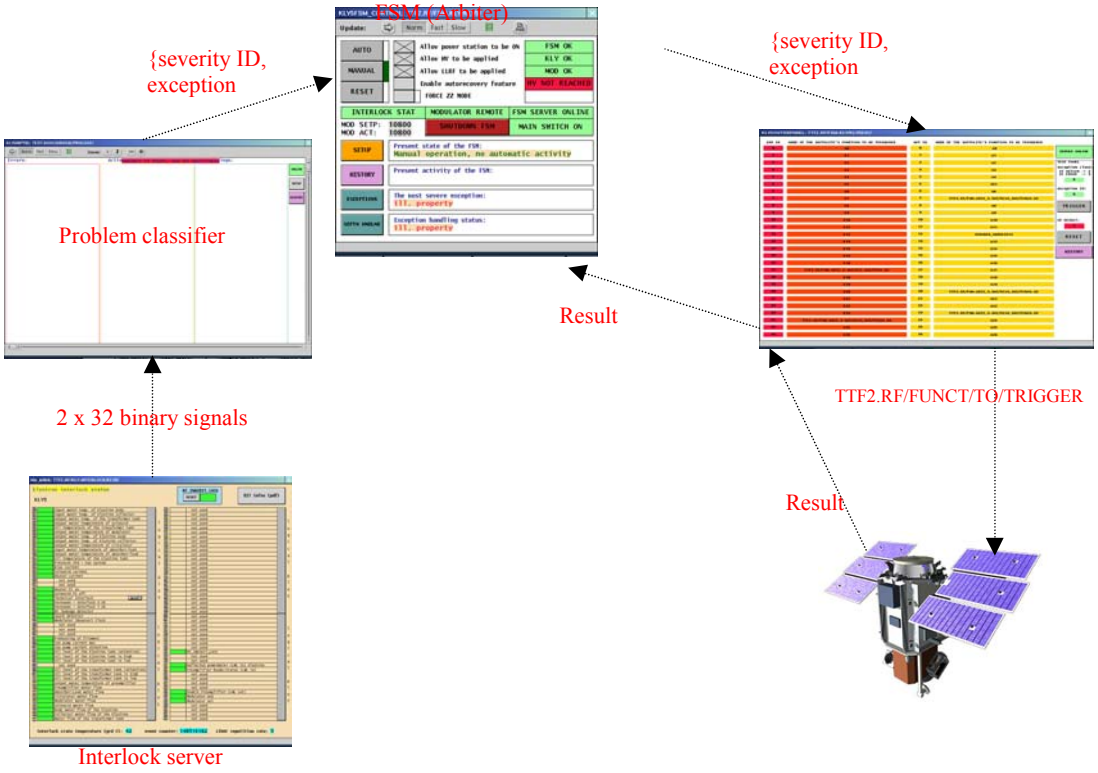

Figure 12 Cooperation of the FSM with exception handler

RF Power station automation - Klystron and preamplifiers nonlinearities characterization and linearization.

The klystron 5 high power chain – characterization:
After installation of the new vector modulator a set of measurements was performed in order to characterize work of the preamplifiers and the klystron itself for the different supplying high voltage settings and driving signal parameters (like different signal amplitude level and phase angle).
In order to provide measured signal representation in amplitude and phase coordinates dedicated Matlab scripts for data processing had been created. They allow to distinguish between nonlinearities introduced by the klystron and preamplifiers in amplitude and this in phase.
The AM/AM and PM/AM characteristics of high power chain including klystron 5 working with standard operation conditions (high voltage level at 115kV, pulse length 1,7ms) are presented in figure 7.
As other measurement shows a phase perturbation (deviation) may not only be caused by the klystron tube but also can be introduced by the second (driving) preamplifier. Comprehensive study on work performance of driving preamplifier (the device that has been proposed for driving new klystrons in VUV or XFEL project) gave rise to defining new requirements for amplifier vendors concerning device phase stability and available power margin.

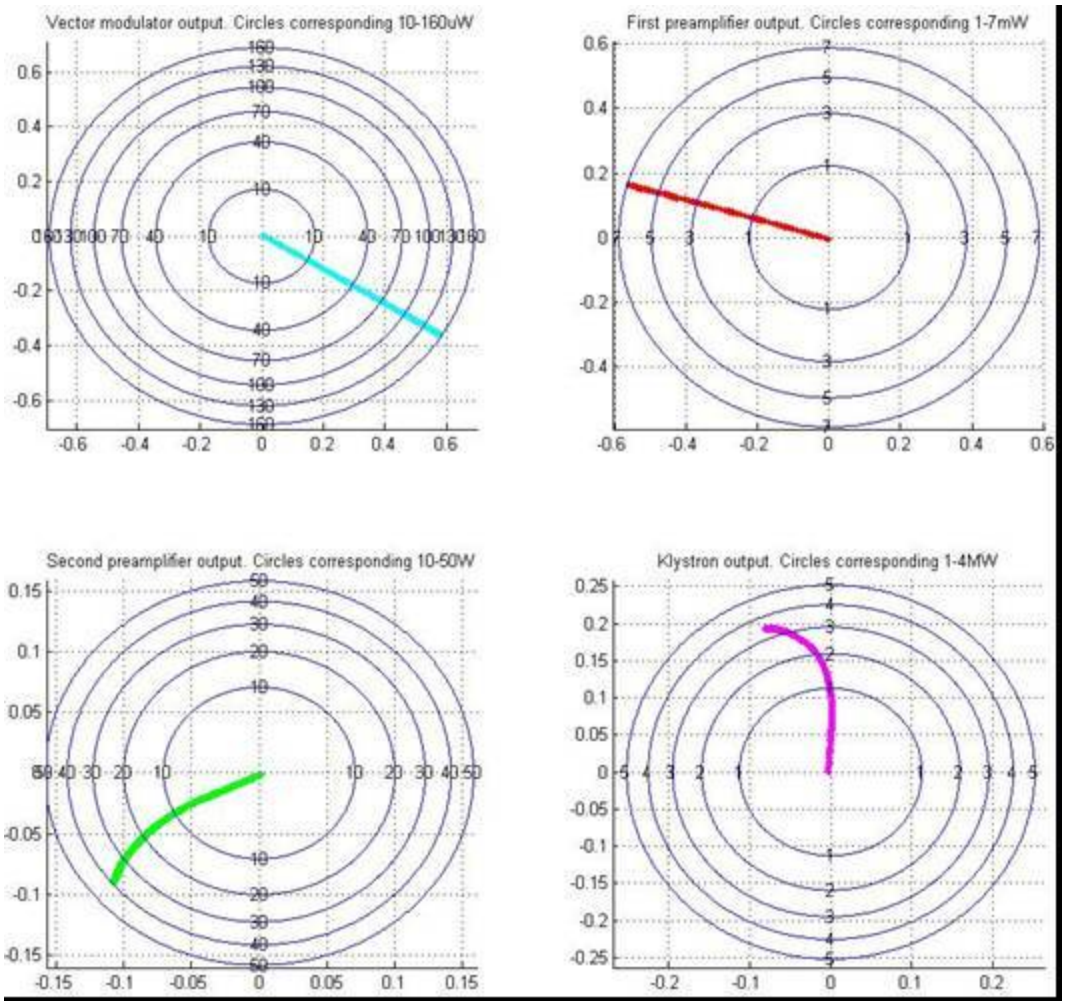

Figure 13 High power chain components response measurement for dedicated driving signal level change.

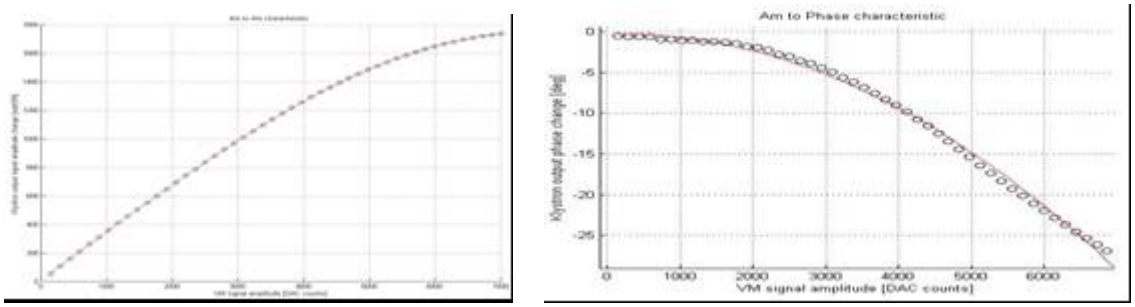

Figure 14. AM/AM and PM/AM characteristics of high power chain (concerning klystron5)

Amplitude and phase deviation caused by the klystron and amplifiers nonlinearities cancellation

In order to provide linear response of the high power chain components for the LLRF field controller driving signal a new idea for HPC characteristic linearization had been proposed. First

test of the linearizer had been performed. Because of the existing system infrastructure and capabilities the most efficient solution would be a compensator working in predistorter configuration. The idea of predistorter base on introducing distortions to requested input signal before it reaches first preamplifier or even vector modulator. Introduced distortions are prepared in such a way that including nonlinear behavior of system the response on given input signal would be linear (constant gain, no phase deviation).
Although different realization of this idea is studied now there were test performed using predistorter designed using Matlab environment .
The test was performed on the high power chain (kly5) connected to the super-conducting cavities modules ACC2 and ACC3 in VUV-FEL accelerator tunnel. During the test both configuration – open and close feedback loop operation were used with and without nonlinearities effects compensation.
In open loop operation just an adaptive feed forward algorithm had been used for shaping the driving signal.

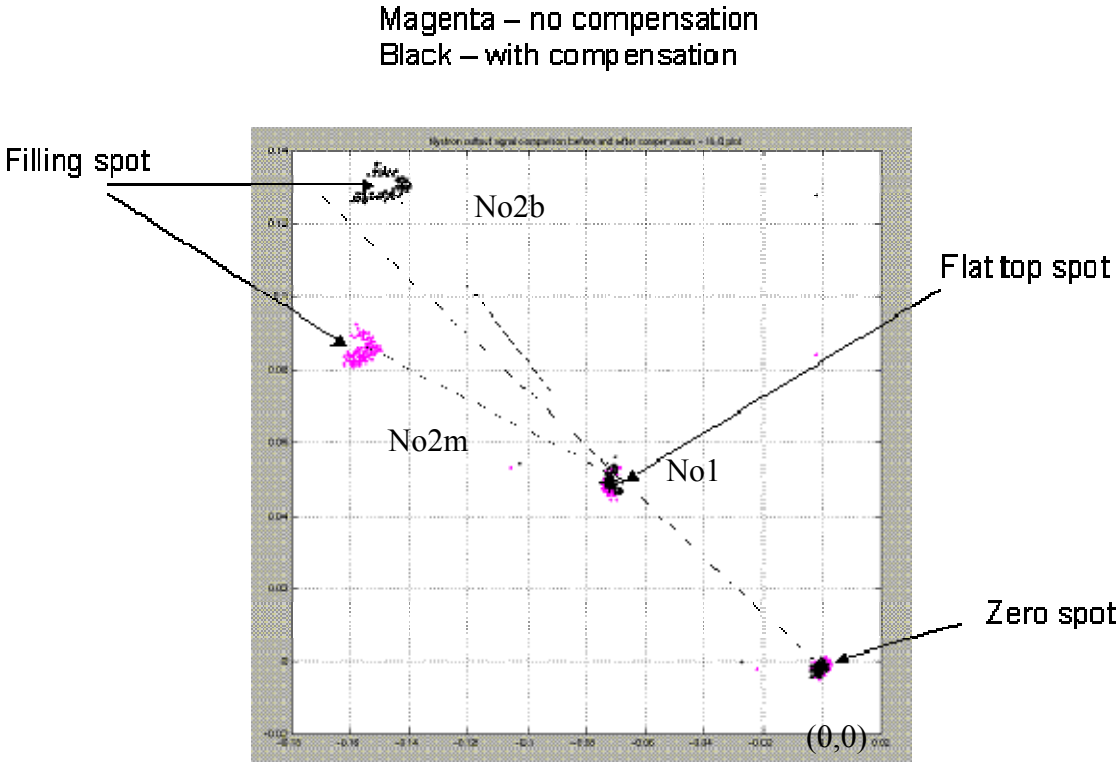

Figure 15. Klystron output measurement – field vector comparison for open loop operation with (black spots) and without (magenta spots) correction - I&Q coordinates.

As it is presented in figure 8. the correction introduced by the predistorter (that had modified the feed forward tables – according to the measured characteristics) shows improvement in the system response. This can be observed from the spots placement (black ones almost in one line) that corresponds to the driving signal phase. As one can notice the distance form the black spot (no2b) to the line that crosses No1 and (0,0) point is shorter in black case than in magenta case (no2m) that corresponds less phase deviation for module work with compensation.

Close loop test also showed that both expected amplitude and phase of the klystron output signal better fits to requested one when the compensator had worked. Especially this driving parameters

improvement could be noticed for signals with higher power level – where nonlinearities are more significant

VUV-FEL LLRF Automation Scheme

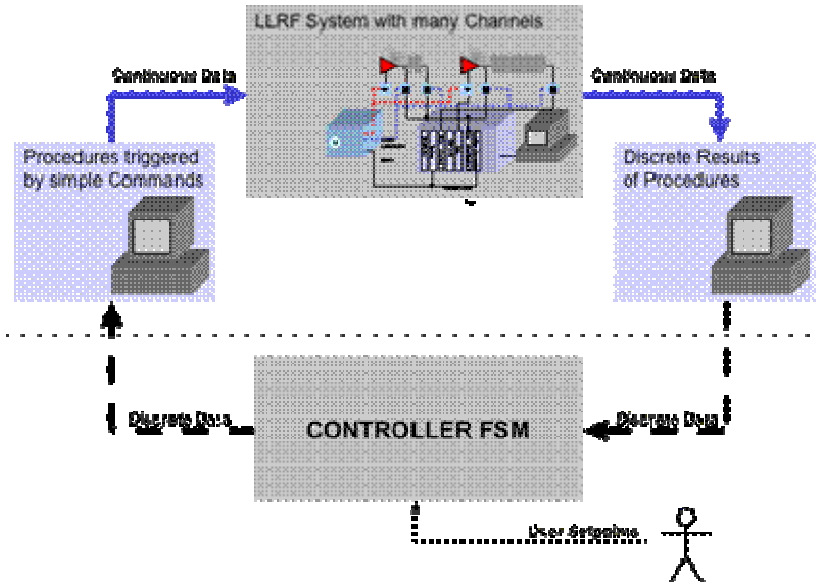

Figure 16: Quantization of the LLRF system by means of procedures.

Finite state machines (FSMs) model time-discrete systems with quantized input and output data flows. The complex VUV-FEL LLRF system surely is not time-discrete and quantized, but an appropriate set of procedures can make it look discrete to the outside world. Figure 1 depicts the major elements of the VUV-FEL LLRF automation scheme. The continuous LLRF system is accessible only via procedures that execute defined tasks like ‘measure data quality’, ‘apply loop phase correction’ or ‘ramp-up the feedback gain’. Every procedure returns a quantized result like ‘data quality is good’, ‘loop phase corrected’ or ‘feedback gain successfully ramped’. Based on this discretization, the controller FSM (see figure 1) can implement a strategy that meets the operator’s specifications. The VUV-FEL LLRF automation scheme has been developed with the premise that the VUV-FEL is a developing system that requires a flexible automation with easily reconfigurable finite state machines and a flexible procedure server that allowes to quickly adapt the system to a changing environment. The attachment of procedures that leads to an appropriate quantization had to be. Subsystem experts shall be able provide their procedures without awareness of the automation scheme. Therefore we developed a three-layer approach to attach procedures to the automation scheme by introducing procedure servers. The procedure server (middle layer) presents itself towards the controller FSM (top layer) as whatever is the preferred communication medium of the FSM implementation. It can, for example, be the accelerators control systems communication protocol. For the implementation at VUV-FEL we chose the DOOCS remote procedure call (RPC) protocol for communication between the FSM and its procedure servers. The procedures (bottom layer) are compiled programs that are executed by the procedure server on request. The subsystem expert is free to choose any toolbox for the implementation of his procedure, he only has to comply to a convention that transports results of

the procedure back to the procedure server. This can easily be done via a local file system, if the procedure server resides on the same physical server as its procedures.

Milestones and deliverables: None defined in contract for this period
Significant achievements and impact:
Implementation of the exception handler for RF station, design of prototype system for klystron linearization.
Deviations from plan: None

9.1.3 Control Optimization

Beam loading compensation using beam monitor signals

At the DESY Vacuum Ultraviolet Free Electron Laser (VUV-FEL) bunch compression and the SASE effect are (amongst other parameters) sensitive to beam energy and beam phase variations. Bunch compression requires bunches accelerated off crest the rf field to obtain an energy chirp from the bunch head to the tail. Variations of the rf phases in the accelerating modules upstream the bunch compressors decrease the compression efficiency. Transient beam loading causes most of these variations.
For optimal treatment of beam loading transients, we started to use information of beam intensity monitors in addition to the rf field probes. In March 2006 we managed to set up first algorithms within FPGAs calculating bunch charge proportional values from bunch to bunch in real time and verified their performance in reality.
Together with the AFF algorithms, tested at the rf gun control, both measures together should significantly improve the control stability in the accelerating modules upstream the bunch compressors significantly. The methods are expected to be fully proofed in praxis towards the end of 2006.

9.2 LLRF cost and reliability

9.2.1 Cost and reliability study

Progress: In line with schedule.

9.2.2 Radiation damage study

Radiation measurements and calibration of RadMon 2.5 detector.
The report concerns development of radiation tolerant read-out system for neutron and gamma radiation monitoring system. The system uses calibrated SRAM-based neutron detector and gamma sensitive RadFET. The memory is continuously scanned. Suitable information is sent to PC computer when SEU is detected. The number of induced SEUs is proportional to neutron fluence. RadFET is based on the dedicated p-type MOS transistor sensitive to gamma. Gamma radiation creates defects in widen MOS gate silicon dioxide and silicon-oxide interface. Because of generated defects MOS parameters are modified, like threshold voltage. Threshold voltage is measured when 10 μA current flows through RadFET. The converted signal is sent to PC computer and collected together with measured SEU in database.

Memory supply voltage was decreased and polyethylene moderator was applied to enhance the sensitivity of SRAM-based detector to neutrons. Four RadMon 2.5 devices were installed in VUV-FEL tunnel. The results of the radiation measurement for 1 and 2 MB memories are presented in figure 9. The first system cooperates with 1 MB SRAM and detected 900 SEU. When the same type memory was installed in 6 cm in diameter moderated the number of SEU increased up to 6500. The same number of SEU were detected by third system using 2 MB (4x512 KB) memory module. When the memory module was housed in 9 cm moderator, 26000 SEUs were detected. Therefore, application of selected memories and suitable moderator allows to increase the sensitivity to neurons almost 30 times. The moderator was designed using MCNP 4a code.

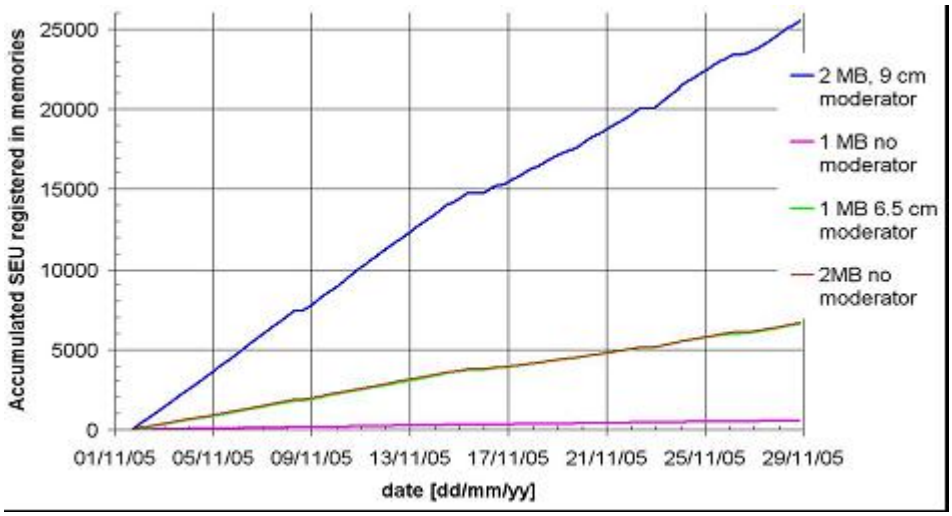

Figure 17. Accumulated SEU number measured in VUV-FEL for 1 and 2 MB memories and two different moderators.

The calibrated system equipped in sensitive SRAM and RadFET were installed in VUV-FEL tunnel for 27 days. The results are presented in figure 2. The neutron detector was calibrated "in-situ" using bubble dosimeters. Thus, the calibration factor was calculated to express the relationship between induced SEUs and neutron fluence. 2 MB memory was supplied form 3V. The shape of registered accumulated gamma dose resembles neutron fluence detected by SRAM, because the bremsstrahlung gamma and photoneutrons are produced during beam and dark current collisions with niobium cavity walls.

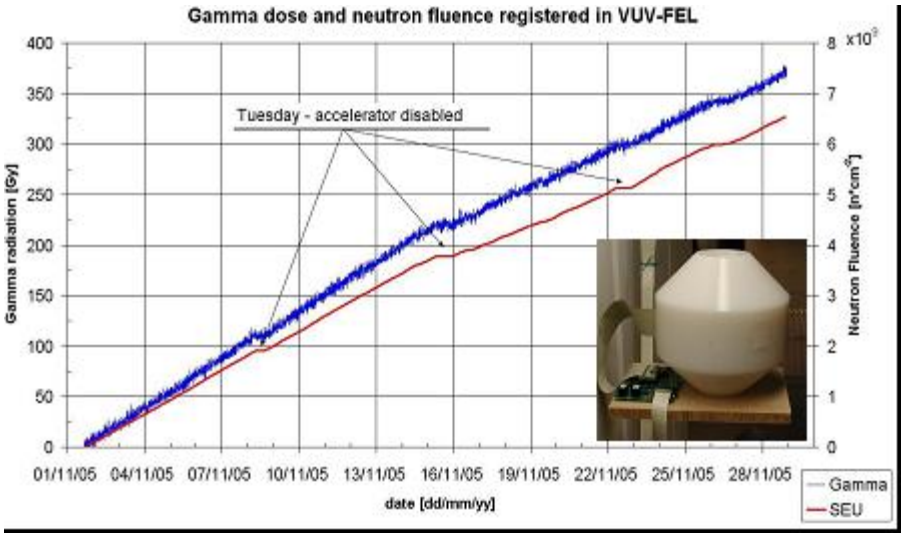

Figure 18. Accumulated neutron fluence and gamma radiation measured in VUV-FEL tunnel within one month.

Radiation tolerant microcontroller – RadMon 3.0

Another version of read-out system was built using radiation tolerant microcontroller implemented in FPGA. The microcontroller has been built using APA 600 FPGA. The device is presented in figure 11. It is a Flash based-FPGA, which stores its configuration in Flash memory. The configuration is used directly from Flash during device's operation. Flash memory is immune to soft neutron induced effects, rendering the FPGA's configuration resistant to unpredictable change due to SEU. However, contents of Flash may be erased by gamma radiation, if exposed to it for extended time. The drawback of using Flash based FPGA is lower maximum frequency, as compared to SRAM-based devices.

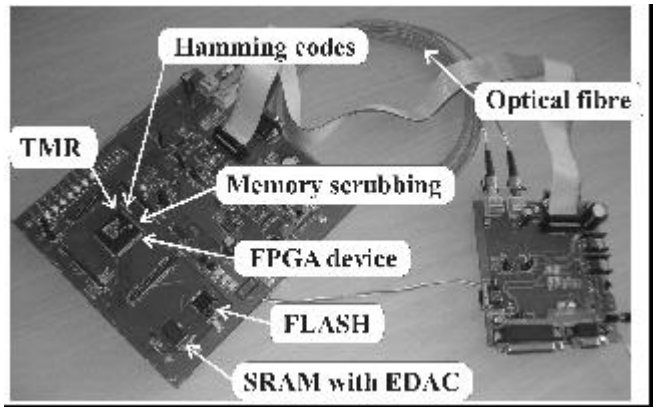

Figure 19. Radiation tolerant microcontroller

Architecture of radiation tolerant microcontroller

The microcontroller is based on the PIC16C57. The basis for development was a description of processor core written in VHDL, published under GNU General Public License (GPL) on

opencores.org. The basis core is significantly limited according to PIC16C57 specification. It is also impaired by several errors. Therefore, some corrections were necessary.
The resources in the microcontroller, which are susceptible to SEUs, can be divided into the two categories

- components based on SRAM, both embedded in the FPGA and external
- Finite State Machines (FSM)

For protection of SRAMs for microcontroller purposes, the scrubbing technique connected with use of the Hamming codes has been applied. This redundancy has to be embedded in the description of the design. No algorithm for automatic or semi-automatic code generation has been implemented for the purpose of this design.
The techniques employed for protecting sequential components, such as FSMs or others, which rely on storing information in distributed memory elements, i.e. flip flops, is TMR. In the design, every D type flip flop is tripled. The three outputs are fed to the inputs of majority voting circuit. The majority voting circuit outputs the value indicated by at least two flip flops. The voting circuit is glitch free. The radiation tolerance or immunity of the majority voter is an important issue. The circuit is not protected against the influence of radiation. The SEU effect poses no threat on proper operation of the circuit, since the voter is purely combinatorial. The complete TMR D type flip flop is extended with error indication output. Whenever one of the sub flip flops is altered by SEU, the single error detection output is set. This may provide information on the level of vulnerability of distributed memory elements of FPGA to SEU. Once a register is mitigated with TMR, it should also be refreshed periodically, not to let errors accumulate. This, however, is done automatically. The clock is always supplied to the register's flip-flops, it is never gated or disconnected. If the condition for writing a new value to the register is not met, the value from output is written back on every active clock edge. This provides sufficient rate of refreshing register's contents.

Application of TRM in Libero IDE
The starting point in applying the TMR scheme is description of a component in VHDL. The next step is to synthesize the component. The process of synthesis is handled by dedicated tools. It follows the process of compilation, which transforms every description into RTL description. The RTL description is then used as a prerequisite for the synthesis process. During synthesis the RTL is mapped to the resources available in a particular FPGA device . Therefore, the synthesis results in a netlist, which can be either an industry standard EDIF netlist or a structural VHDL description. The VHDL description is much more human readable and can be easily modified. Later, every flip-flop in a netlist has to be replaced by an instance of the component, having the same pins as a regular flip-flop, but containing three flip-flop and a voter circuit. Special software tools have been created for this purpose. Then the circuit is synthesized again, followed by a standard place and route (Figure 12).

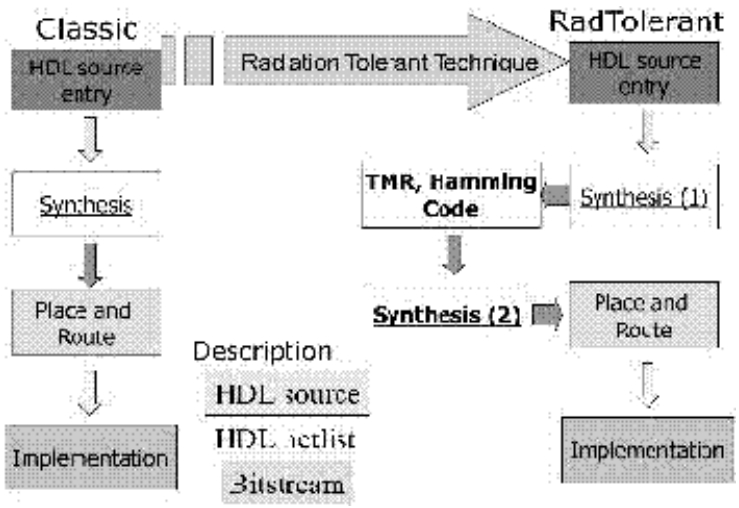

Figure 20. Radiation tolerant microcontroller

Using the radiation-tolerant microcontroller the system measuring the susceptibility of various SRAM modules has been implemented (see Figure 3). The system consists of a microcontroller and UART implemented in FPGA, external FLASH and SRAM program and data memories and a SRAM memory under test. The memory is periodically tested for SEU-induced errors. The results of the tests are periodically sent to a standard PC by a RS-485 or optical link.

The SRAM SEU detector was tested in DESY (Deutsches Elektronen Synchrotron). The test was run during 72 hours. The purpose of the test was to verify the designed MCU's behaviour under the mixed gamma and neutron irradiation. The device was installed in the LINAC II linear lepton accelerator. The SEU detector was placed in about five meters distance from the electron-positron converter, which generates high number of neutrons.
The monitoring station (PC computer running Linux operating system) together with transceiver was placed on the test bench, located in radiation free environment. The communication between PC and detector was carried over 50 meters long full duplex 62.5/125 micron multimode optical fibre. The bitrate was set to 9600 bps. No communication errors were observed. During the test period, 500 SEUs have been observed in the tested SRAM memory and five SEUs in the UART transmitter. The FPGA microcontroller-based detector was able to operate in rush radioactive environment.

The radiation hardened sCore kernel
The sCore is the modern, multitasking kernel, designed for real-time applications. The kernel has Round Robin scheduler and a preemptive environment. The sCore is written in the C++ language to be platform independent. Actually the kernel is implemented on the IA-32 architecture (implementation on the ARM platform is developed and the PowerPC will be next architecture). The most of kernel's structures are static and based on generic objects (C++ templates). This technique allows to avoid a dynamic memory management inside the kernel and moves a object's inheritance from a run-time to a compile-time. Static structures do not required an additional time to allocate memory therefore the system is more predictable and reliable. The basic functionality, such as device drivers manager, memory manager and scheduler were implemented in the kernel. All additional functionality can be realized in tasks outside the kernel.

This principle of operation is similar to the concept of micro-kernels. The sCore memory manager allows to create servers in a separate virtual memory (for a large systems) or in a flat memory shared with the kernel (dedicated for small, embedded systems).

The first version of the sCore kernel

The first version of the sCore kernel does not require Memory Management Unit dedicated to memory management and address translation. Main memory is organized as a flat memory by sCore. Every task can address all memory space. The method of address translation used by sCore on the IA-32 platform is shown on the figure 13.

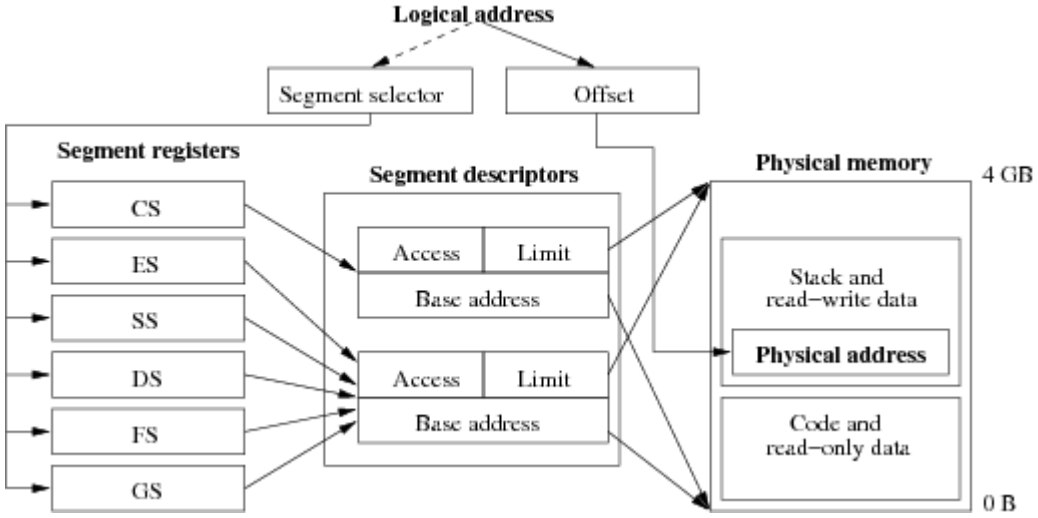

Fig. 21. The scheme of memory addressing in the first version of the sCore kernel.

This simple technique of memory management does not allow to design sophisticated fault tolerant algorithms. The only way to realize SEUs protections was to implement fault tolerant algorithms in special task called EDAC Task. The EDAC Task was described in previous reports. Moreover, a complete microkernel architecture can not be realized using the simple technique of memory management.

The second version of the sCore kernel

The second version of the sCore kernel was based on pagging mechanism. Pagging mechanism is a method to provide virtual address space for every task. Memory Management Unit is required by the second version of sCore. The scheme of address translation on the IA-32 architecture is shown on the figure 14. The main memory is divided equally to parts called pages. The 4 KB page size are used by sCore on the IA-32 platform. Every page is addressed by page table entries (figure 15). Apart from page address, additional attributes are stored in the page table entry. From SEUs protection point of view, the most interesting flags are:

1. *Accessed* (A) – Indicates whether a page has been accessed.
2. *Cache disable* (PCD) -When the PCD flag is set caching of page is not allowed. The issue of cache will be discuss later.
3. *Read-write* (R/W) – Indicates whether a page can be written or page can be only read.
4. *Present* (P) – Most important flag for discussed SEUs tolerant algorithm. When the flag is set the page is in the main memory (in physical sense) and task is allowed to use it. When

the flag is clear and some task tries to use it a page-fault exception (PF) is generated by processor. This flag is mostly used to realize swap technology by modern operating systems but sCore used it for SEUs protection.

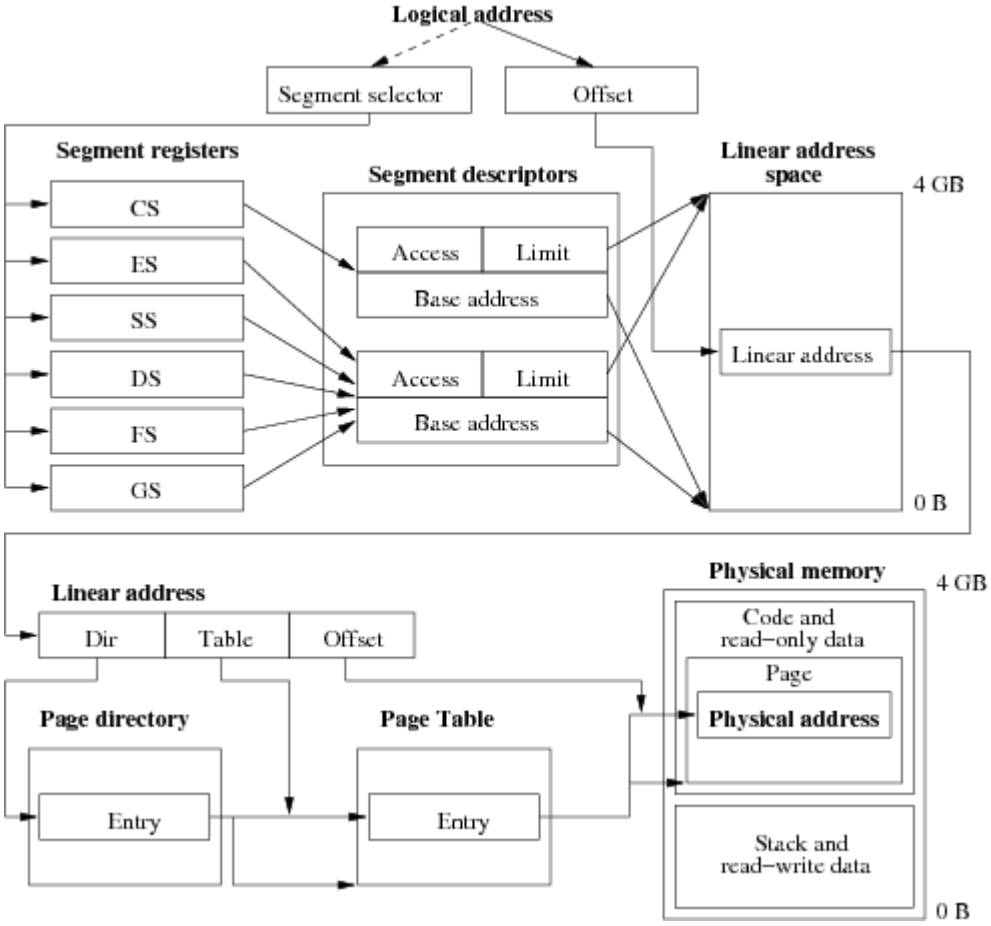

Fig. 22. The scheme of memory addressing in the second version of the sCore kernel.

The address translation manner is the main difference between flat memory model and virtual memory model. The physical address is reflected by logical address (one to one) in the first version of sCore. The second version of kernel allowed to translate any logical address to any physical address. This approach provide mechanism to realize complete microkernel architecture by separating address space for every modules and tasks.

Fig.* 23. *Page table entry.

The SEUs tolerant algorithm
The SEUs tolerant algorithm introduced by the second version of sCore is based on the paging mechanism. When the system is initialized (and also when new task is run) all pages are copied to two memory regions. All pages have cleared present bit (figure. 15) in every page table entries. When any task try to use memory - does not matter what kind, code, data, stack – page fault exception is generated by processor. Interrupt procedure compares page and copies using a triple voting technique. If contents of page is different from contents of copies the correct value is restored. When the task is preemptive by system scheduler all pages with set RW bit used during running time are copied to copies memory region. This mechanism guarantee that task has always valid contents of page (SEUs area corrected by ISR procedure). Compare to EDAC Task this approach is more efficient and reliable, but also slow. In simple words, EDAC Task in second version of sCore is moved from task to ISR procedure.

The influence of cache
Processor cache memory is undesirable and it is switch off. All page table entries have set Page-level Cache Disable.

Milestones and deliverables: None defined in contract for this period
Significant achievements and impact:
Development of a new version of SRAM based radiation on-line monitor RADMON,
development of radiation tolerate operating system.
Deviations from plan: None

9.3 Hardware

9.3.1 Multichannel downconverter

Progress: In line with schedule.

9.3.2 Third generation rf control

Progress: In line with schedule.

9.3.3 Stable frequency distribution

During the reporting period the Master Oscillator (MO) system concept was significantly improved. MO is the signal source for the frequency distribution system. A new MO system layout was developed basing on the experience with the previous MO version. The MO system was split in four 19 “ crates. The block diagram of the MO system is shown in the figure 9.3.3.1.

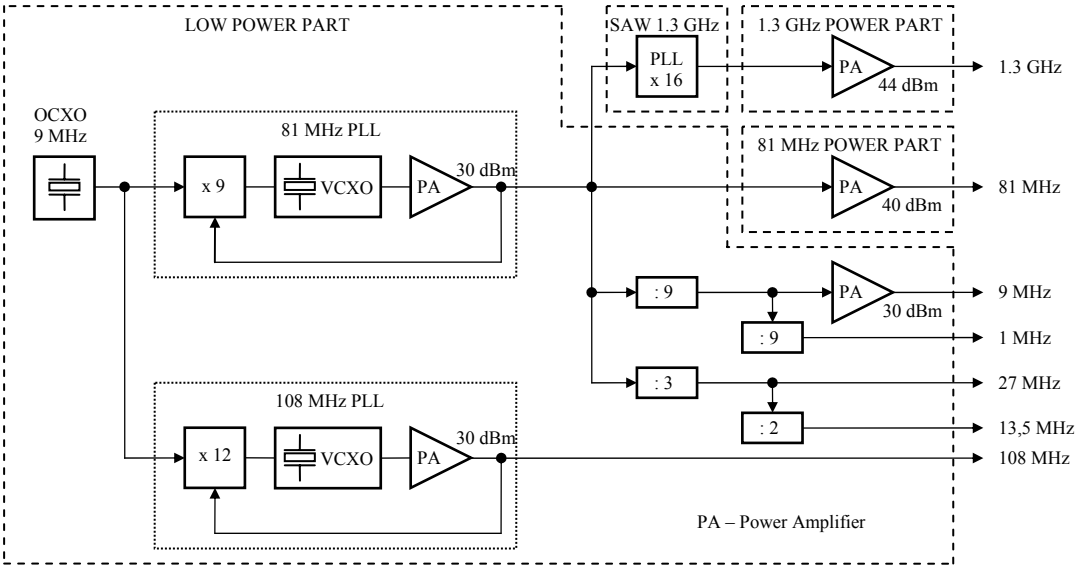

Figure 9.3.3.1 Master Oscillator System block diagram.

The main signal source (strict MO), which is the 9 MHz Oven Controlled Crystal Oscillator (OCXO) was located in the Low Power Part (LPP) of the MO system. A network of frequency multipliers and dividers was used to generate most of the signals with frequencies required in the accelerator system, synchronized with the OCXO. Those signals will be provided directly to the distribution system. The 1.3 GHz signal is generated out of 81 MHz in external PLL module called SAW 1.3 GHz. Both, 1.3 GHz and 81 MHz signals are amplified inside of separate crates called High Power Parts (HPP) intended to provide signal power in the range of 100 W. Those amplified signals will be further distributed with the use of two more crates with signal distribution components. Those crates are not treated as a part of the MO and they will not be addressed in this report.

Detailed design of each MO system crate was performed. As an example see figure 9.3.3.2 for the detailed block diagram of the Low Power Part. More diagrams will not be shown here because of the limited size of this report. The electronic components of the MO subsystems were mostly provided by the company Inwave. Besides the frequency generation and distribution components, each MO crate contains electronic system responsible for MO performance monitoring. Signals from the monitoring circuits can be displayed in the front plates of each crate. Additional connectors have been foreseen to provide those signals to external devices for the online use by the accelerator diagnostic system.

Mechanical design and assembly was performed for each MO crate. See figure 9.3.3.3 for the MO LPP assembly drawing. The LPP components have been assembled on both sides of the metal chassis located in the middle of the LPP crate. Therefore the drawing on the figure 9.3.3.3 contains two layers: top – black and bottom – yellow. Each frequency generation component was assembled in special, shielded housing that is supposed to minimize EMI problems and assure proper heat dissipation ad thermal inertia.

Figure 9.3.3.4 shows the front panel drawings for the MO LPP. Similar drawings have been prepared for each MO system crate but will not be shown here.
MO crates have been assembled and prepared are under tests during the time of writing of this report. See figures 9.3.3.5 and 9.3.3.6 for photographs of the assembled low power part.
In the nearest future the tests of the MO system will be finished in laboratory conditions and the system will be installed in the FLASH facility.

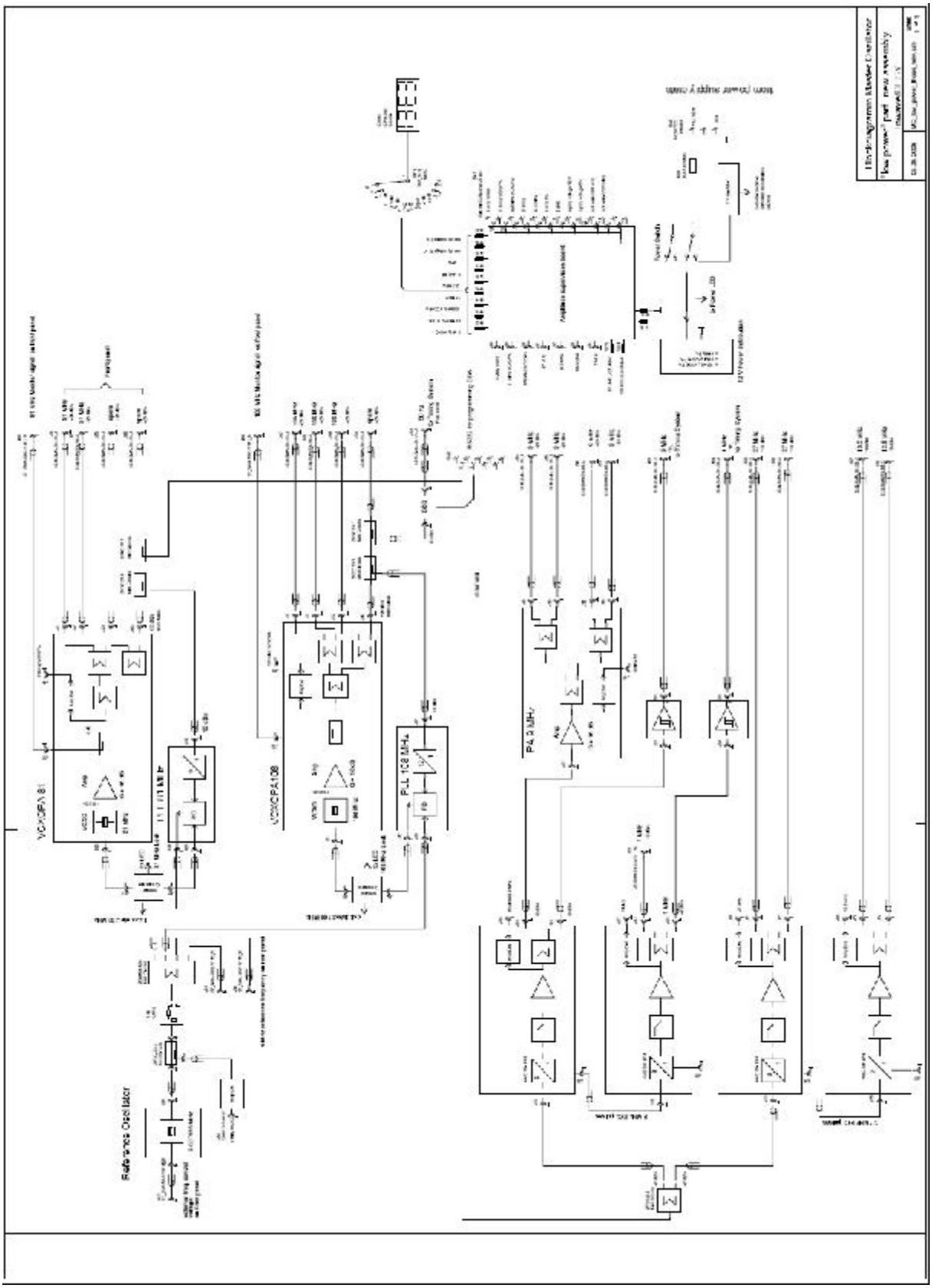

Figure 9.3.3.2. MO Low power part block diagram.

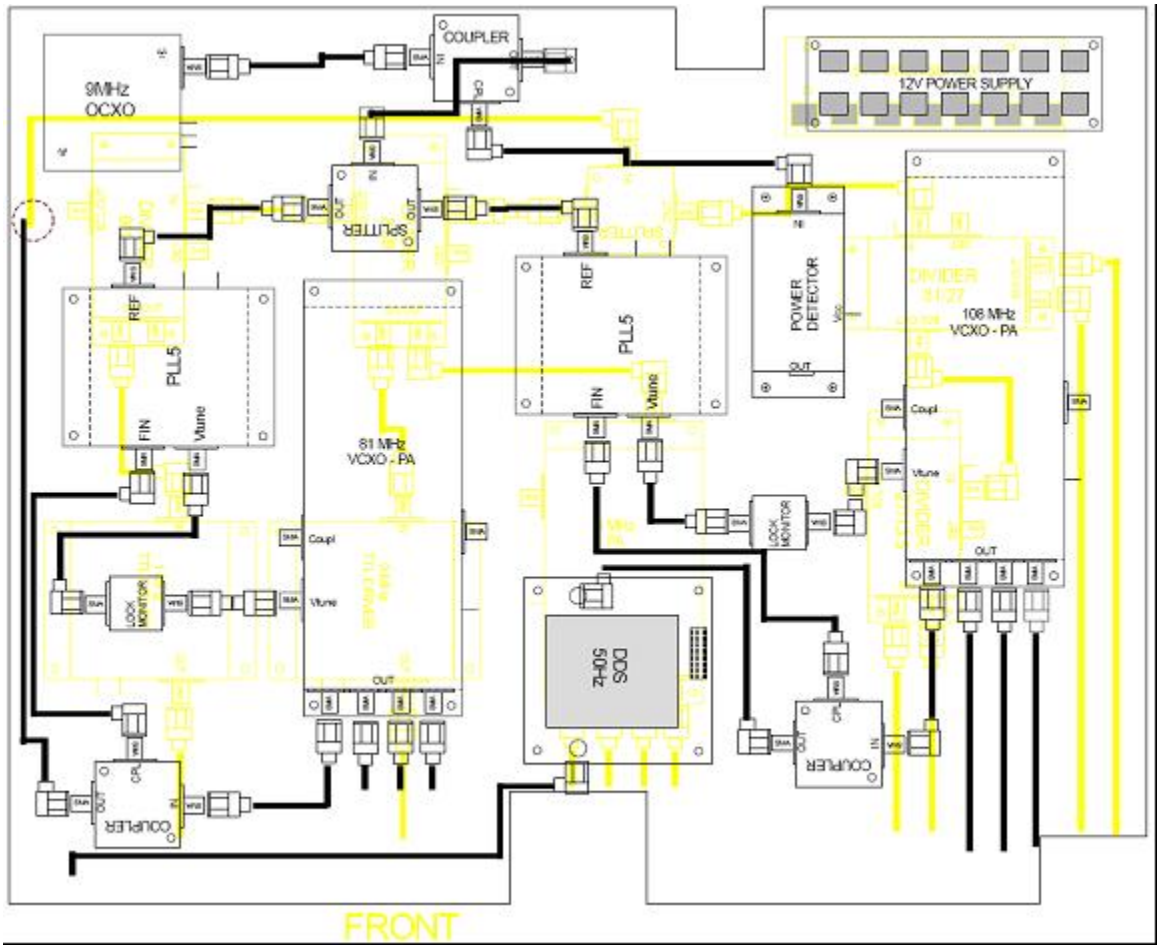

Figure 9.3.3.3 MO LPP assembly drawing

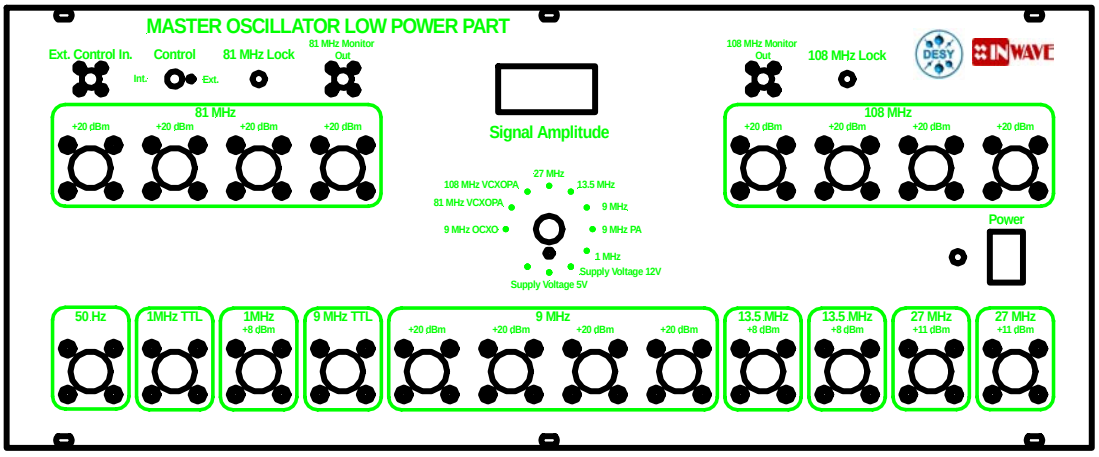

Figure 9.3.3.4 MO LPP front panel drawing.

9.4 Software

9.4.1 Data management development

Progress: In line with schedule.

Task completed in 2005 and final report published. The database is currently under tests in DESY – Hamburg.

Milestones and deliverables: None defined in contract for this period
Significant achievements and impact:
Database and supporting programs installed and exercised.
Deviations from plan: None

9.4.2 RF Gun control

At the DESY Vacuum Ultraviolet Free Electron Laser (VUV-FEL) bunch compression and the SASE effect are (amongst other parameters) sensitive to beam energy and beam phase variations. The electron bunches are created in a rf gun, which does not have field probes.
DSP based rf field control used previously was only able to stabilize the rf output of the klystron. This was due to the lack of processing power and the overall loop latency. The controller was not able to provide satisfying rf field stability in the gun.
Replacing the DSP hardware by the new FPGA-based hardware Simulation Controller (SimCon), we reduced the latency within the digital part significantly. Furthermore SimCon provides sufficient processing power for calculating a probe signal from the forward and reflected power as input for PI and adaptive feed forward (AFF) control.
In March 2006 we qualified the performance of the FPGA based gun rf field control with beam: The field is now well stabilized for SASE operation for short and also for long rf pulses. For rf pulse length in the order of 100 us PI control only is sufficient. Longer rf pulses and bunch trains require the use of AFF control in addition.

Milestones and deliverables: None defined in contract for this period
Significant achievements and impact:
Improved rf gun field stability in user operation at Flash facility
Deviations from plan: None

Update of MS-Project

N°	Task Name	Anfang	Ende
9	**WP9 LOW LEVEL RF (LLRF)**	**Do 01.01.04**	**Fr 08.12.06**
9.1	**Operability and technical performance**	**Do 01.01.04**	**Fr 08.12.06**
9.1.1	**Transient detector**	**Do 01.01.04**	**Fr 08.12.06**
9.1.1.1	Define requirements	Do 01.01.04	Fr 30.01.04
9.1.1.2	Electronics design	Mo 02.02.04	Fr 27.02.04
9.1.1.3	Build prototype and evaluate	Mo 01.03.04	Fr 30.07.04
9.1.1.4	Final design of detector	Mo 02.08.04	Fr 01.10.04
9.1.1.5	Installation and commissioning	Mo 04.10.04	Mi 09.02.05
9.1.1.6	Test with beam	Mi 09.02.05	Fr 08.12.06
9.1.1.7	**Report on transient detector test**	Fr 08.12.06	Fr 08.12.06
9.1.2	**LLRF Automation**	**Do 01.01.04**	**Fr 23.06.06**
9.1.2.1	Dialogue with industrial experts	Do 01.01.04	Fr 27.02.04
9.1.2.2	Develop full specification	Mo 01.03.04	Fr 26.03.04
9.1.2.3	Implement FMS for subsystems	Mo 29.03.04	Fr 29.10.04
9.1.2.4	Test and evaluation	Mo 01.11.04	Mi 23.02.05
9.1.2.5	Implement improvements	Mi 23.02.05	Di 26.04.05
9.1.2.6	Evaluation and acceptance by operators	Di 26.04.05	Fr 23.06.06
9.1.2.7	**Report on LLRF atomization design**	Fr 23.06.06	Fr 23.06.06
9.1.3	**Control optimization**	**Do 01.01.04**	**Fr 13.10.06**
9.1.3.1	Specification of system	Do 01.01.04	Fr 02.04.04
9.1.3.2	Conceptual design of controller	Mo 05.04.04	Fr 30.04.04
9.1.3.3	Performance simulation	Mo 03.05.04	Fr 27.08.04
9.1.3.4	Implementation in DSP hardware	Mo 30.08.04	Mi 02.02.05
9.1.3.5	Implementation and tests on TTF	Do 03.02.05	Fr 13.10.06
9.1.3.6	**Evaluation of test results**	Fr 13.10.06	Fr 13.10.06
9.1.4	**Exceptional handling routines**	**Do 01.01.04**	**Fr 02.12.05**
9.1.4.1	Specification	Do 01.01.04	Fr 23.01.04
9.1.4.2	Design of exceptional handler	Mo 26.01.04	Fr 30.04.04
9.1.4.3	Implementation and test on TTF	Mo 03.05.04	Fr 02.12.05
9.1.4.4	**Report on exceptional handler operation**	Fr 02.12.05	Fr 02.12.05
9.2	**LLRF cost and reliability study**	**Do 01.01.04**	**Fr 27.10.06**
9.2.1	**Cost and reliability study**	**Do 01.01.04**	**Fr 29.09.06**
9.2.1.1	Identify cost drivers of present LLRF	Do 01.01.04	Fr 27.02.04
9.2.1.2	Develop cost reduction ideas	Mo 01.03.04	Fr 02.04.04
9.2.1.3	Build prototypes and evaluate	Mo 05.04.04	Fr 21.01.05
9.2.1.4	Final design of LLRF system	Fr 21.01.05	Fr 29.09.06
9.2.1.5	**Complete design of LLRF system for reduce cost**	Fr 29.09.06	Fr 29.09.06
9.2.2	**Radiation damage study**	**Do 01.01.04**	**Fr 27.10.06**
9.2.2.1	Identify critical electronics issues	Do 01.01.04	Fr 27.02.04
9.2.2.2	Evaluate TESLA radiation	Mo 01.03.04	Fr 02.04.04
9.2.2.3	Develop tests for components	Mo 05.04.04	Fr 28.05.04
9.2.2.4	Procure and assembles test set up	Mo 31.05.04	Fr 23.07.04
9.2.2.5	Data acquisition from radiation tests	Mo 26.07.04	Fr 29.10.04
9.2.2.6	Analyze results and develop countermeasures	Mo 01.11.04	Mi 09.02.05
9.2.2.7	Implement countermeasures and verify	Mi 09.02.05	Fr 27.10.06
9.2.2.8	**Report on radiation damage studies**	Fr 27.10.06	Fr 27.10.06
9.3	**Hardware**	**Do 01.01.04**	**Mi 01.03.06**
9.3.1	**Multichannel downconvertor**	**Do 01.01.04**	**Mi 26.01.05**
9.3.1.1	Study and compare technologies	Do 01.01.04	Fr 27.02.04
9.3.1.2	Select optimum PCB design	Mo 01.03.04	Fr 23.04.04
9.3.1.3	Build prototype and evaluate	Mo 26.04.04	Fr 02.07.04
9.3.1.4	Finalize multichannel down converter	Mo 05.07.04	Fr 03.09.04
9.3.1.5	Determine characteristics	Mo 06.09.04	Mi 26.01.05
9.3.2	**Third generation RF control**	**Do 01.01.04**	**Mo 11.04.05**
9.3.2.1	Integrate system generator with VHDL	Do 01.01.04	Fr 30.01.04
9.3.2.2	Complete specification	Mo 02.02.04	Fr 02.04.04
9.3.2.3	Demonstrate simulator	Mo 05.04.04	Fr 04.06.04
9.3.2.4	Final design of RF electronic board	Mo 07.06.04	Fr 28.01.05
9.3.2.5	Evaluate performance	Mo 03.01.05	Mo 11.04.05
9.3.3	**Stable frequency distribution**	**Do 01.01.04**	**Mi 01.03.06**
9.3.3.1	Complete specification	Do 01.01.04	Mi 04.02.04
9.3.3.2	Concept ional design of frequency	Do 05.02.04	Fr 05.03.04
9.3.3.3	Build prototype and evaluate	Mo 08.03.04	Fr 06.08.04
9.3.3.4	Final design	Mo 09.08.04	Fr 22.10.04
9.3.3.5	Procurement and assembly of subsystems	Mo 25.10.04	Fr 28.01.05
9.3.3.6	Installation and commissioning	Mo 03.01.05	Fr 18.03.05
9.3.3.7	Performance test with beam	Mo 21.03.05	Mi 01.03.06
9.3.3.8	**Report on new LLRF hardware components**	Mi 01.03.06	Mi 01.03.06
9.4	**Software**	**Do 01.01.04**	**Fr 06.10.06**
9.4.1	**Data management development**	**Do 01.01.04**	**Mi 14.09.05**
9.4.1.1	Specification	Do 01.01.04	Fr 30.04.04
9.4.1.2	Conceptional design with DOOCS	Mo 03.05.04	Fr 09.07.04
9.4.1.3	Prototype	Mo 12.07.04	Fr 10.09.04
9.4.1.4	User evaluation	Mo 13.09.04	Fr 05.11.04
9.4.1.5	Finalize design	Mo 08.11.04	Fr 31.12.04
9.4.1.6	Implementation in TTF	Mo 03.01.05	Mi 14.09.05
9.4.1.7	**Report on data management developments**	Mi 14.09.05	Mi 14.09.05
9.4.2	**RF gun control**	**Do 01.01.04**	**Fr 06.10.06**
9.4.2.1	Write specification	Do 01.01.04	Fr 30.01.04
9.4.2.2	Design of controller	Mo 02.02.04	Fr 23.04.04
9.4.2.3	Procurement and assembly	Mo 26.04.04	Fr 27.08.04
9.4.2.4	Installation and test	Mo 30.08.04	Fr 06.10.06
9.4.2.5	**Report on RF gun control tests**	Fr 06.10.06	Fr 06.10.06

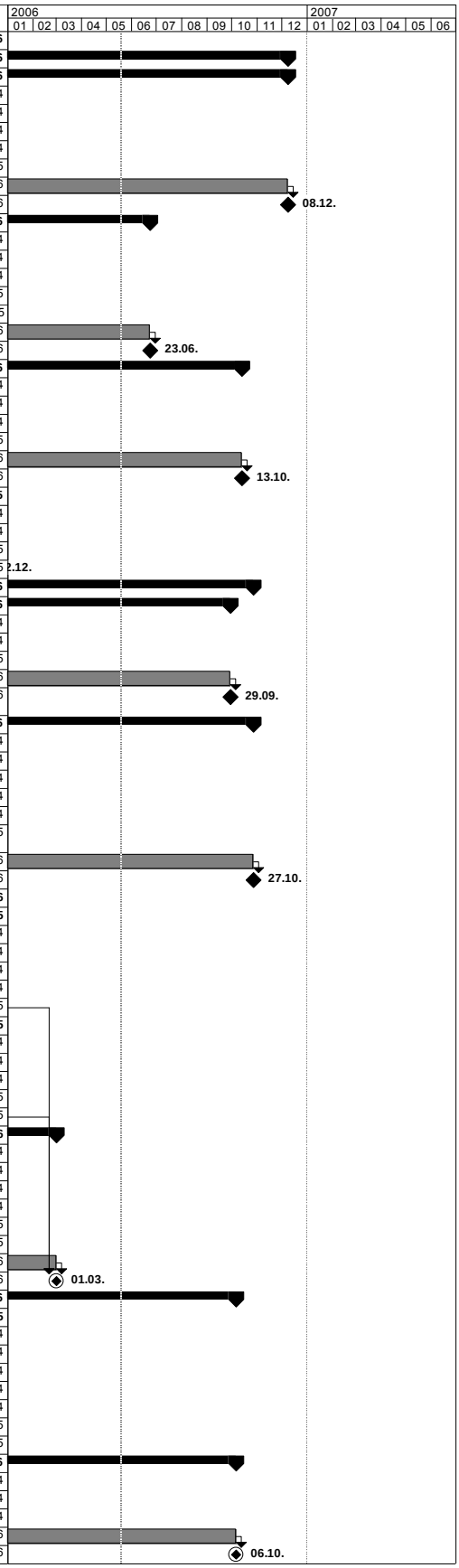

Work package 10: Cryostat integration tests

At the beginning of 2006, we encountered some problems with the cryogenic system necessary to supply helium in CryHoLab. A fatal damage occurred to the valve bellow used to regulate helium level in phase separator. Repair caused one month delay in the experimental schedule.

Moreover fluctuations of the helium bath pressure at 1.7 K damaged RF analysis with a bad signal to noise ratio. At last an acceptable working situation was found avoiding the helium compressor use.

After qualifying tests of nine cells C45, an electronic device has been developed to generate a 200 μs pre-pulse at the klystron with RF power multiplied by four. This improvement was necessary to shorten the cavity filling time and achieved a 800 μs flat top.

a) 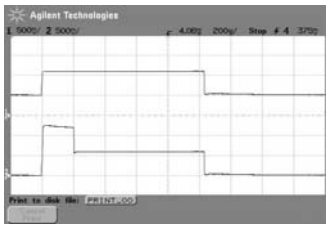 b) 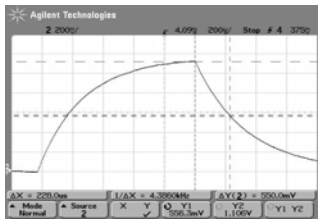 c) 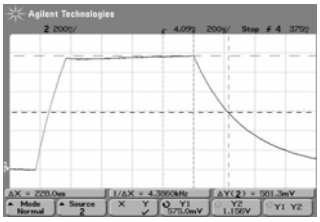

Fig.1 a) injected RF power in cavity without or with pre-pulse (P:1ms or 4P:200μs - P:800μs) b) transmitted RF power from cavity without pre-pulse c) Flat top on transmitted RF power with pre-pulse

After coupler conditioning, the pulsed RF power (P=70 to 130 kW, 800 μs, 6.25 Hz) with pre-pulse (4P, 200 μs) was injected in the 9-cell cavity cooled down at 1.7 K. We got Q_0 (E_{acc}) curve using transmitted power (P_t) and cryogenic measurements to determine cavity losses (P_{cav}). The maximum accelerator field (22 MV/m) is limited by field emission with X-rays detected (figure 2).

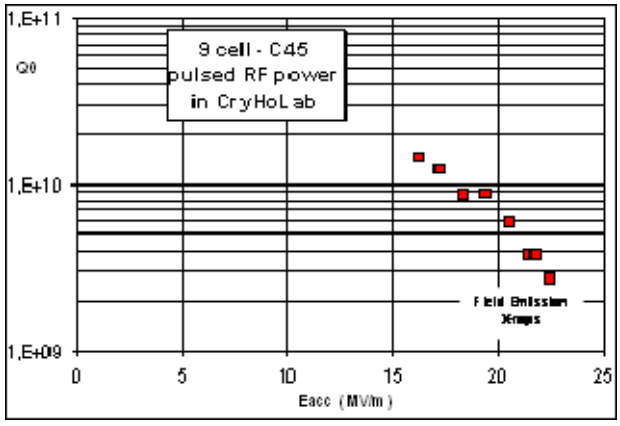

Fig.2 Q_0 vs. E_{acc} for C45 cavity

In such conditions, compensation of Lorentz Force detuning has been achieved (figure 3) using NOLIAC piezoelectric tuners assembled on cold tuning system (figure 4) developed in WP8. At present similar experiments are achieved with PICMA piezoelectric device. These results will be subjected to special reports in few weeks.

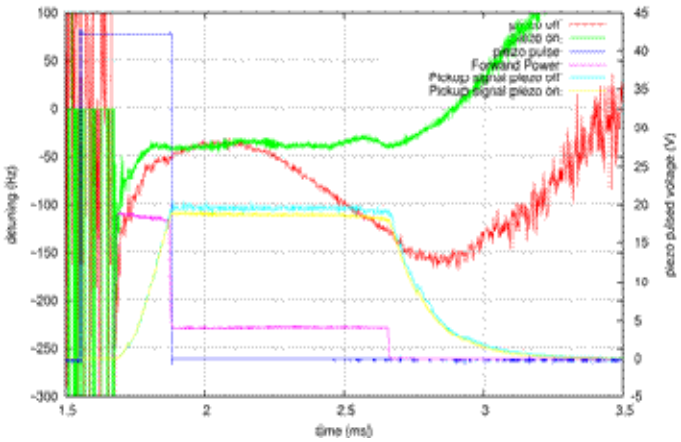

Fig.3 Lorentz Force Detuning for E_{acc}= 20 MV/m (red curve). Compensation using Noliac PZT Tuner on Cold Tuning System (green curve)

Fig.4 Cold Tuning System (CTS) with Noliac or PICMA Piezoelectric Tuners mounted on 9-cell C45 cavity in CryHoLab.

The third tests series planned with magnetostrictive tuner should be delayed after CryHoLab displace from "l'Orme des Merisiers" area to the main Saclay Center. Experiments in CryHoLab will be stopped at the end of May and they will restart in December 2006 according to the schedule

Update of MS-Project

N°	Index WBS		Nom de la tâche
1	**10**		**WP10 CRYOSTAT INTEGRATION TESTS**
2	**10-1**		**Installation Moving**
3	10-1.2		Vertical cryostats moving
4	10-1.1		CRYHOLAB - Liquefier - Klystron moving, commissioning
5	**10-2**		**CRYHOLAB Adaptation to 9 cell**
6	10-2.1		Mechanical adaptations (design-manufacturing-mounting)
7	10-2.2		Low performance cavity and coupler transfert from DESY & LAL
8	10-2.3		Assembly in Cryholab and Cryogenic test
9	10-2.4		High performance coupler - High Power Pulsed Test
10	10-2.5		Magnetic shielding with cryoperm
11	**10-3**		**Integration tests in cryostat (1st test)**
12	10-3.1		CEA Cold Tunning System + Piezo (Assembly & warm tests)
13	10-3.4		Installation of 9-cell & coupler - Cooldown
14	10-3.3		Cold test (CTS + NOLIAC) in CryHoLab
15	10-3.2		Evaluate experimental results
16	**10-5**		**Integration tests in cryostat (2sd test)**
17	10-5.7		Installation of CTS + Piezo PICMA
18	10-5.5		Cold test (CTS + PICMA) in CryHoLab
19	10-5.6		Evaluate experimental results
20	**10-4**		**Integration tests in cryostat (3rd test)**
21	10-4.4		Mechanical adaptation
22	10-4.3		Installation of CTS + MSM Energen
23	10-4.1		Cold test (CTS + ENERGEN) in CryHoLab
24	10-4.2		Evaluate experimental results
25	**10-6**		**Integration tests in cryostat (4th test)**
26	10-6.1		New Coupler TTF V from LAL
27	10-6.2		Evaluate experimental results

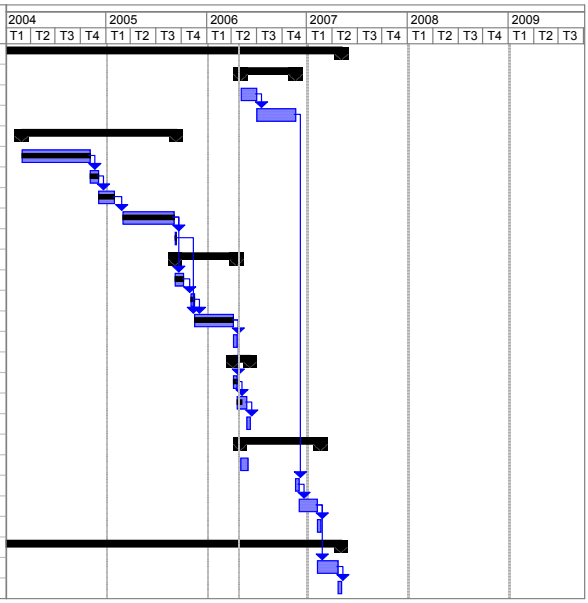

Work package 11: Beam diagnostics

Task 11.1 The Emittance Monitor

In this first period of 2006, two blocks of dedicated shifts were assigned to this experiment. We had the possibility to verify the complete system with the beam. The alignment of the optics must be improved, but the setting was good enough for the first measurements.
The first shifts were used to optimize the beam transport through the by-pass line and trying to obtain the expected beam size at our screen location. The low energy, 450 MeV, and the beam size larger than expected prevented the observation of Diffraction Radiation, but the shifts were useful not only for the calibration of the optical system with the much more intense Optical Transition Radiation, evidencing the presence of a strong background due to synchrotron radiation from the last dipole, at more than 50 meters distance, and of the first successive quadrupoles, whose gradient was very high.
This background was not expected, and even if not completely understood, derives from multiple reflections on the pipe surface, showing a much larger angular distribution that what the distance of the magnetic elements could suggest.
In the second set of shifts the energy was higher, about 630 MeV, but still lower than what expected. The beam size still resulted too large, probably for a not perfectly optimized transport resulting in a higher emittance, so that we were forced to use the largest of the two slits, 1 mm width, for which the observation of DR was surely difficult, in particular because the beam was slightly larger than the slit itself.
The data taken are still under analysis, but we think to have found a way to subtract the background, steering the beam out of the screen with the last steerer. A couple of months will be needed to complete the analysis.
This shifts have teached us that for the future a hardware shielding of the synchrotron radiation background will be required, a much better transport of the beam will be needed, in order to obtain the design beam size, and the final energy of the machine must be reached.
In the following few images, the strong background level and the effect of its subtraction is shown, together with the image of the beam inside the slit, with the tails still hitting the borders.

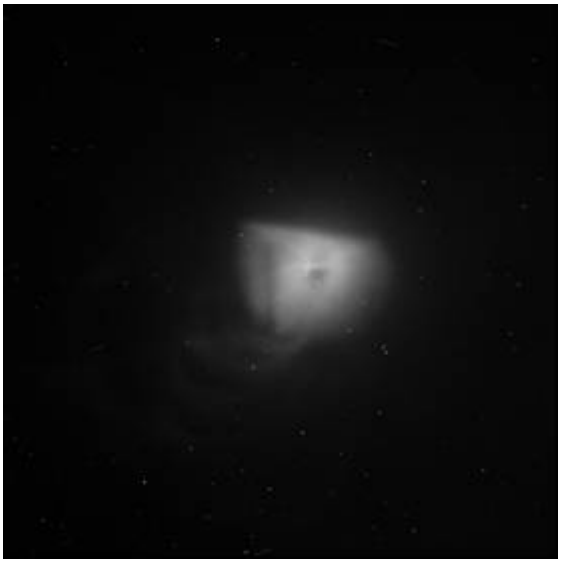

Fig. 1 – OTR with background

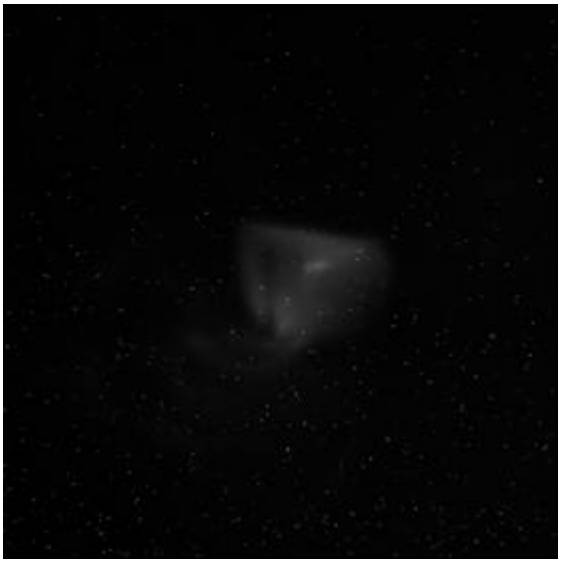

Fig. 2 - Background (not normalised)

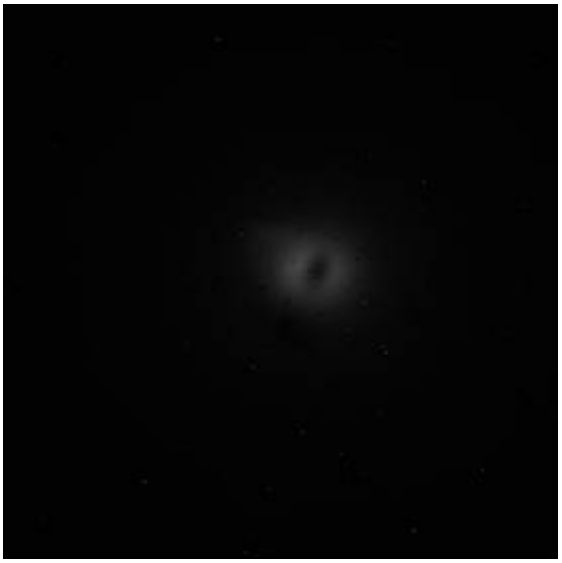

Fig. 3 – OTR after the background subtraction

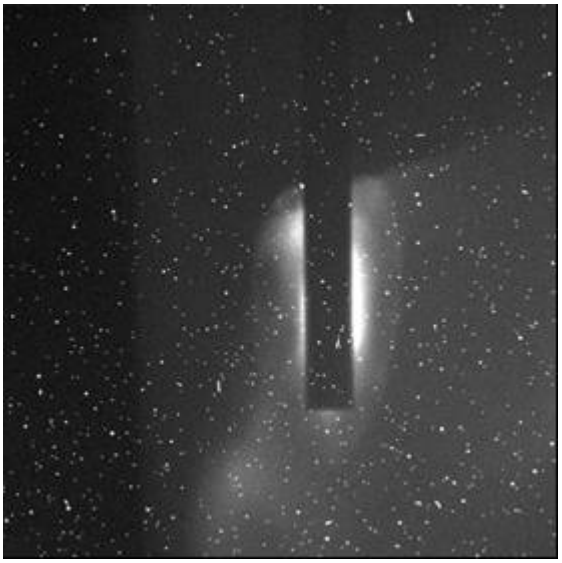

Fig.4 – Beam inside the 1 mm slit

Update of MS-Project

N°	Task Name	Anfang	Ende
11.1	**Beam position monitor**	**Do 01.01.04**	**Mi 12.12.07**
11.1.1	**Present BPM installed in TTF module**	Mi 30.06.04	Mi 30.06.04
11.1.2	Cryogenic measurements on BPM	Do 01.07.04	Fr 06.08.04
11.1.3	Beam tests of BPM on TTF	Mo 09.08.04	Mo 03.10.05
11.1.4	Design of BPM Cavity	Do 01.01.04	Fr 25.03.05
11.1.5	Design of BPM cavity ready	Fr 25.03.05	Fr 25.03.05
11.1.6	Fabrication of BPM Cavity	Fr 25.03.05	Fr 23.12.05
11.1.7	BMP cavity ready	Fr 23.12.05	Fr 23.12.05
11.1.8	Development of new hybrid coupler and electronics	Mo 05.07.04	Mo 05.09.05
11.1.9	Design of Digital Signal Processing	Mo 03.01.05	Mi 17.08.05
11.1.10	**New BPM ready for Installation**	So 01.01.06	So 01.01.06
11.1.11	Beam Tests with new BPM	Mo 02.01.06	Mi 12.12.07
11.1.12	**Evaluation of BPM operation**	Mi 12.12.07	Mi 12.12.07

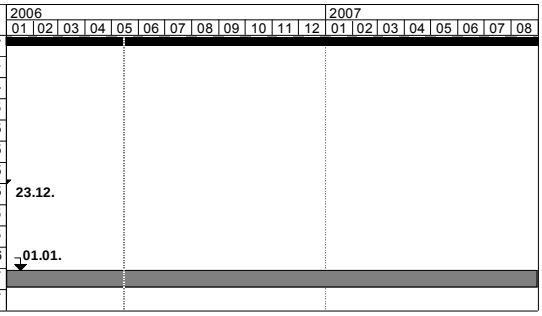

Task 11.2 Beam position monitor

The activity of the last months was dedicated to beam tests on the BPM installed in ACC1 and simulations of different models of BPM to evaluate the resolution and support the choice of the new design. Another part of the activity concerned the fabrication of a new BPM cavity which will be installed near ACC7 on TTF2.

I - Reentrant BPM calibration:

In March 2006, an additional calibration operation was carried out on the BPM installed in ACC1. The TTF2 was operated in single bunch for these measurements which produced statistics and correlations. Two methods were used to calibrate this BPM called 9ACC1.

The first method uses steerers to move the beam. The setting and the relative beam position are calculated in using a transfer matrix between steerers and BPM (made of drifts and accelerating cavities): $\Delta x = R12*\Delta x'$ where $\Delta x'$ is the angle at steerer. The HOMs (High Order Modes) of the cavity 8 installed in the cryomodule ACC1, were minimized thanks to beam moving by steerers. This minimization let adjust the BPM center. The beam tilt was neglected due to the closeness between the BPM 9ACC1and the cavity 8. An offset was added in the software to have a slope around 1 and show the system linearity.

The second method uses 3 BPMs. The relative beam position at the reentrant BPM (9ACC1) is calculated by extrapolation from the other two BPMs.

With the first calibration method (transfer matrix), 9ACC1 shows a linear range around 3-4 mm before saturation. We suppose that this saturation comes from the amplifier or ADC saturation.

The second method gives some results which are not very linear in a range of 3-4mm. The problem may come of the fact that between the first and second BPM the distance is quite long. On the fig.1 and fig.2, the plots of the predicted position calculated with the first method vs the position read by 9ACC1, on X and Y channels are presented:

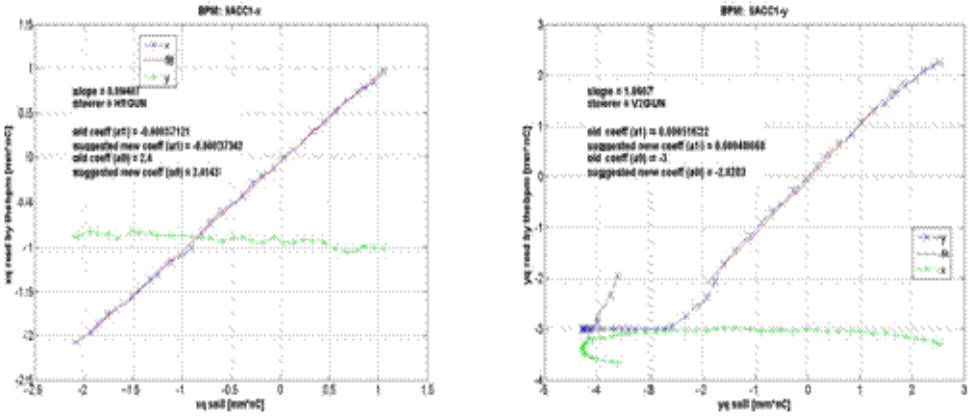

FIGURE 1 & 2. Position read by 9ACC1 vs the predicted position

The raw RMS resolution of the system, measured directly from 9ACC1, is around 50µm on the X channel. In using the correlation between different BPMs, the beam jitter

can be canceled and the real resolution can be estimated which gives a result around 20µm. On the Y channel, the resolution is around 30µm without the beam jitter and around 70µm as a raw measurement.

II Estimation of the Prototype Absolute Resolution

The resolution is limited by the signal to noise ratio of the system. The signal voltage of the BPM is determined by the beam's energy loss to the "TM110" mode and by the external coupling of the coaxial cable.

The noise comes from the thermal noise, the components used in the signal processing. The thermal noise of a system is given by the following equation

$$P_{th} = k_b * T * BW \qquad (1)$$

where k_b is Boltzmann's constant ($1.38*10^{-23}$J/K), BW is defined by the bandwidth of the band pass filter in Hertz, and T is the room temperature in Kelvin.

The noise level present at the output of the cavity BPMs, is amplified by the devices which compose the signal processing. To calculate the noise level, the thermal noise is added to the noise factor and to the gain. The noise level is therefore given by the following equation:

$$P_n = NF * G * P_{th}. \qquad (2)$$

where NF is the total noise figure of the circuit, G is the gain of the signal processing and P_{th} is the thermal noise.

The total noise introduced into the system by the electronics could be evaluated by the noise figure in the cascaded system and is applied by the following formula:

$$NF = F_1 + \frac{F_2 - 1}{G_1} + \frac{F_3 - 1}{G_1 * G_2} + \ldots \qquad (3)$$

where NF is the total noise factor of the signal processing, F_i and G_i are respectively the noise factor and the gain of component i.

To assess the performances of system, a model (cavity+signal processing) was elaborated with Mathcad. The re-entrant cavity model is a resonant R L C circuit, the impulse response of the monopole and dipole modes depends on frequencies and external coupling. The transfer functions of different elements (cables, hybrid couplers, filters, amplifier mixer) which compose the signal processing, are determined by the S parameters measured with a network analyzer. Then those transfer functions are used and combined to simulate the BPM system (RF cavity+signal processing). The transfer function of cables takes the effect of attenuation and dispersion into account.

The following tables 2 and 3 show a comparison between three systems regarding the resolution, noise level and output signal level from the signal processing. The first system corresponds to the BPM installed in ACC1 on TTF2. The second system (ACC1 with BW=110MHz) has the same resonance modes and the same electronics than the re-entrant BPM installed in ACC1 but the filter bandwidth is 110MHz. The gain was adjusted to have a RF signal level around 0 dBm on the Δ channel. The NBPM system (RF cavity + electronics) is the model of the new system as presented in the previous report. The gain was adjusted to have a RF signal level around 0 dBm on the Δ channel, too. A prototype of this system is ready for warm tests with beam on TTF2.

TABLE 2. Signal and noise level for different systems.

System	Signal level on the Δ channel with an offset of 10 µm (dBm)	Noise level (dBm)	Thermal Noise (dBm)
ACC1 with BW=8Mhz	-79	-57.2	-104.9
ACC1 with BW=110Mhz	-5.8	-25.8	-93.5
NBPM	-9.4	-47.4	-93.5

TABLE 3. Resolution for different systems.

System	Resolution with a total monopole rejection (µm)	Resolution calculated (µm)	Offset (µm)
ACC1 with BW=8Mhz	6	6	6.5
ACC1 with BW=110Mhz	1.6	1.8	6.5
NBPM	$155*10^{-3}$	$155*10^{-3}$	1.5

III - Time Resolution

The damping time is known by using the following formula:

$$\tau_{110} = \frac{1}{\pi * BW}. \qquad (4)$$

where BW is the bandwidth in Hertz .

For bunch to bunch measurements, the time resolution has to be smaller than the space between bunches of the machine. On TTF2, bunches space is 110 ns.

Taking a RF cavity, the bandwidth is defined by the relation:

$$BW = \frac{f_{110}}{Q_{l110}}. \qquad (5)$$

with f_{110} which is frequency of the dipole mode and Q_{l110} loaded quality factor for the dipole mode. The time resolution is therefore around 9.5 ns for the new re-entrant BPM. It is lower than the separation between bunches on TTF2, the bunch to bunch measurement is therefore possible.

In reality, the rising time of a signal is 3τ. For bunch to bunch measurements, the time resolution has to be smaller than the distance between bunches ΔT. The system has to verify the following equation:

$$6\tau \le \Delta T \qquad (6)$$

To evaluate the time resolution of the BPM system (cavity+electronics), the Mathcad model is used and gives the simulated output signal after the synchronous detection. The time resolution is therefore defined by the time interval at 5% of the peak voltage from the baseline.

Table 4 shows that the BPM system installed in ACC1 couldn't do bunch to bunch measurements, it was necessary to change the filter bandwidth.

TABLE 4. Time resolution for different systems.

System	Time resolution (cavity)	Time resolution (cavity + electronics)
ACC1 with BW=8Mhz	0.63ns	204ns
ACC1 with BW=110Mhz	0.63ns	20ns
NBPM	9.4ns	40ns

IV - Fabrication of the RF cavity (NBPM)

The RF cavity is fabricated with stainless steel and has a small size (170mm of length, 78 mm for the beam pipe and 152 mm of diameter) as shown Fig.3.

FIGURE 3. BPM Cavity and one of its feedthrough.

The antennas fulfilled the conditions of Ultra High Vaccum (UHV). They are assembled to the cavity by a conflat gasket. To ensure electrical conduction, between the feedthrough and the cavity, a RF contact in CuBe was welded in the coaxial cylinder part. To avoid hydrogen out gassing, a heat treatment at 280°C for 15 days was done on the BPM cavity instead of the usual treatment (950°C for 2h) which may have damaged the RF contact elasticity.

Some RF measurements, presented in the Table 1, were done to verify the RF characteristics (frequencies, quality factor and longitudinal R/Q).

TABLE 1. RF characteristics of the BPM.

Eigen modes	F (GHz)		Q_l		R/Q_l with 5 mm of offset	R/Q_l with 10 mm of offset
	calculated	measured	calculated	measured		
Monopole mode	1.2497	1.254	22.95	22.74	12.87 Ω	12.89 Ω
Dipole mode	1.7194	1.725	50.96.	48.13	0.27 Ω	1.15 Ω

Due to machining tolerances, welding procedure, beam pipe elliptic and the asymmetry of the antennas mounting, some small distortions of the cavity symmetry are generated. The cavity modes become asymmetric in the direction x and can coupled those in the y direction and vice versa, this asymmetry is called cross talk.

Cross-talk isolation measurements were performed on the re-entrant cavity with a network analyzer. The signal is coupled between 2 antennas positioned at 180°, on the others ports a 50Ω load is put. With this measurement, the monopole and dipole modes are excited as shown Fig.4. At the dipole frequency (1.72 GHz), the signal level is -0.805dB.

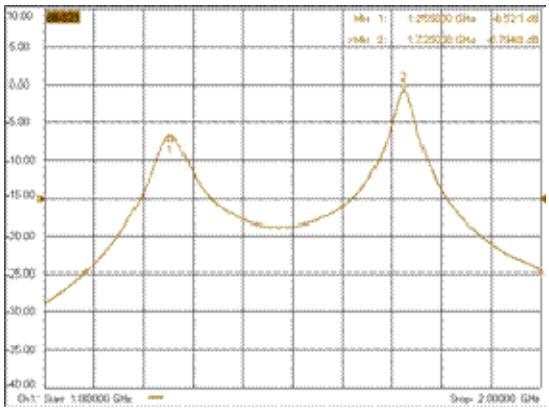

FIGURE 4. Signal level vs frequency

For the second measurements, the signal is coupled between 2 antennas positioned at 90°. The output signals from antennas positioned to 180° are connected by cables to hybrid coupler. On the top of fig.5, the output signals from the Σ channel of the hybrid is shown and in bottom, the measurement is the output signal from the Δ channel of the hybrid.

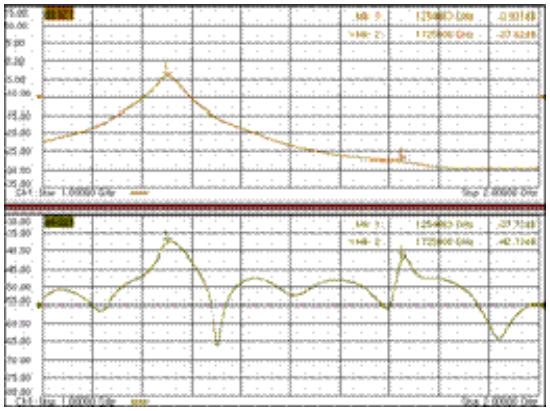

FIGURE 5. Signal level vs frequency

From those measurements, the cross-talk isolation value can be determined to be 41 dB+/- 1dB.

Update of MS-Project

N°	Task Name	Anfang	Ende
11.2	**Beam Emittance Monitor**	**Do 01.01.04**	**Mi 28.05.08**
11.2.1	Slit width simulations	Do 01.01.04	Fr 02.04.04
11.2.2	Slit design	Mo 05.04.04	Fr 02.07.04
11.2.3	Optics simulations	Mo 05.04.04	Fr 02.07.04
11.2.4	Optics appropriations	Mo 05.07.04	Mo 15.08.05
11.2.5	System assembly and tests	Mo 25.10.04	Fr 30.09.05
11.2.6	Mechanical assembly at TTF	Mo 03.10.05	Mi 02.11.05
11.2.7	Optical assembly at TTF	Do 03.11.05	Do 01.12.05
11.2.8	Integration of controls into TTF	Fr 02.12.05	Sa 31.12.05
11.2.9	**Ready for beam test in TTF**	Sa 31.12.05	Sa 31.12.05
11.2.10	Beam tests at TTF	Mo 02.01.06	Fr 02.06.06
11.2.11	Evaluate first beam test result	Fr 02.06.06	Fr 02.06.06
11.2.12	Successive measurements	Mo 05.06.06	Mi 28.05.08
11.2.13	**Final evaluation**	Mi 28.05.08	Mi 28.05.08